Understanding the evolution of nearshore Deepwater Horizon oil spill residues and characterizing them using GC/MS/MS methods

by

Gerald Francis John

A dissertation submitted to the Graduate Faculty of
Auburn University
in partial fulfillment of the
requirements for the Degree of
Environmental Engineering Doctor of Philosophy

Auburn, Alabama
May 7, 2016

Keywords: Oil spill, Deepwater Horizon, tarballs, submerged oil mats
polycyclic aromatic hydrocarbons, dispersants

Approved by

T. Prabhakar Clement (Chair), Professor of Civil Engineering
Joel S. Hayworth, Associate Professor of Civil Engineering
Dongye Zhao, Professor of Civil Engineering
Xinyu Zhang, Associate Professor of Civil Engineering

Abstract

On April 20, 2010, *Deepwater Horizon,* a semi-submersible oil rig exploring for oil in the northern Gulf of Mexico (GOM), exploded. The resulting accident released about 4.8 million barrels of oil into the waters of GOM over a period of 87 days. Oil released from this accident impacted various beaches located along Florida, Alabama, Mississippi, Louisiana and Texas coastline. The weathered oil started arriving on the beaches of Alabama from early June 2010. The oil that washed ashore was in the form of highly viscous, neutrally buoyant, water-in-oil emulsion known as mousse. An unknown quantity of mousse interacted with near-shore sediments, settled down to seafloor transforming into submerged oil mats (SOMs) and surface residual balls (SRBs). SOMs and SRBs continue to impact the beaches of Alabama to this day. The overall goal of this study is to monitor SRBs deposition activities along Alabama's beaches and evaluate the transformation of various PAHs trapped in these oil spill residues when they are exposed to sunlight.

The first part of this study (Chapter 2) summarizes the field sampling activities completed along Alabama's beaches over the past four years (from May 2010 to August 2014). Based on our field observations we conclude the following: (1) virtually all the tarballs found on Alabama's beaches have the characteristics of MC252 oil, (2) the beaches wouldn't return to the expected pre-spill background levels in the next five to ten year period, (3) chemical analysis shows the concentration levels of certain polycyclic aromatic hydrocarbons (PAHs), especially chrysene, almost remaining constant over the past four

years; and (4) the presence of SRBs/SOMs continue to pose long-term environmental risk to the nearshore beach environment.

The second part of this study (Chapter 3) discusses the effects of sunlight on weathering of five groups of PAHs present in MC252 oil and SOMs samples: – (1) C_0- to C_4-naphthalenes, (2) C_0- to C_4-phenanthrenes, (3) C_0- to C_3-dibenzothiophenes, (4) C_0- to C_3-fluorenes, and (5) C_0- to C_4-chrysenes. The PAHs present in both MC252 oil and SOM can be weathered by evaporation and photo-oxidation processes. Among the five groups of PAHs, C_0 to C_4-chrysenes trapped in SOMs have the least weathering rate.

Chrysene and its alkylated homologues (C_0- to C_4-chrysenes) are resistant to various natural weathering processes and could potentially persist in the environmental for a very long time. Therefore, the third section of this effort (Chapter 4) focusses on developing a more efficient GC/MS/MS MRM analytical method for characterizing C_0- to C_4-chrysenes in oil spill residues. The developed method was used to quantify C_0- to C_4-chrysenes in MC252 oil and the estimated concentrations were close to that of values reported in the literature.

The oil from *Deepwater Horizon* accident that washed ashore was predominantly in the form of water-in-oil (W/O) emulsion known as mousse. The environmental risks posed by these emulsions can be considerably reduced if this W/O emulsion can be dispersed rapidly in the deep ocean environment. COREXIT9500A, which was widely used to disperse the released oil, is ineffective in dispersing W/O emulsions. The fourth part of this dissertation (Chapter 5) focusses on developing a method to modify COREXIT9500A by adding polar additives (1-octanol and hexylamine) to enhance its ability to disperse W/O emulsions. Preliminary results show that the addition of these

additives have the potential to enhance the effectiveness of COREXIT9500A to disperse W/O emulsions.

The final section (Chapter 6) summarizes the key findings of this research and also points out some future research recommendations.

Acknowledgments

I would like to thank, my advisor, Dr. T. Prabhakar Clement for his patient guidance and mentorship during my stay at Auburn University. I would also like to thank my co-advisor, Dr. Joel Hayworth for his guidance with the emulsion work. I express my sincere gratitude to the other committee members: Dr. Dongye Zhao and Dr. Xinyu Zhang, for their valuable comments and suggestions and Dr. Muralikrishnan Dhanasekaran for having graciously accepted to serve as the outside reader.

Special thanks to Dr. Fang Yin and Dr. Vanisree Mulabagal, for helping me with scientific discussions, project design, instrument knowledge and making this stay a fruitful experience.

My group colleagues Farhad Jazaei, Yuling Han, Dr. Jagadish Torlapati and Mengyuan Zheng deserve special appreciation for their assistance and cooperation.

Finally, I would like to thank my parents and brothers for their great support and confidence in me. I want to thank the City of Orange Beach, Alabama, USA, the National Science Foundation (NSF), Samuel Ginn College of Engineering, Auburn University, and Marine Environmental Sciences Consortium (MESC) for funding this research.

Table of Contents

List of Tables

List of Figures

List of Abbreviations

EIA	U.S. Energy Information Administration
MC252	Macondo Prospect 252
DWH	Deepwater Horizon
GOM	Gulf of Mexico
SOMs	Submerged oil mats
ESOM	Dichloromethane extract of SOM
SRBs	Surface residual balls
PAHs	Polycyclic aromatic hydrocarbons
BP	British Petroleum
USEPA	United States Environmental Protection Agency
NRC	National research council
OSAT	Operational science advisory team
UC	Unified Command
SCAT	Shoreline Cleanup Assessment Technique
SCCP	Shoreline Cleanup Completion Plan
FOSC	Federal On-Scene Coordinator
GPS	Global Positioning System

NWR	National Wildlife Refuge
mph	miles per hour
LP	Lagoon Pass
GC	Gas chromatograph
MS	Mass spectrometer
GC/MS	Gas Chromatograph/Single Quadrupole Mass Spectrometer
GC/MS/MS	Gas Chromatograph/Triple Quadrupole Mass Spectrometer
EI	Electron ionization
SIM	Single ion monitoring
MRM	Multiple reaction monitoring
TS	Time segment
CE	Collision energy
CID	Collision induced dissociation
IS	Internal standard
RRF	Relative response factor
LOD	Limit of detection
LOQ	Limit of quantitation
SD	Standard deviation
DL	Below detection limit
NIST	National Institute of Standards and Technology
C_0-N	C_0-naphthalene
C_1-N	C_1-naphthalenes

C_2-N	C_2-naphthalenes
C_3-N	C_3-naphthalenes
C_4-N	C_4-naphthalenes
C_0-P	C_0-phenanthrene
C_1-P	C_1-phenanthrenes
C_2-P	C_2-phenanthrenes
C_3-P	C_3-phenanthrenes
C_4-P	C_4-phenanthrenes
C_0-D	C_0-dibenzothiophene
C_1-D	C_1-dibenzothiophenes
C_2-D	C_2-dibenzothiophenes
C_3-D	C_3-dibenzothiophenes
C_0-F	C_0-fluorene
C_1-F	C_1-fluorenes
C_2-F	C_2-fluorenes
C_3-F	C_3-fluorenes
C_0-C	C_0-chrysene
C_1-C	C_1-chrysenes
C_2-C	C_2-chrysenes
C_3-C	C_3-chrysenes
C_4-C	C_4-chrysenes
QSAR	Quantitative Structure Activity Relationship

HOMO	Highest Occupied Molecular Orbital
LUMO	Lowest unoccupied Molecular Orbital
SMILES	Simplified molecular input line entry system
W/O	Water-in-oil emulsion
MC	MC252 oil
EMC	Evaporated MC252 oil
AM	Artificial mousse
USCOE	U.S. Army Corps of Engineers

Chapter 1

Introduction

1.1 Background

Global petroleum and other liquids production in first half of 2015 is approximately 95 million barrels per day and this is expected to continue to increase in future years (EIA, 2015). In order to meet the demand and contain the costs, oil is now extracted from various unconventional sources namely- deep sea drilling, Canadian tar-sands and Venezuelan heavy crude oil deposits which were earlier considered as not economical (Wood et al., 2004). More than half of the oil produced from both traditional and unconventional sources are transported across the globe through maritime routes (EIA, 2014). These oil exploration and transportation activities have increased the risk of oil spills into marine environment resulting from oil tanker accidents, offshore drilling accidents and associated drilling activities (Wang et al., 2005). Most of the world's largest oil spills have resulted from oil tanker accidents, although such spills are relatively rare (Joye, 2013). The *Exxon Valdez* oil spill in 1989 (Peterson et al., 2003), *Hebei Spirit* oil spill in 2007 (Yim et al., 2011), *Prestige* oil spill in 2002 and *Torey Canyon* oil spill in 1967 (Díez et al., 2007) are some of the major spills that resulted from oil tanker accidents. The *Deepwater Horizon* accident in 2010 (Camilli et al., 2010; John et al., 2014; Kostka et al., 2011) and *Ixto*c accident in 1979 (Boehm and Fiest, 1982) are few examples of major oil spills that resulted from offshore drilling accidents.

1.2 Review of notable oil spill accidents

1.2.1 Notable oil tanker accidents

1.2.1.1 Exxon Valdez oil spill

The *Exxon Valdez* oil spill, which occurred on March 24, 1989, released approximately 258,000 barrels of crude oil into the waters of Prince William Sound (Burns et al., 1997). About 2000 miles of coastline was affected. Approximately 41% of the spilled oil stranded in the intertidal zones. Aggressive measures were taken to clean the oiled beaches. Despite these measures, oil spill residues with little or no weathering have been found decades after the spill along various Alaskan beaches (Li and Boufadel, 2010; Peterson et al., 2003). *Exxon Valdez* oil spill was the most researched oil spill that has helped us understand the negative effects of crude oil to the environment. As a result of this spill, several policies have been changed across the globe on how to respond or prevent oil spills into the oceans. Also, better approaches have been developed to manage the spilled oil in order to minimize the environmental impacts (NRC, 2003).

1.2.1.2 Hebei Spirit Oil spill

Hebei Spirit oil spill occurred on December 7, 2007 and approximately 10,900 tons of crude oil was released off the west coast of Korean peninsula. About 375 miles of coastline was affected (Yim et al., 2011). This was Korea's worst oil spill and it was big enough to be considered as one of the world's largest oil spills (Kim et al., 2010). Even after 4 years after the spill, oil was found lingering in the coastal environment (Yim et al., 2012). This oil spill initiated several oil spill related researches in the Republic of Korea.

1.2.1.3 Prestige oil spill

Prestige oil spill occurred on November 13, 2002 off the coast of Spain and released about 60,000 tons of heavy fuel oil (González et al., 2006). The spill affected about 800 km of coastline (Díez et al., 2005). In 2007, researchers have found Prestige oil spill residues in inter-tidal zone; these residues have undergone little or no weathering and were mechanically removed from the coastal environment (Díez et al., 2007).

1.2.1.4 Torey Canyon oil spill

Torey Canyon oil spill occurred on March 16, 1967 off the coast of England and released about 60,000 tons of crude oil (O'Sullivan and Richardson, 1967). It was the first oil spill where large volumes of dispersants were used to disperse the spilled oil. Use of toxic dispersants led to widespread environmental damage and this event initiated the research on the development of less toxic dispersants (Lessard and DeMarco, 2000).

1.2.2 Notable off-shore oil drilling accidents

The off-shore oil drilling accidents mostly result from well blow-outs. The oil spills resulting from blow-outs are very different from that of the oil tanker spills. Usually, the oil from the damaged well will be discharged into the sub-sea environment and the released oil has to travel the entire water column to reach the sea surface (NRC, 2003). Furthermore, oil well blow-outs lead to a point source continuously releasing oil into the ocean until the well-head is capped (Boehm and Fiest, 1982).

1.2.2.1 Ixtoc oil spill

The Ixtoc well blow-out that happened on June 3, 1979 released about 476,000 tons of crude oil into the waters of Gulf of Mexico. The oil released continuously over a period

of 9 months until the well was capped on March 24, 1980 (Gundlach et al., 1981). The resulting spill formed water-in-oil emulsions, known as mousse, and the mousse continued to impact various shores for over two months after the accident (Patton et al., 1981).

1.2.2.2 Deepwater Horizon oil spill

Deepwater Horizon oil spill resulted from a well blow-out accident that occurred on April 20, 2010, released approximately 4.9 million barrels of crude oil into the waters of Gulf of Mexico over a period of 87 days. This incident employed, for the first time, sub-surface application of large quantities of dispersants (Kujawinski et al., 2011). Recent researches have reported that the Deepwater Horizon oil spill residues continue to impact Gulf of Mexico beaches till to-date (Kostka et al., 2011; Mulabagal et al., 2013; Urbano et al., 2013; Yin et al., 2015b).

1.3 Recalcitrance of spilled oil

From the above review of some notable oil spill accidents it is clear that the oil spill remnants in the environment continue to persist for a long time. Several studies have shown how the spilled oil can impact coastal ecosystems (Laffon et al., 2006; Lee et al., 2009; Piatt and Anderson, 1996). Furthermore, these oil spill residues can trap various toxic compounds such as heavy polycyclic aromatic hydrocarbons (PAHs), that are resistant to weathering (Carls et al., 2001; Reddy et al., 2002; Wang et al., 1998b; Wang et al., 1994c; Yin et al., 2015b). The long term environmental impacts of partially weathered crude oil is largely unknown since only a few research efforts have focused on understanding the ecological impacts of weathered oil (Peterson et al., 2003). Therefore, it is important to study and understand the composition of crude oil, how various components of oil behave or weather when released into marine environment, and how

each weathering process affects the oil composition in order to fully assess the impacts of weathered oil on the coastal ecological systems.

1.4 Crude oil chemistry

Crude oils are a complex mixture of thousands of different hydrocarbons and non-hydrocarbons that range from small, volatile to large, non-volatile compounds (Wang and Fingas, 2003; Wang et al., 2006). The compounds in crude oils are classified into five major groups – saturates, olefins, aromatics, resins and asphaltenes (Wang et al., 2006). Saturates are the predominant group of hydrocarbons comprising only carbon and hydrogen with no carbon-carbon double bonds. Olefines or alkenes are characterized with one or multiple carbon-carbon double bonds and are rare in crude oils. Aromatics include both monocyclic and polycyclic aromatic hydrocarbons. Resins are smaller polar compounds and asphaltenes are very large heteroatom containing compounds (Wang et al., 2006). The composition of these five groups various depending on the geological formation of the crude oil (Incardona et al., 2013).

1.5 Fate of Marine Oil Spills

Marine oil spill accidents are harmful to marine environment as well as the human health. It can contaminate the shoreline and impart a long-term damage to the aquatic life and wildlife (Chao et al., 2001). Apart from impacting the natural ecosystem, it is very expensive to clean the oil spill (Bernabeu et al., 2009).

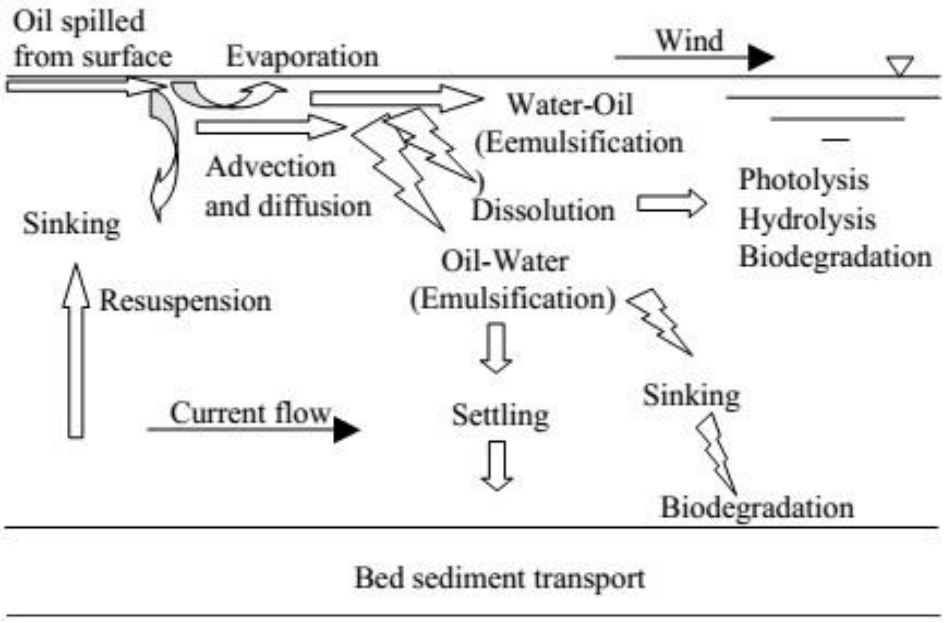

Figure 1.1: Fate of spilled oil in the marine environment (Wang et al., 2005)

In the event of a marine oil spill, the spilled oil weathers through various physical, chemical and biological processes greatly altering its characteristics compared to that of the original source oil. The weathering processes involved are spreading, advection, evaporation, dissolution, emulsification, photo-oxidation, sedimentation and biodegradation (Chao et al., 2001; Garrett et al., 1998; Guo and Wang, 2009; Hamoda et al., 1989; NRC, 2003; Prince et al., 2003).

Spreading aids in the formation of slicks and greatly increasing the surface area of the spilled oil, thus facilitating evaporation, dissolution, possible photo-oxidation and

microbial degradation (Garrett et al., 1998). Evaporation is one of the most important weathering process in many oil spill incidents as this process greatly reduces the spilled volume (Fingas, 1997). Compounds having significant vapor pressure weathers primarily by evaporation (Garrett et al., 1998). Few polycyclic aromatic hydrocarbons and polar compounds dissolves in water and they are eventually degraded by microbial degradation (Garrett et al., 1998; Prince et al., 2003).

Photo-oxidation is another important weathering process for the spilled crude oil in the marine environment as it produces a variety of oxidized products. Photo-oxidized products have high polarity and water solubility and thus contribute to the disappearance of oil slicks (Lee, 2003). Photo-oxidation is the major weathering pathway for higher molecular weight PAHs present in crude oil as many of them absorb light in the ultraviolet or visible wavelengths found in the sunlight (Lee, 2003).

Weathering process also increases the viscosity of the spilled oil and tends to form water-in-oil emulsion known as "chocolate mousse" (Daling and StrØm, 1999; Fingas and Fieldhouse, 2009). Their formation occurs due to various mechanisms and complicate the clean-up efforts as they are hard to recover mechanically, treat or burn. The oil becomes a very less dispersible substance (Daling and StrØm, 1999). It greatly reduces the effectiveness of booms (Hayworth et al., 2011) and dispersants used either to contain or disperse the oil (Lessard and DeMarco, 2000). When W/O emulsions form, it greatly alters the physical properties of oil. For instance, stable W/O emulsion contains 65-80% of water, thus increasing the volume of spill material to be removed by two to five times. Besides the viscosity also increases by a factor of 500, thereby making a liquid product into heavy semi-solid material (Fingas and Fieldhouse, 2003).

1.6 Toxicity of spilled crude oil

Researches has shown that the spilled oil is toxic to both marine and coastal ecosystem (Dubansky et al., 2013; Incardona et al., 2013). The toxicity of crude oil is majorly contributed by specific group of compounds known as polycyclic aromatic hydrocarbons (PAHs) (Incardona et al., 2013). They are class of organic compounds containing two or more fused aromatic rings (Neff, 1979). They are naturally found in organic substances such as crude oil, coal and creosote. They are also formed during incomplete combustion of coal, oil, gas or other organic substances (John et al., 2014). PAHs are known carcinogens and mutagens and due these properties they are classified as hazardous organic compounds (ATSDR, 1995; Liu et al., 2012a; Mumtaz et al., 1996; Urbano et al., 2013). In crude oils, the PAHs are dominated by their alkylated homologues (Wang et al., 2006) and they are more toxic than their parent PAHs (Turcotte et al., 2011). Several PAHs found in crude oil are highly recalcitrant to natural environment and resist weathering. For example, higher molecular weight PAHs were found to be resistant to weathering in an oil spill residue sample of Arrow oil spill which was recovered after 22 years (Wang et al., 1994c). More recently, Yin et al (2015b) studied the *Deepwater Horizon* oil spill residues over a period of four years and reported that the PAHs present in these oil spill residues appear to have very low degradation rates. Furthermore, due to their recalcitrance to natural weathering processes, the relative concentrations of PAHs can increase over time under certain environmental conditions (Wang et al., 1994c). These properties makes PAHs, an excellent group of compounds for chemical characterization and environmental impact assessments (Wang and Fingas, 2003).

1.7 Analytical methods for detecting and quantifying PAHs

The recent advances in analytical methods have led to the development of newer techniques for chemical analysis of various compounds present in crude oil and oil spill residues. Newer techniques include high-performance liquid chromatography (HPLC), gas chromatography (GC), mass spectrometry (MS), infrared spectroscopy (IR), ultraviolet (UV) and fluorescence spectroscopy (FLD), ^{1}H and ^{13}C nuclear magnetic resonance (NMR) and small-angle neutron scattering (SANS) (Fernández-González et al., 2008; Spiecker et al., 2003; Wang et al., 1994a).

Traditionally, PAHs were analyzed using a hyphenated technique such as HPLC/FLD, high resolution capillary GC equipped with flame ionization detector (FID) and capillary GC/MS. More recently, liquid chromatograph coupled to a mass spectrometer (LC/MS) is being used for analysis of PAHs, but this technique is still an upcoming method and still has obstacles for the analysis of PAHs (Song et al., 2011). HPLC/FLD has good sensitivity for PAHs but has a restricted linear range. GC/FID offers ruggedness but has limited selectivity and sensitivity.

Gas chromatograph/mass spectrometer (GC/MS) is the most widely used analytical tool for the analysis of crude oil as it offers better oil separation, characterization and identification (Wang et al., 1994a). It is more suited for analysis of PAHs as it offers simultaneous identification and quantification of a large number of PAHs in complex samples such as environmental samples (Fernández-González et al., 2008).

1.8 Gas Chromatograph/Mass Spectrometer

Gas chromatograph/mass spectrometer (GC/MS) is a technique in which the gas chromatograph (GC) used for separation is directly coupled to a bench top mass

spectrometer (MS) used for detection and identification (McMaster and McMaster, 1998; McNair and Miller, 2009). A gas chromatograph coupled to a single quadrupole mass spectrometer is the most widely used configuration and its schematics is give in Figure 1.2.

GC is a popular, powerful, reasonablly inexpensive and easy to use analytical tool (McMaster and McMaster, 1998). GC works on the principle of a separation method in which the components of a sample partition between two phases, one being stationary

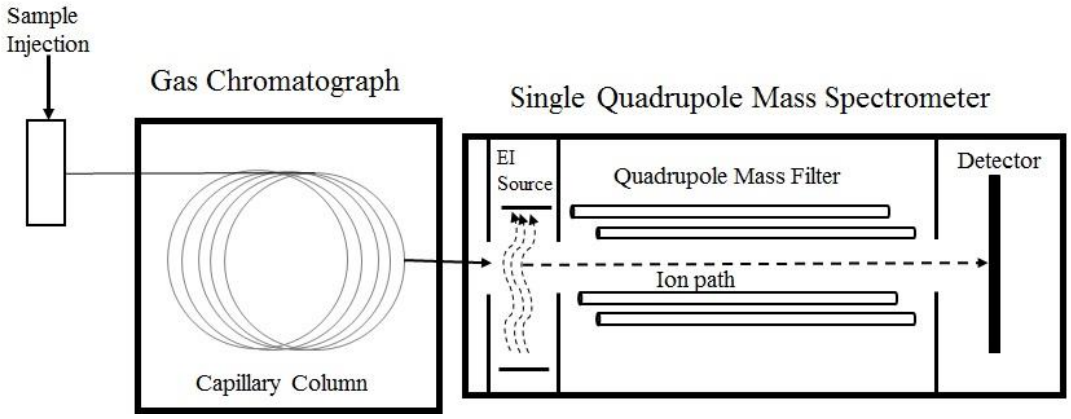

Figure 1.2: A typical GC/MS system

(stationary phase) while the other (mobile phase) moves in a definite direction (McNair and Miller, 2009). Mixtures to be analyzed are injected into the inert gas stream (mobile phase) and swept into a capillary column packed with a solid support (stationary phase). Adsorptive interaction between these phases leads to the differential separation of the components of the mixture, which are then swept in order through a detector flow cell (McMaster and McMaster, 1998).

The mass spectrometer (MS) is an analytical instrument that measures the masses of individual molecules and atoms (Dass, 2001). The MS takes the injected material from the GC, ionizes it in a high vacuum using electron impact (EI) source, propels and focuses

these ions and their fragmentation products through a magnetic mass analyzer (quadrupole), and then collects and measures the amounts of each selected ions in a detector. It is an excellent tool for clearly identifying the structure of a single compound but is less useful when presented with a mixture (McMaster and McMaster, 1998).

This combination of two instruments into one single GC/MS system forms an instrument which is capable of separating mixtures into their individual components, identifying these components and then providing qualitative and quantitative information and chemical structure of each compound (McMaster and McMaster, 1998).

When PAHs are analyzed using GC/MS for identification and quantitation, the GC/MS instrument is operated in electron impact (EI) ionization mode employing selective ion monitoring (SIM) method. This process offers very low detection limits, but requires extensive sample clean-up procedures prior to analysis. Further, the efficiency of detection using SIM method also greatly reduces due to interference ions from the sample matrix (Fernández-González et al., 2008).

1.9 Tandem GC/MS

Recent advances in mass spectrometry have led to the development of tandem GC/MS also known as triple quadrupole mass spectrometer (or GC/MS/MS). The triple

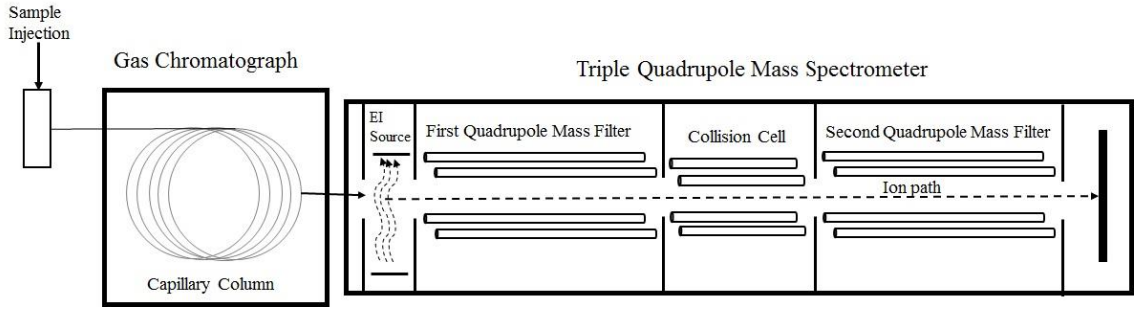

Figure 1.3: A typical GC/MS/MS system

quadrupole mass spectrometer in reality is an instrument made by coupling two mass analyzers (quadrupoles) separated by a collision cell (Hoffmann and Stroobant, 2001; McMaster and McMaster, 1998). The schematics of a GC/MS/MS instrument is given in Figure 1.3.

The working of a triple quadrupole mass spectrometer is described as follows. The mass spectrometer takes the injected material from the GC, ionizes it using electron impact ionization, propels and focuses these ions and their fragmentation products to the first mass analyzer (first quadrupole). The first quadrupole performs mass selection of a specified ion from the mixture of ions and passes on this selected ion to collision cell. The selected ion is called *precursor ion*. The precursor ion collides with inert gas like nitrogen in the collision cell and undergoes further fragmentation. The fragments of precursor ions are called *product ions*. The product ions are then propelled to the second quadrupole which performs mass selections of specified ions and then passes on these selected product ions to the detector (Dass, 2001; McMaster and McMaster, 1998). A unique feature about triple quadrupole mass spectrometer is its molecular specificity, which is offered by the link between the precursor ion and all its product ions (Dass, 2001). This allows greater certainty and minimizes matrix interferences.

1.9.1 Advantages of GC/MS/MS

A very low detection limits can be achieved using GC/MS/MS compared to GC/MS. Abdulkadar et al (2003) analyzed benzo(a)pyrene present in olive oil using both GC/MS and GC/MS/MS methods and reported that limit of detection (LOD) offered by GC/MS is 500 pg/µl, whereas GC/MS/MS offered 5 pg/µl, a 100 times lower LOD. Wong et al (2010) compared the GC/MS and GC/MS/MS analytical methods for monitoring

pesticides in ginseng powder and reported that LOD for GC/MS was 48 – 53 µg/kg and for GC/MS/MS, LOD is 6 – 7 µg/kg. Goncales et al (2006) analyzed various soil samples for pesticides and observed a 4-10 times lower LOD using GC/MS/MS compared to that of GC/MS. GC/MS and GC/MS/MS LOD values for PAHs, pesticides and polychlorinated biphenyl residues in soil/sediments samples were compared; GC/MS LOD ranged between 0.01 and 0.5 ng/g, whereas for GC/MS/MS LOD ranged between 0.001 to 0.019 ng/g (Camino-Sánchez et al., 2011). GC/MS/MS even offers lower LOD compared to LC/MS/MS for some PAHs like benzo(a)pyrene (Johnson, 2012).

GC/MS/MS offers excellent selectivity and sensitivity. Pitarch et al. (2007) quantified various semi-volatile organic compounds in water samples and concluded that GC/MS/MS methods can lead to excellent selectivity and sensitivity. Varlet et al (2007) analyzed several PAHs in smoked salmon and reported a five-fold increase in sensitivity for PAHs in GC/MS/MS compared to that of GC/MS. This allows for simple sample preparation and clean-up procedures (Haib et al., 2003).

GC/MS/MS allows for monitoring a large number of target compounds simultaneously. Vidal et al (2002) demonstrated the viability of monitoring 31 pesticide residues simultaneously using GC/MS/MS in fruits and vegetables. In 5 years period, Walorczyk (2007) successfully developed a GC/MS/MS method for simultaneously monitoring 122 gas chromatography amenable pesticide residues in complex matrices such as cereal grains. Given the advantages and versatility of the GC/MS/MS, it could be best utilized for analyzing various compounds present in complex matrices such as oil spill residues.

1.10 Deepwater Horizon Accident

On April 20, 2010, *Deepwater Horizon*, a semi-submersible oil exploration drilling rig while exploring for oil in northern Gulf of Mexico in Macondo Prospect 252 well (MC252), experienced catastrophic well blow-out and exploded. The resulting accident released about 4.8 million barrels of oil into the waters of Gulf of Mexico over a period of 87 days. Oil related to the accident impacted the coasts of Florida, Alabama, Mississippi, Louisiana and Texas. The released oil experienced various ocean weathering processes such as evaporation, dissolution, emulsification, photo-oxidation and microbial degradation. The weathered oil started arriving on the beaches of Alabama from early June 2010 onwards. The weathered oil that arrived was predominantly in the form of water-in-oil emulsions known as mousse. A portion of this mousse interacted with the near-shore sediments and settled to the bottom of seafloor forming submerged oil mats (SOMs) and surface residual balls (SRBs). The SOMs and SRBs continue to impact the beaches of Alabama. The fate of these oil spill residues are largely unknown.

1.11 Scope and objective of this dissertation

The persistence of remnant oil in the coastal environment after a major oil spill is a common worldwide environmental problem. The objective of this dissertation is to conduct field studies to monitor the oil spill residues deposition patterns in beaches located along the Alabama shoreline and analyze those oil spill residues using novel GC/MS/MS methods. This dissertation is organized into five chapters with each chapter focusing on specific set of objectives and tasks and they are briefly discussed below.

The objective of this first introduction chapter is to provide a general overview of oil spills, discuss about the chemicals present in crude oils and review the analytical methods used for analyzing these chemicals.

The objective of the second chapter is to summarize a field study that focused on monitoring oil spill residues deposition patterns for over four years along Alabama's beaches located in between Orange Beach and the Fort Morgan.

The objective of third chapter is to investigate the effects of sunlight on transforming various alkylated PAHs trapped in DWH oil spill residues. Some of the recent studies published in the current literature indicate that the DWH oil weathered rather rapidly when it was floating over the ocean. The weathering rates appears to have slowed down considerably once the oil sank in the nearshore environment. Based on these observation we hypothesized that sunlight must have played a substantial role in weathering the oil spill when it was floating offshore. The objective of this effort is to test this working research hypothesis.

The objective of fourth chapter is to develop a novel GC/MS/MS method for detecting and quantifying an important group of PAHs – chrysene and its alkylated homologues (C_0- to C_4-chrysenes). Our preliminary studies have shown that C_0- to C_4-chrysenes are one of the most recalcitrant compounds trapped in DWH oil spill residues collected from Alabama's beaches. Therefore, we focused on developing a more robust and efficient GC/MS/MS method for analyzing C_0- to C_4-chrysenes.

The objective of fifth chapter is to better understand some of the physical weathering processes, particularly the emulsification process that occurred offshore. The

goal is to modify some of the currently available dispersants and study their effectiveness in dispersing water-in-oil emulsions that were formed by offshore mixing processes. The aim is to identify some chemical additives that can modify commercially available dispersants to destabilize and disperse water-in-oil crude oil emulsions.

The final chapter provides a summary of the key finding of this dissertation and also points out some possible future research directions.

Chapter 2

Assessment of DWH accident related SRBs deposition along Alabama's beaches

2.1 Introduction

On April 20, 2010, the *Deepwater Horizon* (DWH) drilling platform exploring for oil on the Macondo Prospect (MC252) in the Gulf of Mexico (GOM) exploded, resulting in the release of a U.S. Government-estimated 780 million liters of crude oil into the GOM over a period of 87 days (McNutt et al., 2012; Team, 2010). From early June 2010 to August 2010, a considerable amount of oil washed onto northern GOM sandy beaches in Florida, Alabama, Mississippi, and Louisiana (Hayworth et al., 2011; Hayworth and Clement, 2011b; Michel et al., 2013b; OSAT-3, 2013). Figure. 2.1 is a generalized cross-section of a typical northern GOM beach, defining the system and also illustrating areas of beach potentially impacted from MC252 oil. Oil impacting these beaches was predominantly in the form of water-in-oil (W/O) emulsions, a highly viscous, neutrally buoyant material also known as mousse. Earlier studies have shown that MC252 W/O emulsions were weathered during transit from the MC252 wellhead to the northern GOM coastline, principally by volatilization of low molecular weight compounds and other physio-chemical processes (Liu et al., 2012a; Yin et al., 2015b). Once formed, W/O emulsions are extremely difficult to destabilize, even when treated with dispersants (Hayworth and Prabakhar Clement, 2012). In the vicinity of the shoreline, an unknown amount of emulsified oil interacted with suspended solids and sank to the sandy bottom

surface, forming immobile deposits of submerged oil mats (SOMs), and mobile surface residual balls (SRBs). Earlier studies have shown that MC252 SOMs and SRBs are predominantly composed of sand (75–95% by mass) (Hayworth et al., 2011; OSAT-1, 2010; OSAT-2, 2011), and that the formation of the majority of SOMs and SRBs found along Alabama's beaches occurred in the surf zone along sandy beaches, rather than in the deeper areas of the continental shelf. An unknown amount of emulsified oil also became stranded on backshore areas of the beach as a result of storm events during the initial period of oiling (June–August, 2010). Over time, SOMs and SRBs have been discontinuously buried, exposed, broken apart, and mechanically eroded as a result of natural coastal dynamics (Dalyander et al., 2014; OSAT-3, 2013), and there is an indirect evidence that fragmenting SOMs continue to provide new SRBs into Alabama's beach system, joining existing SRBs which continue to be reworked over time (Dalyander et al., 2014; Hayworth et al., 2011; Michel et al., 2013b; OSAT-3, 2013).

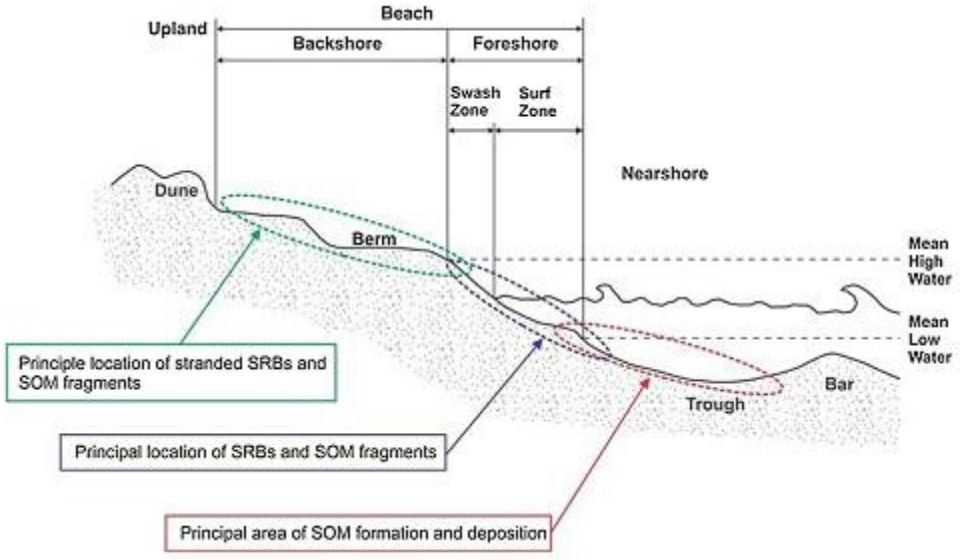

Figure 2.1: Generalized cross-section of northern GOM beach and areas impacted by MC252 oil ((USCOE), 2002)

The Unified Command (UC), a group comprised of federal, state, and private entities (including the responsible party, British Petroleum (BP)), was tasked by law to coordinate most aspects of the response to the DWH accident (website, 2014). In the months following the first arrival of oil on Alabama's shoreline, the UC has directed and guided many cleanup activities designed to remove various forms of oil debris from GOM beaches and nearshore waters. These activities included extensive assessment of shoreline oiling by the UC-managed Shoreline Cleanup Assessment Technique (SCAT) program (Michel et al., 2013b), excavation of large backshore areas of the beaches to remove buried oil, removal of submerged SOMs from discrete foreshore locations, and deployment of cleanup crews to walk the beaches and collect SRBs in the backshore and foreshore by hand (Hayworth and Clement, 2011b; Michel et al., 2013b; OSAT-3, 2013).

In November, 2011, the UC published a document entitled Shoreline Cleanup Completion Plan ((SCCP), 2011), defining the process to be used in Florida, Alabama, Mississippi, and Louisiana to ''deem that removal actions are complete for all segments that were never impacted by MC252 oil, where end-points have been met, or where the Federal On-Scene Coordinator (FOSC) determines current conditions are no longer a threat to the environment, or where further removal actions may cause more harm than good.'' For Alabama's residential and amenity beaches, shoreline cleanup endpoints are defined as ''no visible MC252 oil, or as low as reasonably practicable, considering the allowed treatment methods and net environmental benefit.'' Based on their interpretation of beach conditions in Alabama, the UC announced the end of active, routine shoreline cleanup efforts in Alabama on June 7, 2013 (BP, 2014).

Since the DWH accident in April 2010, our research team has closely monitored Alabama's primary beaches from the Alabama–Florida border to Mobile Bay (Figure. 2.2). Our interests have mainly been to observe and document the physical and chemical evolution of MC252 oil in Alabama's sandy beach system. This chapter has included many sampling events along Alabama's beaches and nearshore waters (from May 2010 to August 2014). We have also discussed the concentration levels of some PAHs which were quantified by using a GC/MS/MS based MRM method. Note parts of this chapter were recently published in a Marine Pollution Bulletin journal article, which was co-authored by this author (Hayworth et al., 2015).

2.2 Background

The principle sandy beach region of Alabama's Gulf coast, which constitutes our study area, is approximately 50 km (31 miles) in length, extending from the Florida–Alabama border in the east to the eastern side of the entrance to Mobile Bay (Figure 2.2). Also shown in Figure. 2 are sampling locations (GPS coordinates are given in Table 1) referenced later in this paper. This stretch of shoreline is bounded in the east by Perdido Bay, a relatively small and shallow estuary (approximately 73 km^2; 2 m average depth) contained within the Perdido Bay watershed; and in the west by Mobile Bay, a large but also relatively shallow estuary (1070 km^2, 3 m average depth) within the Mobile Bay watershed. Along this shoreline are the coastal communities of Orange Beach, Gulf Shores, and Fort Morgan. Also, two Alabama state parks (Gulf, and Fort Morgan State Parks) and a federal wildlife refuge (Bon Secour National Wildlife Refuge (NWR)) are located along this shoreline (Figure. 2). Tidal motion is diurnal along Alabama beaches, with a normal tidal range of approximately 30–60 cm. Along this low-to-medium energy

coastline, average wave heights are approximately 30 cm, with maximum heights of approximately 1.5 m (excluding storm events).

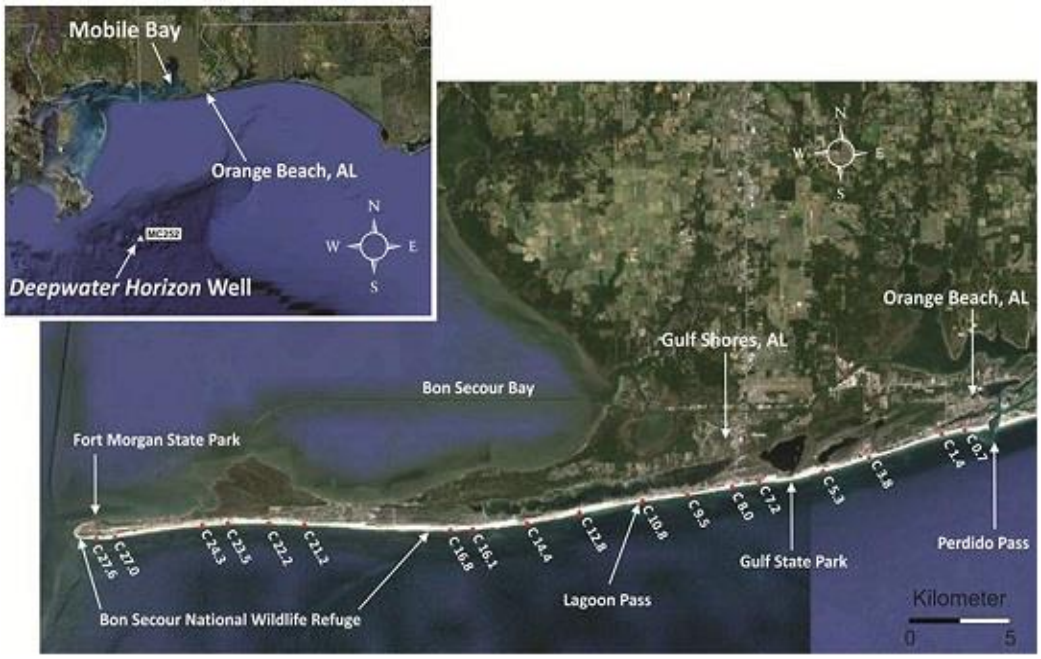

Figure 2.2: Location map of Alabama's 50 km of primary northern GOM beaches, showing important beach locations and sampling locations

2.3 Field survey methods

Figure. 2.3 presents a timeline of important events related to Alabama's beaches in the wake of the DWH disaster, along with the sampling events completed by our research team. The period of time before the first arrival of oil on Alabama's beaches (prior to June 4, 2010) is referred to in this paper as the pre-arrival period; the period of time during UC active cleanup on Alabama's beaches (June 4, 2010–June 7, 2013) is referred to as the cleanup period; and the period of time following cessation of active beach cleanup (from June 8, 2013 forward) is referred to as the post-cleanup period. Our research team has completed 20 field surveys along Alabama's beaches between May, 2010 and August,

2014; Table 2-2 provides further information about these surveys. This includes 1 survey during the pre-arrival period, 15 surveys during the cleanup period, and 4 surveys during the post-cleanup period. Two types of surveys were completed: (1) observation with random sampling (11 surveys), and (2) observation with detailed sampling (8 surveys). Observation with random sampling surveys included visual observation of beach conditions and oil cleanup activities at various locations along the 50 km study area, and collection of random samples of SOM fragments and SRBs found in the backshore and foreshore areas of the beach. Observation with detailed sampling surveys included all observational components, along with the sampling of SRB/SOM fragments at several beach locations. Our sampling efforts employed a 2- or 3-member team, collecting all SRB/SOM fragments in the foreshore region above the swash zone, over a fixed time period of approximately 30 min surveying about 1 km on either side of the sampling access point. All samples collected during the surveys were preserved on ice and transported to our laboratory for archiving and chemical analysis. Additionally, GPS coordinates of all sampling locations were recorded, and photographs of important field observations were obtained. Event-specific survey information is summarized in Table 2-2.

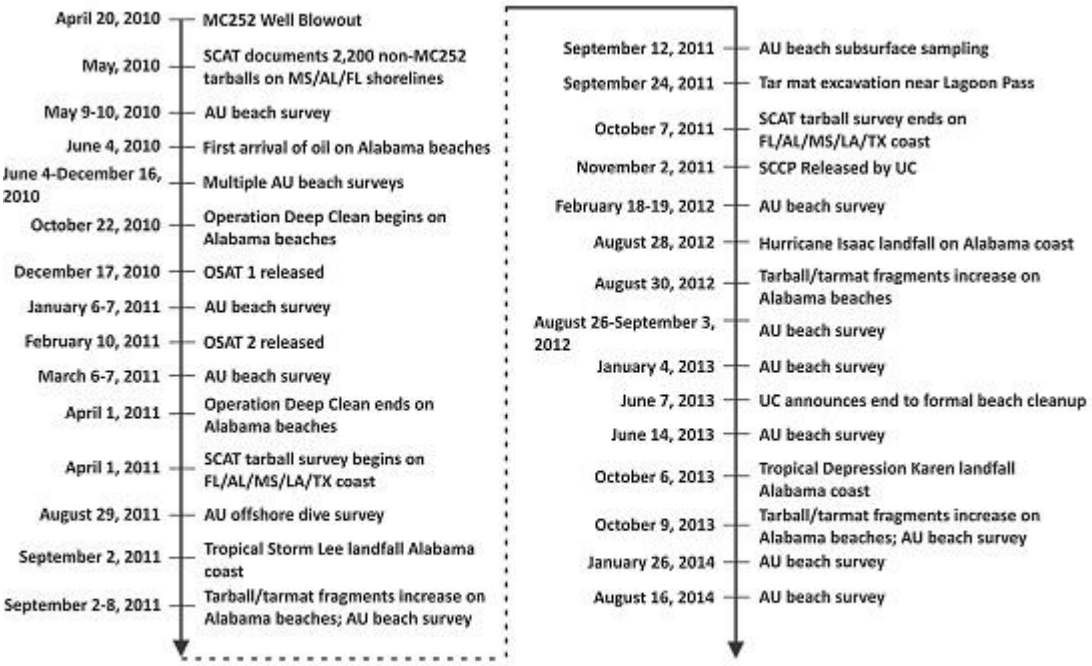

AU: Auburn University research team; SCAT: shoreline cleanup assessment techniques; MC252: Macondo Prospect, Mississippi Canyon Block 252; OSAT: Operational Science Advisory Team; SCCP: Shoreline Cleanup Completion Plan; UC: Unified Command

Figure 2.3: Timeline of important events related to Alabama's beaches following the DWH disaster, along with sampling events of our research team

Table 2-1: Sampling locations on Alabama's principal GOM beaches

Location	Latitude/N	Longitude/W
C0.7	30°16'14.88"	87°34'16.32"
C1.4	30°16'7.32"	87°34'57.00"
C3.8	30°15'31.92"	87°37'12.67"
C5.3	30°15'11.58"	87°38'38.27"
C7.2	30°14'54.76"	87°40'35.26"
C8.0	30°14'47.60"	87°41'24.61"
C9.5	30°14'35.48"	87°42'48.02"
C10.8	30°14'25.85"	87°44'11.01"
C12.8	30°14'7.62"	87°46'6.59"
C14.4	30°13'51.72"	87°47'42.40"
C16.1	30°13'42.48"	87°49'23.34"
C16.8	30°13'41.46"	87°50'5.28"
C21.2	30°13'49.86"	87°54'33.84"
C22.2	30°13'52.32"	87°55'39.47"
C23.5	30°13'52.08"	87°56'54.78"
C24.3	30°13'48.72"	87°57'41.94"
C27.0	30°13'29.94"	88°0'21.84"
C27.6	30°13'27.90"	88°0'57.96"

2.4 Field survey results

2.4.1 Pre-arrival period

A pre-arrival period observational survey of Alabama's beaches was completed on May 9–10, 2010. This survey was performed after the MC252 blowout (April 20, 2010), but prior to first arrival of oil on Alabama's beaches (around June 4, 2010). The 50 km length of our study area was surveyed by accessing the beaches at selected locations within Orange Beach, Gulf Shores State Park, Bon Secour National Wildlife Refuge, and Fort Morgan State Park (Figure. 2), and walking approximately 0.5 km in both directions around the access points. The purpose of this observational survey was to establish background conditions of the beaches, primarily with respect to existing pre-MC252 oil contamination. Other studies have indicated that tar balls can be found on northern GOM beaches as a

result of oil discharges from existing wells and pipelines, natural seeps, and oil-bearing vessels in the GOM ((SCCP), 2011). These tar balls, however, are typically highly weathered, predominantly asphaltenic, hard, black material, with little or no odor. We observed no tar balls of any kind along Alabama's beaches during our pre-arrival survey.

2.4.2 Cleanup period

2.4.2.1 Observation with random sampling surveys, June–December, 2010

Seven observation with random sampling surveys were conducted after oil first arrived on Alabama's beaches (around June 4, 2010) and prior to the beginning of BP's Operation Deep Clean on Alabama's beaches (January 1–April 1, 2011), which was designed to remove oil from the backshore surface and subsurface (Table 2-2). Some of these surveys are discussed in Hayworth et al., 2011 (Hayworth et al., 2011), in the context of comparisons with results from two of the UC's Operational Science Advisory Team reports (OSAT-1, 2010; OSAT-2, 2011). During this time period the presence of MC252 oil on Alabama's beaches was widespread, and many beach areas were inundated with MC252 oil. As noted earlier, pre-arrival surveys demonstrated the absence of non-MC252 oil on Alabama's beaches; therefore, the possibility that any oil found on these beaches after June 4, 2010 may have had a source other than from MC252 is highly unlikely. SOM fragments are usually differentiated from SRBs principally by their physical characteristics: as shown in Figure. 2.4, SOM fragments typically have rough edges whereas SRBs are oval-shaped, with no rough edges. Although cleanup crews continuously worked to remove oil from backshore and foreshore beach areas, during this

period we observed continuous deposition of SOM fragments, especially after weather events that resulted in higher than average surf conditions.

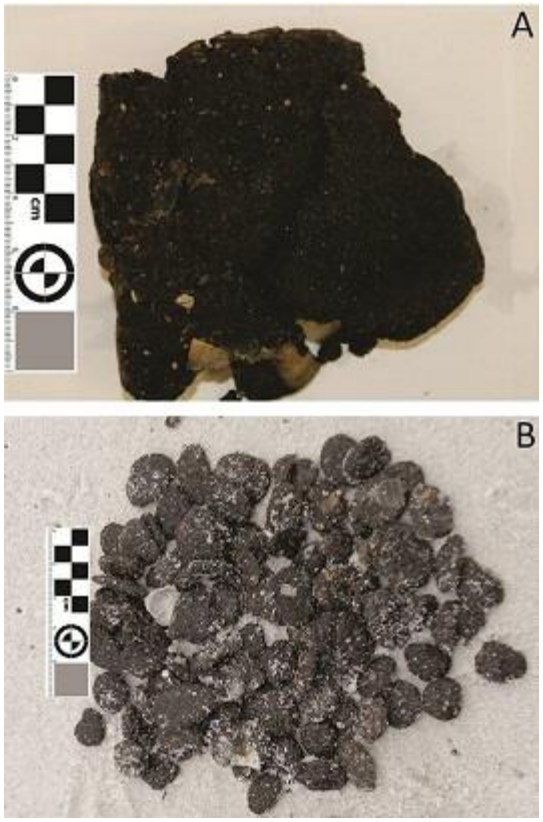

Figure 2.4: Example photographs showing physical differences between (A) SOM fragment; and (B) SRBs found on Alabama's beaches

2.4.2.2 Observation with random sampling surveys, January–March, 2011

Two observation with random sampling surveys were conducted in January and March, 2011, principally to assess the effectiveness of BP's Operation Deep Clean along Alabama's beaches (Table 2-2). The primary objective of Operation Deep Clean was to locate and remove oil buried in backshore areas of Alabama's amenity beaches. Beaches within Gulf and Fort Morgan State Parks, and Bon Secour National Wildlife Refuge were not subject to this method of oil removal. The general approach was to use a small auger drill to complete shallow borings to identify potential cleanup sites. The main approach

used for deep cleaning involved excavation of sand from an identified cleanup area (approximately 100–1000 m^2) to a depth of approximately 2–4 m, sifting the sand through a large mechanical sieve, and replacement of sieved, ‘‘clean’’ sand. Our observations indicated the sifting process was effective at removing solid constituents (like shells, sticks, and other large materials), and some buried oil debris. Further details of BP’s deep-clean operations and its implications are summarized in Hayworth and Clement et al (2011).

Table 2-2: Survey information

Survey	Date	Period	Type
1	May 9 – 10, 2010	P	O
2	June 4 – 10, 2010	C	O/RS
3	July 14 – 16, 2010	C	O/RS
4	August 15 – 18, 2010	C	O/RS
5	September 12 – 13, 2010	C	O/RS
6	October 12 – 14, 2010	C	O/RS
7	November 10 – 13, 2010	C	O/RS
8	December 15 – 16, 2010	C	O/RS
9	January 6 – 7, 2011	C	O/RS
10	March 6 – 7, 2011	C	O/RS
11	September 2 – 8, 2011	C	O/RS
12	September 12, 2011	C	O/RS
13	September 24, 2011	C	O/DS
14	February 18 – 19, 2012	C	O/DS
15	August 26 – September 3, 2012	C	O/DS
16	January 4, 2013	C	O/DS
17	June 14, 2013	PC	O/DS
18	October 9, 2013	PC	O/DS
19	January 26, 2014	PC	O/DS
20	August 16, 2014	PC	O/DS

P: pre-arrival; C: cleanup; PC: post-cleanup; O: observational; RS: random sampling; DS: detailed sampling

2.4.2.3 Observation with random sampling surveys, September 2–24, 2011

The first effects of Tropical Storm Lee (which degraded to a tropical depression just prior to landfall) began along the Alabama coast on September 2, 2011 and the effects lingered for over two days. Our research team was present on Alabama’s beaches before,

during, and after this storm event (Table 2-2). The storm center made landfall in coastal Louisiana, with more powerful winds and storm surge affecting coastal areas to the east. The Alabama coastline experienced sustained winds between 21 and 23 m/s (48– 51 mph) between September 3, 2011 and September 5, 2011, with wind gusts between 24 and 26 m/s (54–59 mph). Strong onshore winds from the storm along the northern GOM coast produced elevated water levels from Louisiana eastward into the Florida Panhandle for several days. Storm tides of 1–2 m (3–5 ft) were reported in Alabama, and values of 0.6–1 m (2–3 ft) were observed in portions of the Florida Panhandle. The highest storm surge in Alabama was 1.3 m (4.4 ft), measured at the National Ocean Service tide gauge at the Coast Guard Sector-Mobile station, near the north end of Mobile Bay (Brown, 2011). During the active, high-energy phase of the storm, the beaches within the study area were remarkably free of SRBs and SOM fragments, although substantial perturbation to shoreline morphology and mobilization of sand along the shoreline occurred. However, during the relaxation phase of the storm (September 7, 2011–September 8, 2011), a substantial increase in the amount of SRBs and SOM fragments appearing on the backshore and foreshore portions of the beaches was observed. This behavior has also been noted by others (Dalyander et al., 2014). Our research team collected a number of SRBs (1–4 cm (longest length)) and large SOM fragments (tens of cm longest length) from several sites along the coastline, and transported them to our laboratory for archiving and analysis. During this survey, an area with an elevated number of SOM fragments and SRBs (relative to other beach locations) was found near Lagoon Pass in Gulf Shores, Alabama (Figure. 2.2). This suggested the possible presence of SOMs in the foreshore portion of this beach location, which was confirmed during a follow-up excavation on September 24, 2011 by

BP, National Oceanic and Atmospheric Administration (NOAA), Alabama Department of Environmental Management (ADEM), and our research team. A long-arm excavator was used to remove a top layer of sand approximately 1–2 m thick prior to locating an SOM approximately 25 m from the shoreline. Samples of SOM material were collected and split between our research team and the teams from BP, NOAA, and ADEM. These samples were transported to the respective analytical facilities for comparative chemical analysis.

2.4.2.4 Observation with detailed sampling survey, February 18–19, 2012

In mid-February 2012, a major cold front moved across the region, bringing high winds with gusts between 9–13 m/s (20–30 mph), and moderate to high surf conditions (0.6–1.2 m; 2–4 ft). The effects of these conditions along Alabama's beaches were similar to those observed during and following Tropical Storm Lee. During the relaxation phase of the storm (February 18–19, 2012), elevated SOM fragments and SRBs were observed at many locations along the Alabama shoreline. We performed a detailed survey of SOM fragments and SRBs at 18 sampling locations (Figure. 2.2; Tables 2.1 and 2.2). At each location, a 3-member team manually collected as many SOM fragments and SRBs in excess of 1 cm (longest length) as possible by surveying about 0.5 km on either side of the access point. The size of collected SOM fragments and SRBs ranged from 1 to 4 cm (longest length). The entire survey took about ten hours. SRB/SOM fragment distribution (number and weight), collected during the survey is given in Table 2-3 and the relative spatial variation in SRB activity are shown in Figure. 2.5. All samples were transported to our laboratory for archiving and chemical analysis.

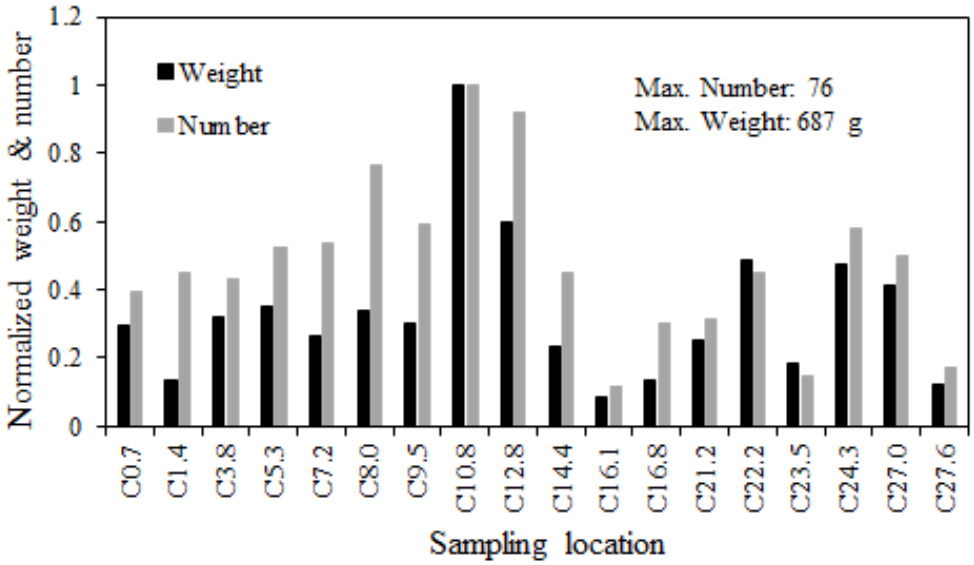

Figure 2.5: Results from sampling event on February 18 – 19, 2012, showing number and weight of SRBs and SOM fragments collected at sampling locations shown in Figure 2.2. Sampling at each location approximately 30 min duration. Normalized by maximum number and maximum weight collected at location C10.8 (in vicinity of Lagoon Pass, Alabama)

2.4.2.5 Observation with detailed sampling survey, August 26–September 2, 2012

Tropical Storm Isaac entered the GOM on August 27, 2012, gradually strengthened while moving north, and became a hurricane on August 28, 2012, while centered about 140 km southeast of the mouth of the Mississippi River. The hurricane slowed while approaching the coast of Louisiana, making landfall at the mouth of the Mississippi River on August 29, 2012 (Berg, 2012). The Alabama coastline experienced sustained winds of approximately 23 m/s (52 mph) on August 28, 2012, with wind gusts up to 28 m/s (62 mph). Strong onshore winds from the storm along the northern GOM coast produced elevated water levels from Louisiana eastward into the Florida Panhandle for several days. Storm tides of 1–2 m (3–5 ft) were reported in Alabama; the highest storm surge was 1.4

m (4.5 ft), measured at the National Ocean Service tide gauge at the Coast Guard Sector-Mobile station, near the north end of Mobile Bay (Berg, 2012). Conditions observed on Alabama's beaches during our survey were similar to those observed during Tropical Storm Lee. During the active, high-energy phase of the storm, the beaches within the study area appeared free of SRBs and SOM fragments, although substantial perturbation to shoreline morphology and mobilization of sand along the shoreline occurred. However, during the relaxation phase of the storm (August 30, 2012–September 2, 2012), a considerable amount of SOM fragments and SRBs appeared on the backshore and foreshore portions of the beaches.

On September 2–3, 2012, we completed a detailed survey of Alabama's beaches following an approach similar to that used during the February 18–19, 2012 survey (Table 2-2). Impact to the beaches from Hurricane Isaac was extensive, and a large amount of SRB/SOM fragments were deposited on the beaches during the relaxation phase of the storm. At each sampling location, we only collected SRB/SOM fragments well above 1 to 2 cm (longest length), in the foreshore area above the swash zone, over a fixed time of approximately 30 min. The size of the SRB/SOM fragments collected primarily ranged from 2 to 7 cm (longest length). The amount of SRB/SOM fragments (by weight) collected during this survey at each sampling location is given in Table 2-3, and the spatial variation in SRB activity are shown in Figure. 2.6. Approximately 11 kg (25 lbs) of SRB/SOM fragments were collected, with the majority recovered near Lagoon Pass (approximately 2.7 kg (6 lbs)).

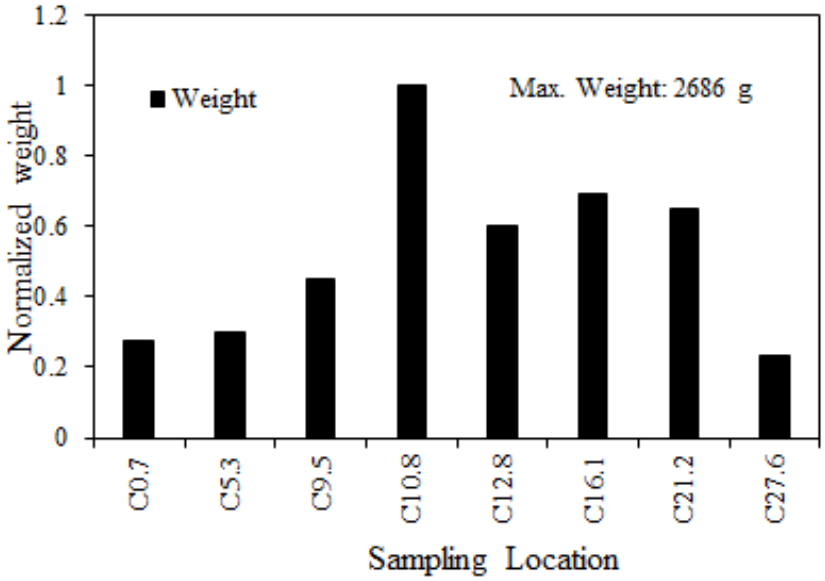

Figure 2.6: Results from sampling event on September 2–3, 2012, following Hurricane Isaac, showing weight of SRBs and SOM fragments collected at sampling locations shown in Fig. 2.2. Sampling at each location approximately 30 min duration. Only SRBs and SOM fragments exceeding about 2 cm (longest length) were collected. Normalized by maximum weight collected at location C10.8 (in vicinity of Lagoon Pass, Alabama)

2.4.3 Additional beach surveys

One additional detailed sampling survey was conducted during the cleanup period (January 4, 2013), and 4 additional detailed sampling surveys were completed during the post-cleanup period (June 14, 2013; October 9, 2013; January 26, 2014; and August 16, 2014). Sampling results are given in Table 2-3, and SRB activities recorded at various locations are shown in Figures. 2.7 – 2.11. These surveys produced results similar to those described above; some noteworthy observations are presented below.

2.4.3.1 January 4, 2013 observation and detailed sampling survey

Five sampling locations were considered in this survey, and sampling protocol was similar to that previously noted: SRB/SOM samples were collected by surveying the foreshore region above the swash zone on either side of the access point for a fixed time period of approximately 30 min. Weather and surf conditions during this sampling event were calm. SRB/SOM fragments ranged in size from 1 to 4 cm (longest length) and the results are summarized in Figure. 2.7.

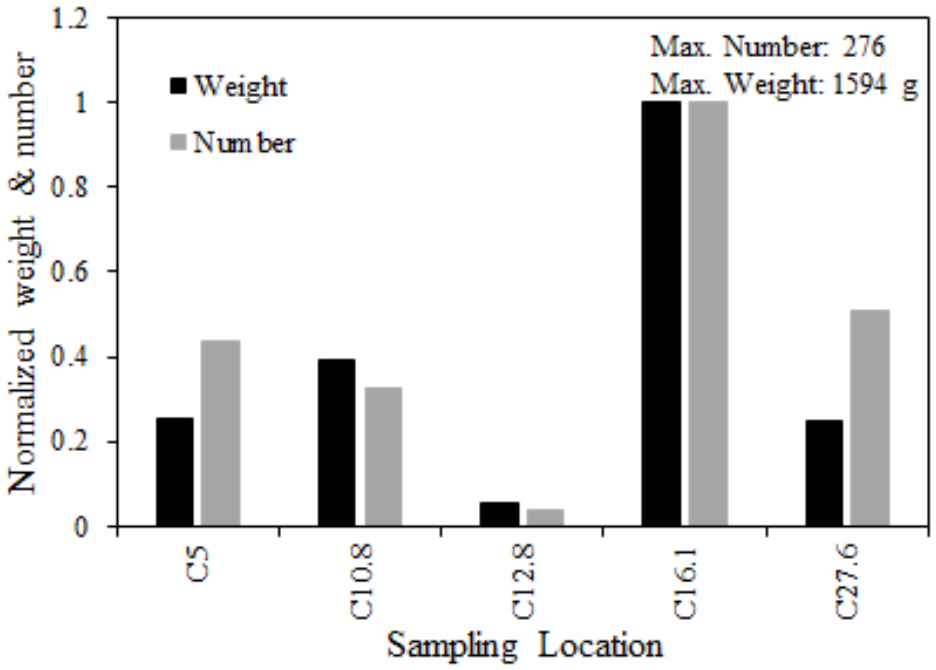

Figure 2.7: Results from sampling event on January 4, 2013, showing weight of SRBs and SOM fragments collected at sampling locations shown in Fig. 2.2. Sampling at each location approximately 30 min duration. Normalized by maximum number and weight collected at location C16.1 (Bon Secour National Wildlife Refuge, Alabama).

2.4.3.2 June 14, 2013 observation and detailed sampling survey

This was the first survey conducted after UC terminated active cleanup on Alabama's beaches on June 7, 2013. Because of time constraints, only two sampling locations were considered. Sampling protocol was similar to that noted above for January 4, 2013 survey. Weather and surf conditions during this sampling event were calm. SRB/SOM fragments ranged in size from 1 to 4 cm (longest length) and the results are summarized in Figure. 2.8.

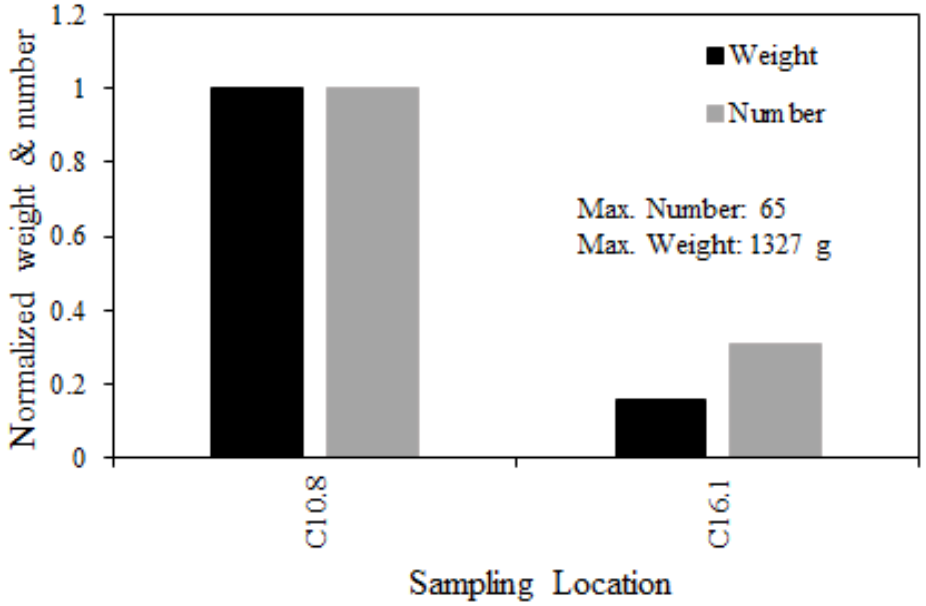

Figure 2.8: Results from sampling event on June 14, 2013, following end of active beach cleanup, showing weight of SRBs and SOM fragments collected at sampling locations shown in Fig. 2.2. Sampling at each location approximately 30 min duration. Normalized by maximum number and weight collected at location C10.8 (in vicinity of Lagoon Pass, Alabama).

2.4.3.3 October 9, 2013 observation and detailed sampling survey

This survey was conducted during the relaxation phase of Tropical Storm Karen, which degenerated into a tropical depression approximately 140 km from the Alabama coast on October 6, 2013. Top sustained winds along Alabama's coast were approximately 13 m/s (30 mph) on October 7, 2013, while storm tides were approximately 0.3–0.6 m (1–

2 ft). The same 5 sampling locations considered during the January 4, 2013 survey were sampled during this survey, with similar sampling protocols. Sampling took place during the relaxation phase of the storm. SRB/SOM fragments ranged in size from 1 to 7 cm (longest length) and the results are summarized in Figure. 2.9.

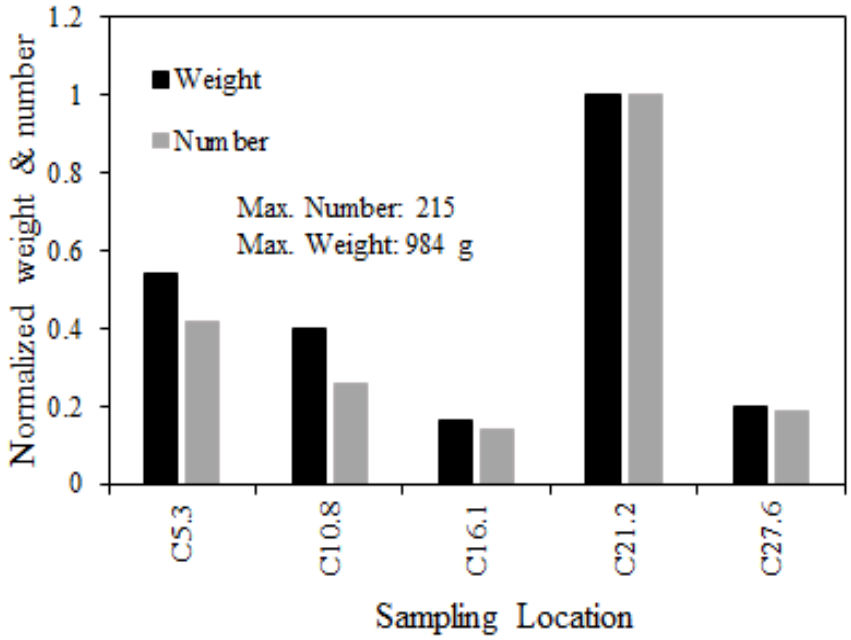

Figure 2.9: Results from sampling event on October 9, 2013, following relaxation phase of Tropical Storm Karen, showing weight of SRBs and SOM fragments collected at sampling locations shown in Fig. 2.2. Sampling at each location approximately 30 min duration. Normalized by maximum number and weight collected at location C21.2 (in vicinity of Fort Morgan, Alabama).

2.4.3.4 January 26 and August 16, 2014 observation and detailed sampling surveys

For both surveys, four sampling locations were considered, and sampling protocol was similar to that noted above for January 4, 2013 survey. Weather and surf conditions during both sampling events were calm. SRB/SOM fragments ranged in size from 1 to 4 cm (longest length) and the results are summarized in Figures. 2.10 and 2.11.

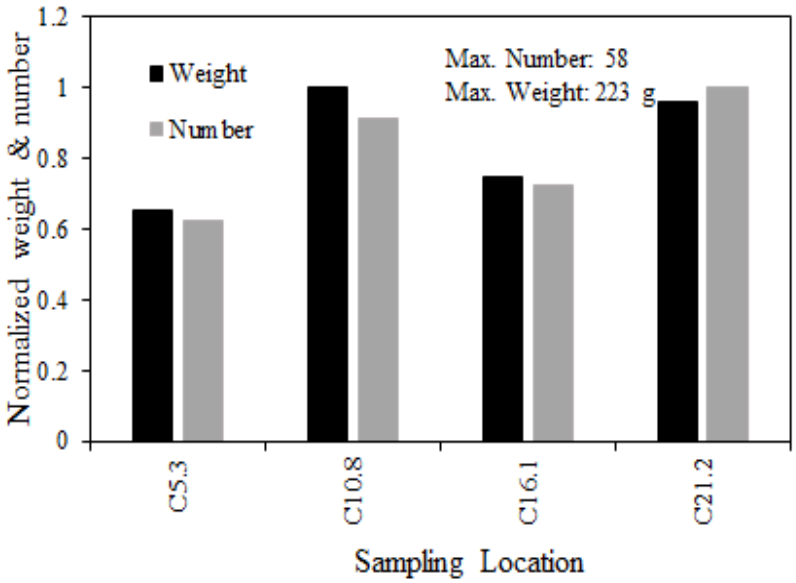

Figure 2.10: Results from sampling event on January 26, 2014, showing weight of SRBs and SOM fragments collected at sampling locations shown in Fig. 2.2. Sampling at each location approximately 30 min duration. Normalized by maximum number (collected at location C10.8, in vicinity of Lagoon Pass, Alabama), and maximum weight (collected at location 21.2, in vicinity of Fort Morgan, Alabama).

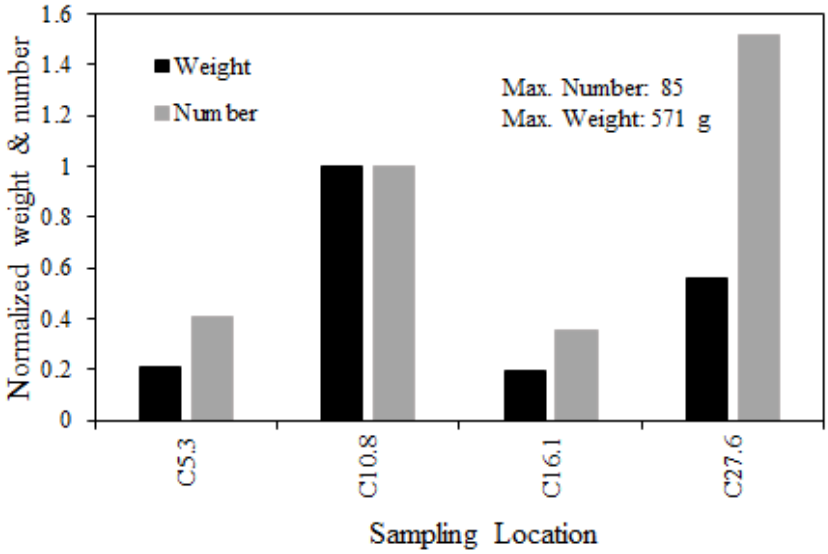

Figure 2.11: Results from sampling event on August 16, 2014, showing weight of SRBs and SOM fragments collected at sampling locations shown in Fig. 2.2. Sampling at each location approximately 30 min duration. Normalized by maximum number (collected at location C21.2, in vicinity of Fort Morgan, Alabama), and maximum weight (collected at location 10.8, in vicinity of Lagoon Pass, Alabama).

Table 2-3: Summary of detailed sampling survey results

Date	Location	Weight (g)	Number	N/W ratio
February 18 – 19, 2012	C0.7	201	30	0.1493
	C1.4	93.4	34	0.3640
	C3.8	219	33	0.1507
	C5.3	241.7	40	0.1655
	C7.2	183.1	41	0.2239
	C8.0	232.2	58	0.2498
	C9.5	205.6	45	0.2189
	C10.8	686.7	76	0.1107
	C12.8	410.1	70	0.1707
	C14.4	159	34	0.2138
	C16.1	60	9	0.1500
	C16.8	92	23	0.2500
	C21.2	174	24	0.1379
	C22.2	335	34	0.1015
	C23.5	126	11	0.0873
	C24.3	328	44	0.1341
	C27.0	283	38	0.1343
	C27.6	86	13	0.1512
September 2 – 3, 2012	C0.7	745		
	C5.3	799		
	C9.5	1209		
	C10.8	2686		
	C12.8	1618		
	C16.1	1853		
	C21.2	1753		
	C27.6	628		
January 4, 2013	C5.3	405.2	120	0.2962
	C10.8	625	90	0.1440
	C12.8	88.1	11	0.1249
	C16.1	1594.1	276	0.1731
	C27.6	391.4	140	0.3577
June 14, 2013	C10.8	1326.5	65	0.0490
	C16.1	211.1	20	0.0947
October 9, 2013	C5.3	534.2	90	0.1685
	C10.8	392	55	0.1403
	C16.1	162.7	30	0.1844
	C21.2	984	215	0.2185
	C27.6	196.8	40	0.2033
January 26, 2014	C5.3	117.8	23	0.1952
	C10.8	570.6	56	0.0981
	C16.1	108.9	20	0.1837
	C27.6	320.8	85	0.2650
August 16, 2014	C5.3	145	36	0.2483
	C10.8	223	53	0.2377
	C16.1	167.2	42	0.2512
	C21.2	213.6	58	0.2715

2.5 Chemical analysis of SRBs/SOMs

2.5.1 Sample Details

MC252 oil was supplied by British Petroleum. First beached oil in the form of mousse was collected on June 11, 2010. SRB/SOMs samples collected over a period of 3 years at Lagoon Pass (LP) in Gulf Shores, AL, USA (GPS coordinates - N30°14'25.55" W87°44'16.58") were analyzed for PAHs. The sample details are given in Table 2-4. The oil content in the SRB samples were estimated using previous established procedures (Yin et al., 2015a; Yin et al., 2015b) and are given in Table 2-4.

Table 2-4: Sampling date and oil content in SRBs collected from Lagoon Pass for the past three years

Sample	Collection Date	%Oil Content
LP1	September 8, 2011	17
LP2	February 19, 2011	24
LP3	September 2, 2012	22
LP4	February 15, 2013	15
LP5	June 14, 2014	17
LP6	August 16, 2014	16

2.5.2 Fractionation and Analysis

Column chromatographic fractionation was conducted according to procedure given elsewhere (John et al., 2014; Wang et al., 1994a). A glass column (10.1 mm diameter and 200 mm length) was plugged with glass wool, and about 3 g of activated silica gel was added to the column, followed by 1 g of anhydrous sodium sulfate. The column was then charged with 20 mL of hexane. 25 mg of oil was weighed into a 12 mL

vial and then spiked with surrogates. For SRBs, 25 mg oil equivalent was weighed into the 12 mL vial and then spiked with surrogates. It was then extracted with 1 mL hexane and transferred to the column. The samples in the 12 mL vial was then extracted with 1 mL of hexane and transferred to the column. The vial was then sequentially washed with 2 mL of hexane, with 1 mL in each step, and the contents were transferred to the column. All solvents eluted from the column prior to this step were discarded. 12 mL of hexane was then used to elute aliphatic hydrocarbon fractions from the sample. The hexane-eluted fraction was labeled as F1. Next, a 50% hexane and 50% dichloromethane solvent mixture (15 mL) was used to elute all aromatic hydrocarbon fractions, and this fraction was labeled as F2. The F1 and F2 fractions were concentrated under a gentle stream of nitrogen gas and then reconstituted in 10 mL of hexane and hexane:dichloromethane solvent mixture (ratio of 1:1) for each fraction, respectively. F2 fraction was spiked with *p*-terphenyl-d_{14}.

Five groups of alkylated PAHs and seventeen other PAHs in F2 fraction were analyzed using single ion monitoring (SIM) and multiple reaction monitoring (MRM) modes, respectively, employing previously established analytical procedures(Yin et al., 2015a; Yin et al., 2015b). The GC and MS parameters for analysis of F2 fractions both in SIM and MRM modes are given in appendix Tables A2 and A3, respectively.

2.5.3 PAHs quantitation

Five groups of alkylated PAHs and seventeen PAHs were quantified using previously developed quantitation methods (Wang et al., 1994a; Yin et al., 2015a; Yin et al., 2015b). The five groups of alkylated PAHs are quantified as follows: Group 1, C_0-naphthalene was quantified using naphthalene; C_1-naphthalenes using 2-

methylnaphthalene; C_2-naphthalenes using 2,6-dimethylnaphthalene; C_3- and C_4-naphthalenes using 2,3,5-trimethylnaphthalene. In Group 2, C_0-phenanthrene was quantified using phenanthrene; C_1- to C_4-phenanthrenes using 1-methylphenanthrene. In Group 3, C_0- to C_3-dibenzothiophenes were quantified using dibenzothiophene. In Group 4, C_0- to C_3-fluorenes were quantified using fluorene. In Group 5, C_0- to C_4-chrysenes were quantified using chrysene. Seventeen other PAHs that were quantified in F2 fraction are biphenyl, acenaphthylene, acenaphthene, anthracene, fluoranthene, pyrene, benzo(a)anthracene, benzo(b)fluoranthene, benzo(j)fluoranthene, benzo(k)fluoranthene, benzo(e)pyrene, benzo(a)pyrene, perylene, dibenz(a,c)anthracene, dibenz(a,h)anthracene, indeno(1,2,3,-cd)pyrene and benzo(ghi)perylene. The internal standard *p*-terphenyl-d_{14} chromatographic peak area was used to normalize the PAHs chromatographic peak areas.

The concentration of PAHs in MC252 oil, Mousse, LP1, LP2, LP3, LP4, LP5 and LP6 are presented in Table 2-5. The concentration of PAHs in SRB samples collected over a period of 4 years show no sign depletion compared to that of first arrived oil in June 2010

Table 2-5: Concentration of PAHs in MC252, Mousse, LP1, LP2, LP3, LP4, LP5 and LP6

Compound	Concentration mg/kg of oil							
	MC252	Mousse	LP1	LP2	LP3	LP4	LP5	LP6
C_0-Naphthalene	583 ± 15	DL	DL	DL	DL	DL	DL	DL
C_1-Naphthalenes	1940 ± 41	DL	DL	DL	DL	DL	DL	DL
C_2-Naphthalenes	3147 ± 116	0.70±0.09	0.88±0.06	0.59±0.03	0.58±0.07	1.1±0.1	1.05±0.08	0.85±0.06
C_3-Naphthalenes	2452 ± 111	8±1	9±1	4.0±0.6	5.5±0.3	12.0±0.3	13.7±0.7	10.1±0.2
C_4-Naphthalenes	2110 ± 112	37±5	47±7	25±4	32±2	61±2	64±1	59±2
C_0-Phenanthrene	213 ± 5	28±3	32.6±0.3	23.6±0.4	24.5±0.8	10.2±0.3	9.1±0.8	3.0±0.2
C_1-Phenanthrenes	928 ± 21	285±8	346±4	292±5	276±9	183±7	131±2	32±3
C_2-Phenanthrenes	1019 ± 20	437±3	601±8	521±5	472±12	517±4	445±2	286±13
C_3-Phenanthrenes	619 ± 10	281±1	403±54	353±5	318±10	412±4	390±2	339±12
C_4-Phenanthrenes	321 ± 4	152±9	233±2	207±4	185±6	253±9	232±1	215±7
C_0-Dibenzothiophene	53 ± 2	2.7±0.3	2.8±0.4	2.4±0.3	2.7±0.2	4.7±0.2	7.7±0.1	2.4±0.5
C_1-Dibenzothiophenes	75 ± 2	16±2	19±2	16±2	16±1	15.2±0.4	15.8±0.3	6.3±0.5
C_2-Dibenzothiophenes	99 ± 4	43±4	57±7	51±6	48±3	62±2	62±1	40±1
C_3-Dibenzothiophenes	74 ± 2	36±3	51±7	46±5	43±3	59±2	57±2	45±1
C_0-Fluorene	131 ± 5	0.58±0.03	0.60±0.05	0.41±0.04	0.50±0.03	0.66±0.03	1.27±0.04	0.45±0.05
C_1-Fluorenes	333 ± 9	17±2	23±3	18±2	21±2	23.7±0.8	25±1	15±2
C_2-Fluorenes	416 ± 15	42±3	62±9	59±7	62±5	80±3	85±3	53±4
C_3-Fluorenes	362 ± 17	72±8	105±12	101±12	99±8	141±5	141±2	117±7
C_0-Chrysene	54.7 ± 0.8	46±4	65±8	59±6	53±4	75±2	67±1	60±2
C_1-Chrysenes	121 ± 1	63±4	90±12	82±8	74±6	109±4	96±1	90±2
C_2-Chrysenes	152 ± 2	44±2	67±9	61±6	55±5	82±3	72±1	69±1
C_3-Chrysenes	107 ± 2	17.3±0.8	28±4	25±3	24±3	35±2	33±2	30±1
C_4-Chrysenes	65 ± 2	7.7±0.5	13±2	11±1	10±1	16.0±0.7	15±1	13.0±0.5
Biphenyl	200 ± 6	DL	DL	DL	DL	DL	DL	DL
Acenaphthylene	61 ± 1	DL	DL	DL	DL	DL	DL	DL
Acenaphthene	70 ± 1	DL	DL	DL	DL	DL	DL	DL
Anthracene	12.5 ± 0.7	1.0±0.1	1.4±0.2	1.2±0.2	1.3±0.1	1.57±0.08	1.72±0.09	1.18±0.04
Fluoranthene	15.8 ± 0.4	3.9±0.7	5.3±0.6	4.5±0.5	4.1±0.4	5.7±0.2	5.4±0.5	4.5±0.2
Pyrene	21.1 ± 0.6	6.8±0.6	10±1	9±1	8.0±0.7	11.3±0.3	11.1±0.1	9.5±0.5
Benzo(*a*)anthracene	16.4 ± 0.4	0.35±0.05	0.58±0.07	0.50±0.05	0.46±0.05	0.64±0.03	0.60±0.04	0.67±0.05
Benzo(*b*)fluoranthene	14.0 ± 0.4	6.4±0.7	9±1	8.3±0.9	7.6±0.7	11.1±0.2	9.75±0.01	8.8±0.1
Benzo(*k*)fluoranthene	5.93 ± 0.08	1.5±0.3	2.2±0.3	1.9±0.3	1.7±0.2	2.37±0.08	2.16±0.04	2.0±0.1
Benzo(*j*)fluoranthene	5.9 ± 0.1	0.90±0.07	1.3±0.2	1.1±0.2	1.01±0.07	1.5±0.1	1.4±0.1	1.2±0.1
Benzo(*e*)pyrene	18.3 ± 0.6	8±1	11±1	10±1	9.4±0.9	13.6±0.3	12.0±0.1	11.4±0.2
Benzo(*a*)pyrene	6.49 ± 0.07	0.36±0.05	0.44±0.02	0.38±0.02	0.39±0.04	0.44±0.05	0.46±0.06	0.48±0.04
Perylene	7.7 ± 0.4	0.26±0.02	0.34±0.03	0.28±0.02	0.27±0.02	0.34±0.03	0.34±0.01	0.28±0.02
Dibenz(*a*,*c*)anthracene	10.2 ± 0.3	0.5±0.1	0.73±0.06	0.57±0.07	0.54±0.07	0.71±0.06	0.69±0.04	0.84±0.07
Dibenz(*a*,*h*)anthracene	8.88 ± 0.07	0.8±0.3	1.2±0.2	1.0±0.3	0.9±0.1	1.10±0.08	1.04±0.06	0.8±0.2
Indeno(1,2,3,-*cd*)pyrene	8.7 ± 0.2	0.6±0.2	0.9±0.1	0.7±0.1	0.59±0.08	0.8±0.2	0.71±0.08	0.6±0.1
Benzo(*gh*i)perylene	8.6 ± 0.1	1.9±0.5	2.9±0.4	2.5±0.3	2.3±0.2	3.3±0.1	2.89±0.05	2.9±0.1
Total	15866	1714	2382	2047	1892	2206	2013	1533

DL – detection limit

2.5.4 Ecological concern for SOM/SRB residues

The chemical analysis of SOM/SRBs collected over a period of four years show that the concentration of PAHs remains almost the same as that of the first arrived oil which washed on the beaches on June 2010. Mulabagal et al (2013) characterized several petroleum biomarkers in several SRBs collected along the Alabama's shoreline and stated that virtually all tarballs found on the beaches of Alabama are from the MC252 oil. Further, it is also reported that the compounds present in SOMs/SRBs are not degrading.

2.6 Conclusion

Based on the observations presented here and based on data available in various recently published literature, the following conclusions can be made.

- SOMs/SRBs are still present in the Alabama's beach system and it is unlikely that these beaches would return to background tarball levels over a period of six months as estimated by Shoreline Cleanup Completion Plan.
- Based on the physical characteristics of SRBs found on Alabama's beaches over the past four years, it is concluded that virtually all "tarballs" currently found on Alabama's beaches match the characteristics of MC252 SRBs (Mulabagal et al., 2013).
- A chemical analysis of SRB samples recovered four years after the spill on August 2014, show that the PAHs concentration levels present in SRBs are similar to those observed in the mousse sample collected in June 2010. This data is consistent with the more comprehensive data collected in other published recent studies (Yin et al., 2015b).

- The presence of SRBs in the near-shore environment could pose a potential long-term ecological risk to Alabama's shoreline. In particular, organisms which reside or frequent near-shore along MC252 oil-impacted beaches may have a heightened potential for chronic exposure to, or consumption of, toxic compounds.

Chapter 3

Effect of sunlight on transformation of polycyclic aromatic hydrocarbons present in submerged oil spill residues

3.1 Introduction

The *Deepwater Horizon* (DWH) accident in April 2010 released an estimated 5.3 × 10^8 kg of oil and 1.8 × 10^8 kg of gas (Aeppli et al., 2012) from the Macondo well (MC252) over a period of 87 days (Hayworth et al., 2015). It was estimated that about 25% of the released oil either evaporated or dissolved, 3% was skimmed, 5% was burnt, 8% was chemically dispersed, 16% was naturally dispersed and 17% was captured and 26% remained in the water (Atlas and Hazen, 2011; Lehr et al., 2010b; OSAT-1, 2010). A fraction of the remaining oil in the water may have deposited in the near vicinity of the MC252 well (Chanton et al., 2015; Lehr et al., 2010b) and the remaining oil washed ashore or transported by deeper ocean currents.

A considerable amount of oil related to the spill washed ashore on the white sandy beaches of Alabama from early June 2010 onwards and continued until mid-August 2010 (Hayworth and Clement, 2011b; Yin et al., 2015b). The spilled oil that washed ashore on Alabama's beaches was pre-dominantly in the form of water-in-oil emulsion, a highly viscous and neutrally buoyant brownish material known as "mousse". An unknown quantity of this mousse interacted with suspended solids near the shoreline, became

negatively buoyant and sank to the bottom, forming immobile submerged oil mats (SOMs) and mobile surface residual balls (SRBs) (Hayworth et al., 2015). The SRBs and SOMs are predominantly composed of sand (75-95%) by mass (Hayworth and Clement, 2011b; OSAT-1, 2010; OSAT-2, 2011). Overtime, due to natural coastal dynamics, these SOMs and SRBs are being discontinuously buried, exposed and broken apart (Dalyander et al., 2014; Hayworth and Clement, 2011b; Hayworth et al., 2015; Michel et al., 2013c; OSAT-3, 2014). The remnant oil in SOMs and SRBs is stripped of easily weathered compounds and have higher concentrations of various hazardous chemicals including polycyclic aromatic hydrocarbons (PAHs) which can be toxic to both human and ecological systems (Liu et al., 2012a; Mulabagal et al., 2013; Urbano et al., 2013; Yin et al., 2015a).

PAHs are group of organic compounds containing two or more fused aromatic rings and are one of the most important groups of toxic environmental compounds present in crude oil (Neff, 1979). Due to their carcinogenic and mutagenic properties, PAHs are classified as hazardous organic compounds (ATSDR, 1995; Mumtaz et al., 1996; Yin et al., 2015b). Well over 100 PAHs have been identified and currently several of them are classified as priority pollutants by the US Environmental Protection Agency (USEPA, 1993). Recent studies have shown that PAHs present in SOMs and SRBs found along the northern Gulf of Mexico shoreline appear to have very low degradation rates (Hayworth et al., 2015; McDaniel et al.; Mulabagal et al., 2013; Natter et al., 2012; Turner et al., 2014; Yin et al., 2014). The reason why the DWH oil spill residues show little or no degradation is still not known.

When crude oil is released into the marine environment, it undergoes various natural weathering processes including spreading, advection, evaporation, dissolution,

photo-oxidation, emulsification, sedimentation and microbial degradation (Dutta and Harayama, 2000; Garrett et al., 1998; Guo and Wang, 2009; Hall et al., 2013; Hamoda et al., 1989; NRC, 2003; Prince et al., 2003; Wang et al., 2005). Evaporation is one of the most important weathering processes in many oil spill incidents as this process greatly reduces the volume of the spilled oil (Fingas, 1997). Few PAHs and polar compounds can also dissolves in water and the dissolved species are eventually degraded by microbial processes (Garrett et al., 1998; Prince et al., 2003).

However, photo-oxidation is one of the most important weathering processes for the spilled crude oil in the marine environment and it produces a variety of oxidized products. Photo-oxidized products typically have higher polarity and water solubility and thus can contribute to the disappearance of oil slicks (Dutta and Harayama, 2000; Lee, 2003). Photo-oxidation is a major degradation pathway for higher molecular weight PAHs present in the crude oil as many of them absorb light in the ultraviolet or visible wavelengths found in the sunlight. Photo-oxidation also increases the susceptibility of crude oil to biodegradation (Dutta and Harayama, 2000). However photo-oxidation process could also increase the net environmental toxicity of the oil to the marine environment (Lee, 2003).

Chemical analysis of various DWH oil spill residues collected along the northern Gulf of Mexico coast confirms that PAHs present in the spilled oil has undergone considerable photo-oxidation during its transit from the well-head to the shoreline, but when the oil was buried into SOMs/SRBs, the degradation processes appeared to have slowed down (Yin et al., 2015b). It is highly likely that after the burial near the shoreline

the remnant oil in the form of SOMs and SRBs were devoid of sunlight and thus the major degradation pathway (photo-oxidation) for PAHs should have been hindered.

SOMs and SRBs continue to wash ashore on the beaches of northern Gulf of Mexico to this day. Therefore it is important to understand the long-term ecological impacts of PAHs present in these oil spill residues when they are re-exposed to sunlight. The primary objective of this study is to understand the fate of PAHs present in SOM deposits when they are re-exposed to sunlight.

3.2 Experimental

3.2.1 Samples

MC252 reference crude oil was supplied by British Petroleum (BP) and is referred as DWH oil. SOM was excavated on September 24, 2011 at Gulf Shores, AL, USA (GPS coordinates - N30.24, W87.74) (Figure 3.1). This SOM was sampled and used for the experiment.

Figure 3.1**:** Excavation and collection of SOM from intertidal region

3.2.2 Materials

The organic solvents dichloromethane and hexane used in this study were of analytical grade or higher. The solvents, silica gel (60–200 μm), and anhydrous sodium sulfate (ACS grade) were purchased from VWR International (Suwanee, GA). C_{30} ββ-hopane (17β(H),21β(H)-hopane) standard was purchased from Chiron, Trondheim, Norway. A mixture of twenty-seven PAHs (naphthalene, 1-methylnaphthalene, 2-methylnaphthalene, 2,6-dimethylnaphthalene, 2,3,5-trimethylnaphthalene, biphenyl, acenaphthylene, acenaphthene, fluorene, phenanthrene, 1-methylphenanthrene, anthracene, dibenzothiophene, fluoranthene, pyrene, benzo(a)anthracene, chrysene, benzo(b)fluoranthene, benzo(j)fluoranthene, benzo(k)fluoranthene, benzo(e)pyrene, benzo(a)pyrene, perylene, dibenz(a,c)anthracene, dibenz(a,h)anthracene, indeno(1,2,3,-cd)pyrene and benzo(ghi)perylene) was purchased from Agilent Technologies, Wilmington, DE. A mixture of four deuterated standards containing naphthalene-d_8, acenaphthene-d_{10}, phenanthrene-d_{10} and benzo(a)pyrene-d_{12} was purchased from Ultra Scientific Analytical Solutions (North Kingstown, RI). These four deuterated compounds were used as surrogates (SS). Internal standard (IS) *p*-terphenyl-d_{14} (purity 98.5%) was purchased from AccuStandard (New Haven, CT, USA). Chromatographic separation of various PAH compounds was achieved using a J&W DB-EUPAH (Agilent Technologies) column (20 m × 180 μm × 0.14 μm). The back flush setup used Agilent Technologies inert fused silica column (0.7 m × 150 μm × 0 μm; 450 °C).

Activated silica gel was prepared according to procedure given in Wang et al (1994a). Silica gel was serially rinsed three times with 250 mL acetone, hexane and dichloromethane and then left to dry for 12 h in a fume hood. After drying, silica gel was

heated in an oven at 40–50 °C for 8 h and then activated at 180 °C for 20 h. Anhydrous sodium sulfate was purified by heating at 400 °C for 4 h and then cooled and stored in tightly sealed glass containers.

3.2.3 Estimation of oil content in SOM

The oil content in SOM was determined using methods described in our previous studies (Mulabagal et al., 2013; Yin et al., 2015b). About 1 g of the homogenized sample was extracted using 10 mL of dichloromethane. The extraction step was repeated four times and the remaining solid residues in the vial were dried and weighed to determine the oil content of SOM. The oil content of SOM is 12.8%.

3.2.4 DWH and ESOM sample preparation for sunlight exposure experiment

About 2.5 g of DWH oil was dissolved in dichloromethane and made upto 5 mL to give an effective concentration of 0.5 g/mL of oil.

About 19.5 g of SOM (2.5 g oil equivalent) was taken and mixed thoroughly with equal quantities of anhydrous sodium sulfate (USEPA, 1996, 2007a, b). 50 mL of dichloromethane was added and sonicated for 10 minutes. The extract was collected and then the extraction step was repeated for another two times. The extracts were combined and then concentrated under a gentle stream of nitrogen and reconstituted in dichloromethane to obtain a final extract concentration of 0.25 mg/mL and was designated as ESOM. Lower concentration of ESOM solution was used as it was easier to handle this solution using syringes at lower concentration levels.

3.2.5 Sunlight exposure experiment

About 100 µl of DWH solution was added to a petri dish, spread uniformly and the solvent was allowed to evaporate to give an effective weight of 50 mg of oil (see Figure 3.2). DWH samples were divided into three sets – 1) first set of samples were placed in a laboratory fume hood to be used for laboratory control, 2) second set of samples were exposed to sunlight and 3) third set of samples were placed along side with second set of samples in a covered box, so this set of samples were exposed to same weather elements as that of second set except that of sunlight. The first, second and third set of samples were designated as "DWH lab control", "sunlight-exposed" and "sunlight-control", respectively. For ESOM, 200 µl was added to give an effective weight of 50 mg of oil in each petri dish. For SOM, 50 mg (390 mg) of oil equivalent was weighed on to the petri dish. For SOM and ESOM, similar to that of DWH, "sunlight-exposed" and "sunlight-control" samples were prepared. The sunlight-exposed and sunlight-control samples of DWH, SOM and ESOM were then exposed to sunlight from 10 am to 4 pm (see Figure 3.3) and in-between exposures and rainy and cloudy days the samples were stored at -15°C. The samples were collected for analysis after 1, 2, 4, 8, 16, 32 and 64 hours of exposure. Hourly solar radiation data was provided by AWIS Weather Services weather station located in Auburn, AL, USA (GPS co-ordinates - 32.60 N, 85.50 W). Summation of hourly solar radiation data was computed for the respective exposure times and presented in Table 3-1.

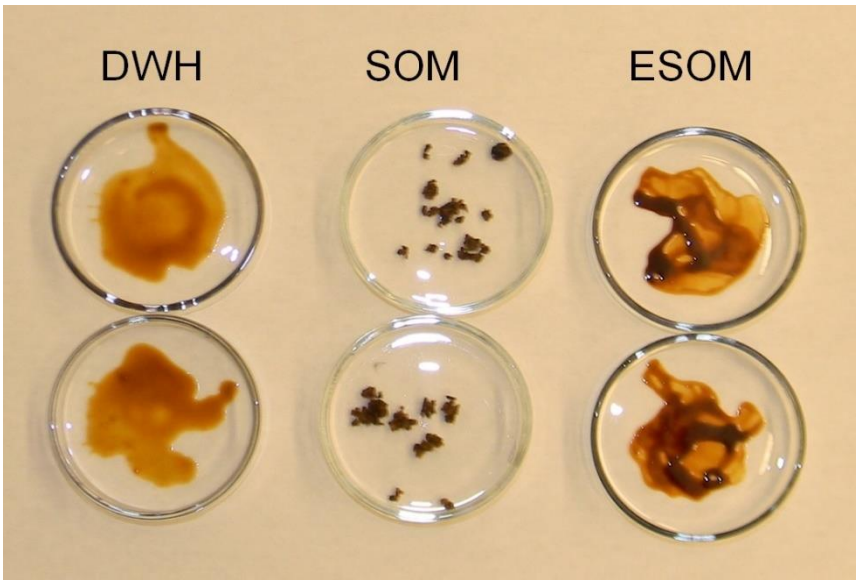

Figure 3.2: Sample preparation

Table 3-1: Solar radiation at different exposure times

Time (hours)	DWH	SOM & ESOM
	Total amount of solar radiation (W-hr/m^2)	Total amount of solar radiation (W-hr/m^2)
0	0	0
1	551	819
2	910	1525
4	1943	2583
8	5470	3950
16	9379	8665
32	18278	21413
64	37080	43798

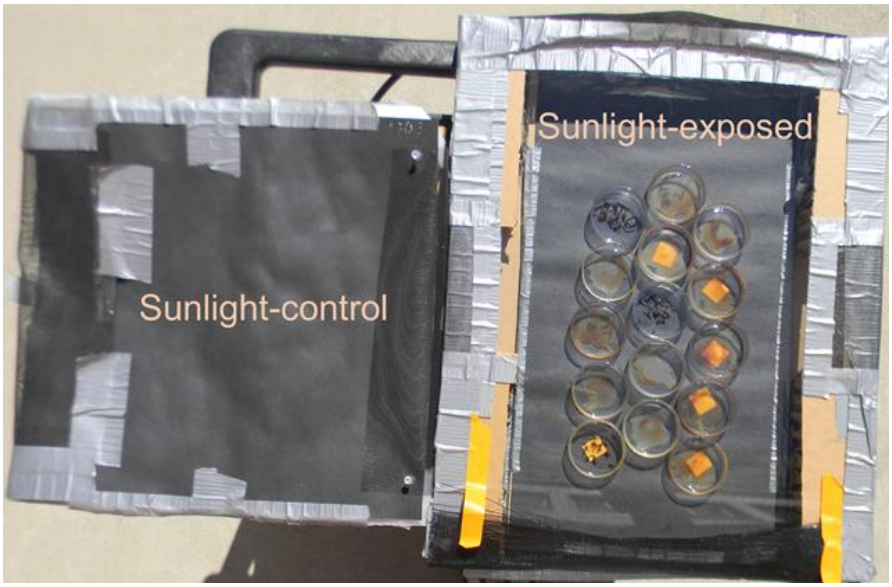

Figure 3.3: Experimental setup for exposing samples to sunlight

3.2.6 Extraction and column chromatographic fraction for irradiated samples

The DWH lab control, sunlight-exposed and sunlight-control samples of DWH and ESOM were spiked with surrogates and extracted with 3 × 1 mL of dichloromethane and transferred to a 12 mL vial. The extract were then concentrated under a gentle stream of nitrogen. For SOM, the samples were transferred to a 12 mL vial and then spiked with surrogates.

Column chromatographic fractionation was conducted according to procedure given elsewhere (John et al., 2014; Wang et al., 1994a). A glass column (10.1 mm diameter and 200 mm length) was plugged with glass wool, and about 3 g of activated silica gel was added to the column, followed by 1 g of anhydrous sodium sulfate. The column was then charged with 20 mL of hexane. The samples in the 12 mL vial was then extracted with 1 mL of hexane and transferred to the column. The vial was then sequentially washed with

2 mL of hexane, with 1 mL in each step, and the contents were transferred to the column. All solvents eluted from the column prior to this step were discarded. 12 mL of hexane was then used to elute aliphatic hydrocarbon fractions from the sample. The hexane-eluted fraction was labeled as F1. Next, a 50% hexane and 50% dichloromethane solvent mixture (15 mL) was used to elute all aromatic hydrocarbon fractions, and this fraction was labeled as F2. The F1 and F2 fractions were concentrated under a gentle stream of nitrogen gas and then reconstituted in 10 mL of hexane and hexane:dichloromethane solvent mixture (ratio of 1:1) for each fraction, respectively. F1 fraction was spiked with $C_{30}\beta\beta$-hopane and F2 fraction was spiked with *p*-terphenyl-d_{14}.

3.2.7 Instrument analysis and quantitation

F1 and F2 fractions were both analyzed using Agilent Gas Chromatograph (7890) coupled to Triple Quadrupole Mass Spectrometer (7000B). F1 fraction was analyzed for hopanes and steranes using Single Ion Monitoring (SIM) mode. Five groups of alkylated PAHs and seventeen other PAHs in F2 fraction were analyzed using SIM and multiple reaction monitoring (MRM) modes, respectively, employing previously established analytical procedures (Yin et al., 2015a; Yin et al., 2015b). The GC and MS parameters for F1 fraction operated in SIM mode were given in appendix Table A1. The GC and MS parameters for F2 fraction operated in SIM and MRM modes were given in appendix Tables A2 and A3, respectively.

Hopanes peak areas were computed by integrating appropriate chromatographic peaks observed at *m/z* of 191. $C_{30}\beta\beta$-hopane was used as internal standard for F1 fractions and its chromatographic peak area was used to normalize other hopanes chromatographic peak area. Five groups of alkylated PAHs and seventeen PAHs were quantified using

previously developed quantitation methods (Wang et al., 1994a; Yin et al., 2015a; Yin et al., 2015b). The five groups of alkylated PAHs are quantified as follows: Group 1, C_0-naphthalene was quantified using naphthalene; C_1-naphthalenes using 2-methylnaphthalene; C_2-naphthalenes using 2,6-dimethylnaphthalene; C_3- and C_4-naphthalenes using 2,3,5-trimethylnaphthalene. In Group 2, C_0-phenanthrene was quantified using phenanthrene; C_1- to C_4-phenanthrenes using 1-methylphenanthrene. In Group 3, C_0- to C_3-dibenzothiophenes were quantified using dibenzothiophene. In Group 4, C_0- to C_3-fluorenes were quantified using fluorene. In Group 5, C_0- to C_4-chrysenes were quantified using chrysene. Seventeen other PAHs that were quantified in F2 fraction are biphenyl, acenaphthylene, acenaphthene, anthracene, fluoranthene, pyrene, benzo(a)anthracene, benzo(b)fluoranthene, benzo(j)fluoranthene, benzo(k)fluoranthene, benzo(e)pyrene, benzo(a)pyrene, perylene, dibenz(a,c)anthracene, dibenz(a,h)anthracene, indeno(1,2,3,-cd)pyrene and benzo(ghi)perylene. The internal standard *p*-terphenyl-d_{14} chromatographic peak area was used to normalize the PAHs chromatographic peak areas.

3.2.8 Assessment of weathering using hopane

C_{30}αβ-hopane was used as an internal conservative biomarker (Mulabagal et al., 2013; Wang et al., 1994c; Yin et al., 2015a; Yin et al., 2015b) to determine the weathering levels of SOM and ESOM compared to that of the source oil DWH. C_{30}αβ-hopane response in the original crude oil source sample was quantified by first computing a ratio H_{oil}, which is the peak area of C_{30}αβ-hopane in crude oil to the peak area of C_{30}ββ-hopane. Similarly hopane ratio for the weathered samples, $H_{weathered}$, which was the peak area of C_{30}αβ-hopane in a weathered oil spill sample to the peak area of C_{30}ββ-hopane is computed.

The %weathering was then computed using the following equation (eqn(3.1)) (Mulabagal et al., 2013).

$$\%weathering = \left(1 - \frac{H_{oil}}{H_{weathered}}\right) X\ 100 \qquad eqn(3.1)$$

The weathering of SOM and ESOM compared to that of DWH oil is 34% and 41% respectively.

3.2.9 %PAHs remaining

Organic compounds present in crude oil weather concurrently and therefore is necessary to use a non-degrading organic compound as a conservative marker to normalize the concentration of compounds measured in environmental samples (Douglas et al., 1996). C_{30}αβ-hopane was again used as a conservative marker for normalization as it is known to be recalcitrant to volatilization, biodegradation and photo-degradation (Aeppli et al., 2014; Prince et al., 1994; Radović et al., 2014). H_{oil} and $H_{weathered}$ were computed as described in previous section. These ratios were used to compute the hopane normalizing factor, $H_{oil}/H_{weathered}$, which was then used to estimate the amount of target PAHs remaining in the samples using the following equation (Douglas et al., 1996; Radović et al., 2014; Yin et al., 2015b).

$$\%PAHs\ remaining = \left(\frac{PAH\ in\ weathered\ sample}{PAH\ in\ reference\ oil} \times \frac{H_{oil}}{H_{weathered}}\right) \times 100 \qquad eqn(3.2)$$

3.2.10 Estimation of physical and chemical properties

165 PAHs were used as training set to estimate the physical and chemical properties (Appendix Table A3 to A7). These compounds were selected from National Institute of Standards and Technology (NIST) Formula Brower webpages (NIST, 2011a, b, c, d, e, f, g, h, i, j, k, l, m, n, o, p, q, r, s, t, u, v, w). The selection of these 165 compounds was based on different alkylation in the molecule. This selection was made to capture the variation in physical and chemical properties in due to different alkylation in the same homologue. *ChemSketch* was used to generate SMILEYS (Simplified molecular input line entry system) notation for the training set. *Vapor Pressure* was computed using the QSAR model *MPBPWIN* in *EPI Suite*. The energy difference between *Highest Occupied Molecular Orbital to the Lowest Unoccupied Molecular Orbital* (*HOMO-LUMO*) was calculated at PM3 level using Spartan Student v6 software.

3.3 Results

3.3.1 Source Identification

The SOM sample is analyzed first to confirm its origin. In terms of physical characteristics, it matched to that of MC252 residual oil characteristics reported in various studies - sticky, brownish material with considerable amount of sand and strong petroleum odor (Mulabagal et al., 2013; OSAT-2, 2011; Yin et al., 2015b). The sample was further analyzed for hopanes and steranes for chemical fingerprinting using analytical procedures described in our previous studies (Mulabagal et al., 2013; Wang et al., 1994a, b; Yin et al., 2015b). Source-specific hopane diagnostic ratios are used for source crude oil identification and the ratios used for source identification are T_s/T_m, C_{29}/C_{30}, $C_{31}(S)/C_{31}(S+R)$, $C_{32}(S)/C_{32}(S+R)$, $C_{33}(S)/C_{33}(S+R)$, $C_{34}(S)/C_{34}(S+R)$ and

$C_{35}(S)/C_{35}(S+R)$ (Mulabagal et al., 2013). The source-specific hopane diagnostic ratios for both DWH and SOM are computed and plotted on a radar plot (Figure 3.4). The source-specific diagnostic ratios for both the samples matches closely and gives the first confirmation that the source for SOM is DWH oil.

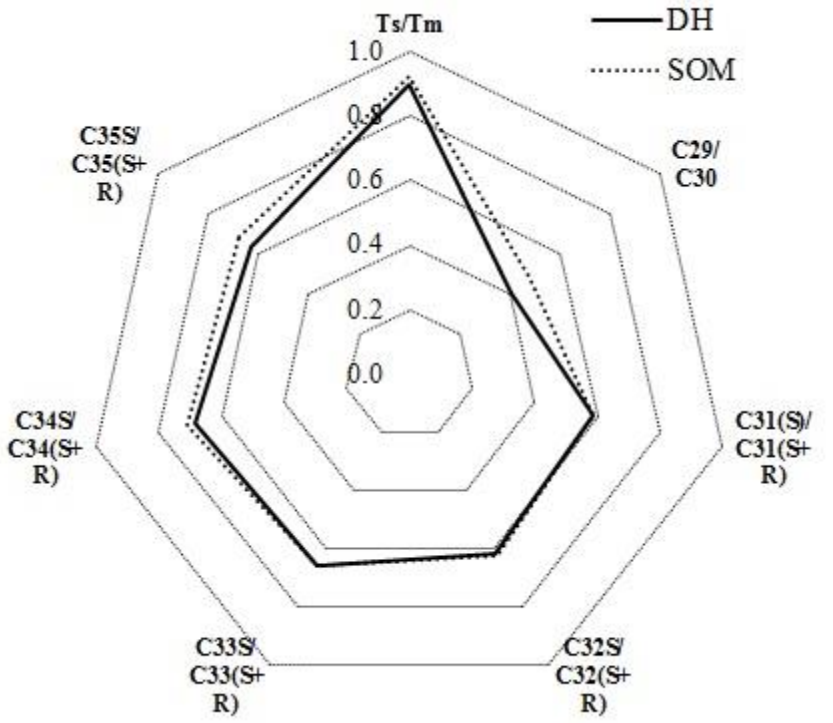

Figure 3.4: Comparison of hopane diagnostic ratios of DH and SOM

Steranes dataset is used to provide additional confirmation for identifying the source of the oil spill residue. The extracted ion chromatogram for steranes (*m/z* 217) for both DWH and SOM is compared (Figure 3.5). The chromatograms match provides another confirmation that the source for SOM is DWH oil.

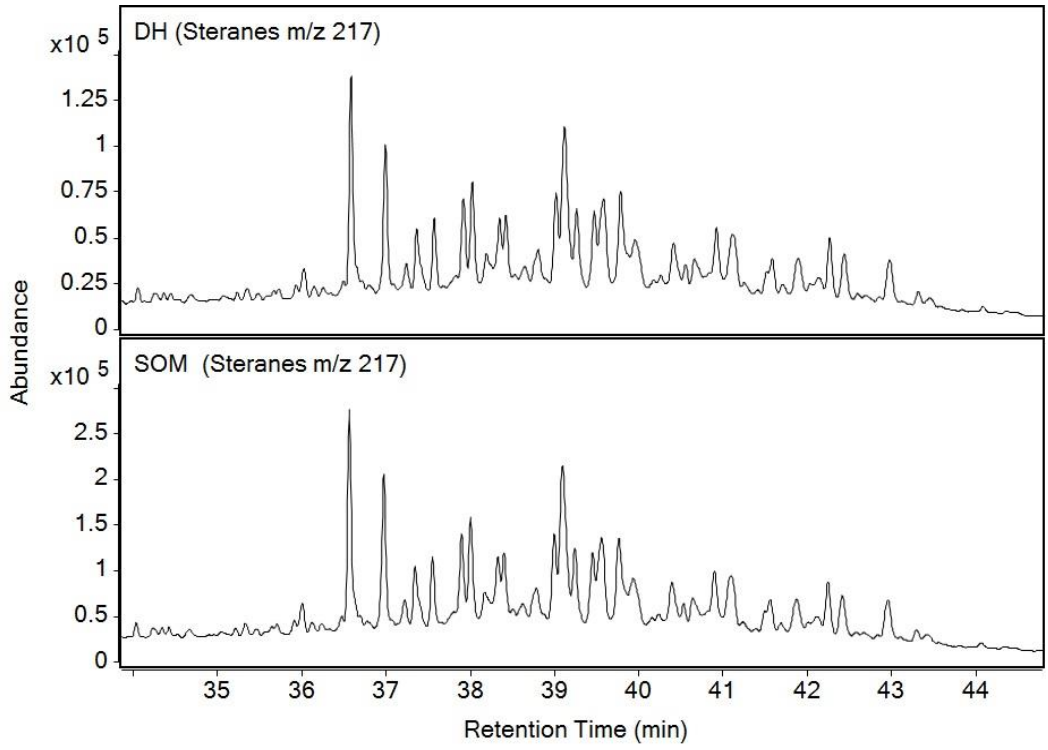

Figure 3.5: Comparison of extracted ion chromatograms of steranes (m/z of 217) for DH and SOM

3.3.2 Comparison of PAHs measured in DWH, EDWH, SOM and ESOM

The PAHs present in DWH, SOM and ESOM are estimated and presented in Table 3-2. The % PAHs remaining in SOM and ESOM compared to that of DWH is also presented in Table 3-2. The total amount of target PAHs in DWH is 15864 mg/kg oil. PAHs in DWH is dominated by naphthalene and its alkylated homologues.

The total amount of PAHs in SOM is 3077 mg/kg of oil and only 13% of total PAHs are remaining in SOM compared to that of DWH oil. Likewise, the total amount of PAHs in ESOM is 2861 mg/kg of oil and only 11% of total PAHs are remaining in ESOM compared to DWH oil. The total PAHs remaining in SOM and ESOM is dominated by four groups of PAHs – phenanthrene and its alkylated homologues, dibenzothiophene and its alkylated homologues, fluorene and its alkylated homologues and chrysene and its alkylated homologues. Since the PAHs in oil and oil spill residue is dominated by five groups of PAHs, the effect of sunlight is monitored only for these five groups of PAHs.

Table 3-2: Concentration of PAHs in DWH oil, SOM and ESOM and %PAHs remaining in SOM and ESOM compared to DWH oil

Compound	DWH oil	SOM		ESOM	
	Concentration mg/kg	Concentration mg/kg	PAHs remaining in SOM %	Concentration mg/kg	PAHs remaining in ESOM %
C_0-naphthalene	583 ± 15	3.48 ± 0.02	0%	3.35 ± 0.02	0%
C_1-naphthalenes	1940 ± 41	3.47 ± 0.03	0%	3.264 ± 0.005	0%
C_2-naphthalenes	3147 ± 116	5.0 ± 0.2	0%	4.47 ± 0.02	0%
C_3-naphthalenes	2452 ± 111	52 ± 4	2%	38.9 ± 0.4	1%
C_4-naphthalenes	2110 ± 112	143 ± 12	5%	109 ± 1	3%
C_0-phenanthrene	213 ± 5	55 ± 2	16%	48.4 ± 0.7	13%
C_1-phenanthrenes	928 ± 21	498 ± 14	36%	441 ± 5	30%
C_2-phenanthrenes	1019 ± 20	778 ± 17	51%	707 ± 8	43%
C_3-phenanthrenes	619 ± 10	430 ± 11	46%	409 ± 5	41%
C_4-phenanthrenes	321 ± 4	218 ± 4	45%	209 ± 3	41%
C_0-dibenzothiophene	53 ± 2	9.5 ± 0.3	9%	8.36 ± 0.06	7%
C_1-dibenzothiophenes	75 ± 2	32 ± 1	28%	27.2 ± 0.3	22%
C_2-dibenzothiophenes	99 ± 4	75 ± 2	52%	64.4 ± 0.9	42%
C_3-dibenzothiophenes	74 ± 2	64 ± 1	60%	55.7 ± 0.9	50%
C_0-fluorene	131 ± 5	5.4 ± 0.1	1%	4.93 ± 0.05	1%
C_1-fluorenes	333 ± 9	50 ± 3	10%	40.2 ± 0.9	7%
C_2-fluorenes	416 ± 15	127 ± 7	20%	106 ± 2	16%
C_3-fluorenes	362 ± 17	149 ± 10	27%	149 ± 2	25%
C_0-chrysene	54.7 ± 0.8	55.5 ± 0.9	67%	64.0 ± 0.5	75%
C_1-chrysenes	121 ± 1	80 ± 2	43%	99.1 ± 0.9	51%
C_2-chrysenes	152 ± 2	62 ± 3	26%	81.2 ± 0.7	33%
C_3-chrysenes	107 ± 2	30 ± 2	16%	38.7 ± 0.4	21%
C_4-chrysenes	65 ± 2	19 ± 1	16%	22.3 ± 0.3	19%
Biphenyl	200 ± 6	2.83 ± 0.01	1%	2.67 ± 0.02	1%
Acenaphthylene	61 ± 1	3.38 ± 0.07	4%	3.21 ± 0.04	3%
Acenaphthene	70 ± 1	4.12 ± 0.07	4%	3.81 ± 0.01	3%
Anthracene	12.5 ± 0.7	5.8 ± 0.2	30%	5.4 ± 0.1	26%
Fluoranthene	15.8 ± 0.4	11.5 ± 0.2	48%	11.21 ± 0.07	42%
Pyrene	21.1 ± 0.6	13.5 ± 0.4	42%	13.6 ± 0.2	38%
Benzo(a)anthracene	16.4 ± 0.4	5.34 ± 0.05	22%	5.11 ± 0.04	18%
Benzo(b)fluoranthene	14.0 ± 0.4	14.3 ± 0.1	67%	13.9 ± 0.2	59%
Benzo(k)fluoranthene	5.93 ± 0.08	5.75 ± 0.02	64%	5.46 ± 0.03	54%
Benzo(j)fluoranthene	5.9 ± 0.1	5.05 ± 0.03	57%	4.82 ± 0.02	49%
Benzo(e)pyrene	18.3 ± 0.6	16.42 ± 0.08	59%	16.13 ± 0.08	52%
Benzo(a)pyrene	6.49 ± 0.07	5.56 ± 0.02	57%	5.24 ± 0.02	48%
Perylene	7.7 ± 0.4	5.63 ± 0.03	48%	5.31± 0.04	41%
Dibenz(a,c)anthracene	10.2 ± 0.3	7.59 ± 0.03	49%	7.19 ± 0.01	42%
Dibenz(a,h)anthracene	8.88 ± 0.07	8.00 ± 0.02	59%	7.57 ± 0.02	50%
Indeno(1,2,3-cd)pyrene	8.7 ± 0.2	7.79 ± 0.02	59%	7.36 ± 0.03	50%
Benzo(ghi)perylene	8.6 ± 0.1	7.90 ± 0.03	60%	7.55 ± 0.05	52%
Total PAHs	15866	3077	13%	2861	11%

3.3.3 Sunlight exposure

The %PAHs remaining in samples at different exposure times in DWH lab control, DWH, SOM and ESOM sunlight-control and sunlight-exposure are presented in Figures 3.6 – 3.9.

3.3.3.1 Lab control DWH

The % PAHs remaining in DWH lab control samples at different kinetic points are presented in Figure 3.6. In DWH lab control samples, the weathering process is majorly through evaporation. As the exposure time in fume hood increases, depletion of C_0-, C_1-, C_2-, C_3- and C_4-naphthalenes increases. As exposure time increases, C_0-phenanthrene shows little depletion, but its alkylated homologues – C_1-, C_2-, C_3- & C_4-phenanthrenes shows no depletion. Depletion of C_0-dibenzothiophene increases with increase in time, but its alkylated homologues - C_1-, C_2-, C_3- & C_4-dibenzothiophenes shows no depletion with increase in exposure time. C_0-, C_1- and C_2- fluorenes depletion increases with increase in exposure time, but C_3-fluorenes shows no depletion. C_0-, C_1-, C_2-, C_3- and C_4-chrysenes shows no depletion with increase in exposure time.

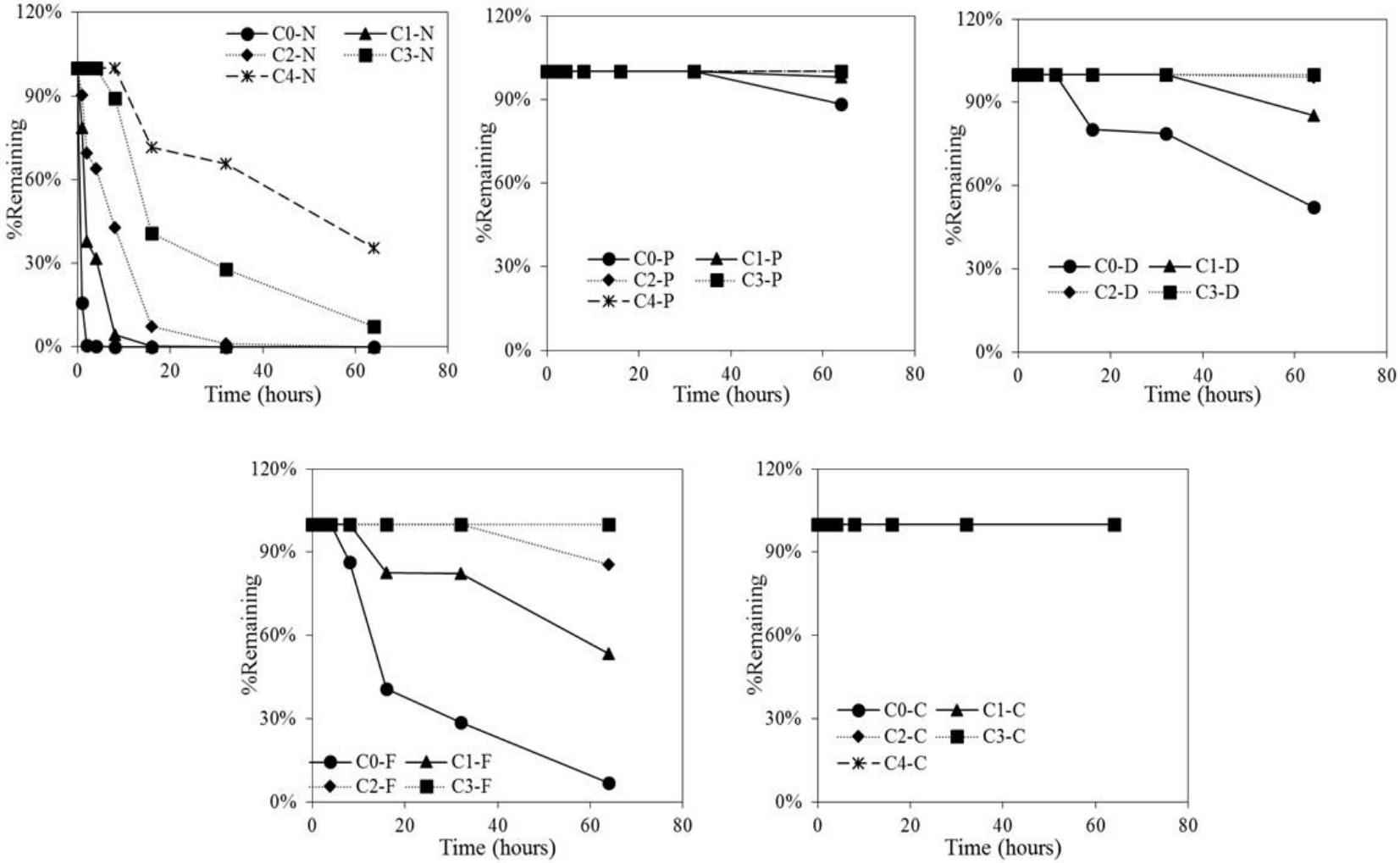

Figure 3.6: % PAHs remaining in Lab control DWH at different kinetic points

3.3.3.2 DWH

The %PAHs remaining in DWH in sunlight-control and sunlight-exposure samples are presented in Figure 3.7. C_0-, C_1-, C_2-, C_3- and C_4-naphthalenes deplete as soon as the samples are exposed to sunlight irrespective whether the samples are sunlight-control or sunlight-exposure samples. The naphthalene compounds present in sunlight-exposure samples weathers at a faster rate compared to that of control samples.

In sunlight-control samples, C_0-, C_1-, C_2-, C_3- and C_4-phenanthrenes weathering decreases with increase in alkylation and C_4-phenanthrenes shows no weathering even after 64 hours of exposure in sunlight-control sample. In sunlight-exposure samples, C_0-, C_1-, C_2-, C_3- and C_4-phenanthrenes weathering increases with increase in exposure time and at the end of 64 hours of sun light exposure more than 95% of phenanthrene and its alkylated homologues have weathered.

Weathering of C_0-, C_1-, C_2- and C_3-dibenzothiophenes in both sunlight-control and sunlight-exposure samples increases with increase in exposure time. In sunlight-exposure samples, at the end of 64 hours of exposure more than 97% of the compounds have weathered.

C_0-, C_1-, C_2- and C_3-fluorenes weather as soon as the samples are exposed to sunlight irrespective whether the samples are sunlight-control or sunlight-exposure samples. The fluorene compounds present in sunlight-exposure samples weathers at a faster rate compared to that of sunlight-control samples.

C_0-, C_1-, C_2-, C_3- and C_4-chrysenes shows little or no weathering in sunlight-control samples. In sunlight-exposure samples, weathering of C_0-, C_1-, C_2-, C_3- and C_4-chrysenes increases with increase in exposure time and alkylation.

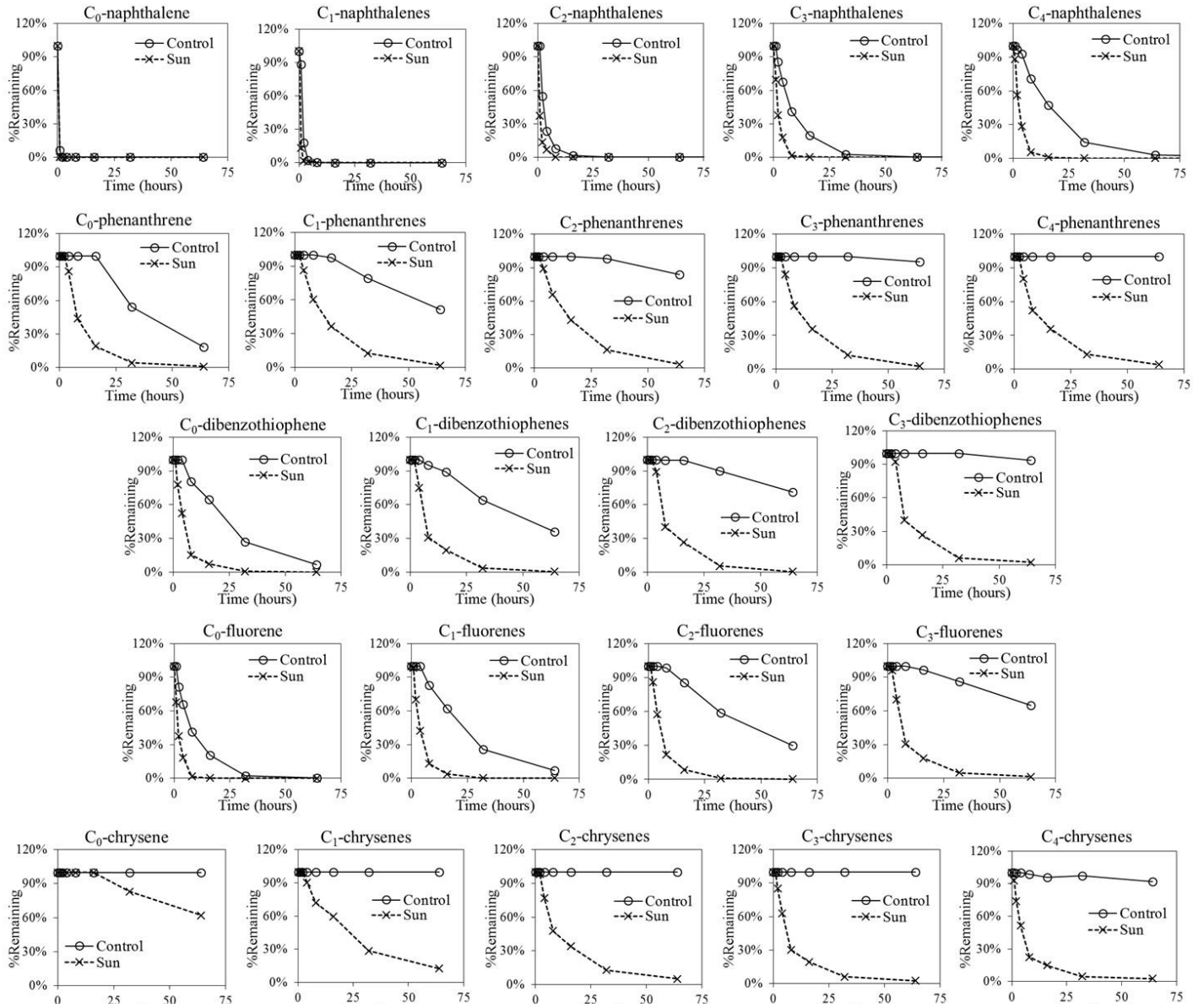

Figure 3.7: PAHs remaining in DWH samples at different kinetic points

3.3.3.3 SOM

The weathering of PAHs present in SOM in sunlight-control and sunlight-exposure samples are presented in Figure 3.8. To begin with, the SOM sample is stripped of C_0-, C_1-, C_2- and C_3-naphthalenes. The remaining C_4-naphthalenes present in SOM weather as soon as the samples are exposed to sunlight irrespective whether the samples are sunlight-control or sunlight-exposure samples. The C_4-naphthalenes present in sunlight-exposure samples depletes at a faster rate compared to that of control samples.

In sunlight-control samples, C_0-, C_1-, C_2-, C_3- and C_4-phenanthrenes weathering decreases with increase in alkylation. In sunlight-exposure samples, C_0-, C_1-, C_2-, C_3- and C_4-phenanthrenes weathering increases with increase in exposure time and at the end of 64 hours of exposure more than 95% of compounds have depleted.

In sunlight-control samples, C_0-, C_1-, C_2- and C_3-dibenzothiophenes weathering decreases with increase in alkylation. In sunlight-exposure samples, C_0-, C_1-, C_2- and C_3-dibenzothiophenes weathering increases with increase in exposure time and at the end of 64 hours of sunlight exposure more than 97% of the compounds have depleted.

C_0-, C_1-, C_2-, and C_3-fluorenes remaining in SOM deplete as soon as the samples are exposed to sunlight irrespective whether the samples are sunlight-control or sunlight-exposure. The C_0-, C_1-, C_2- and C_3-fluorenes compounds present in sunlight-exposure samples weather at a faster rate compared to that of sunlight-control samples.

C_0-, C_1-, C_2-, C_3- and C_4-chrysenes present in SOM samples shows little or no weathering either in sunlight-control or sunlight-exposure samples even after 64 hours of exposure to sunlight.

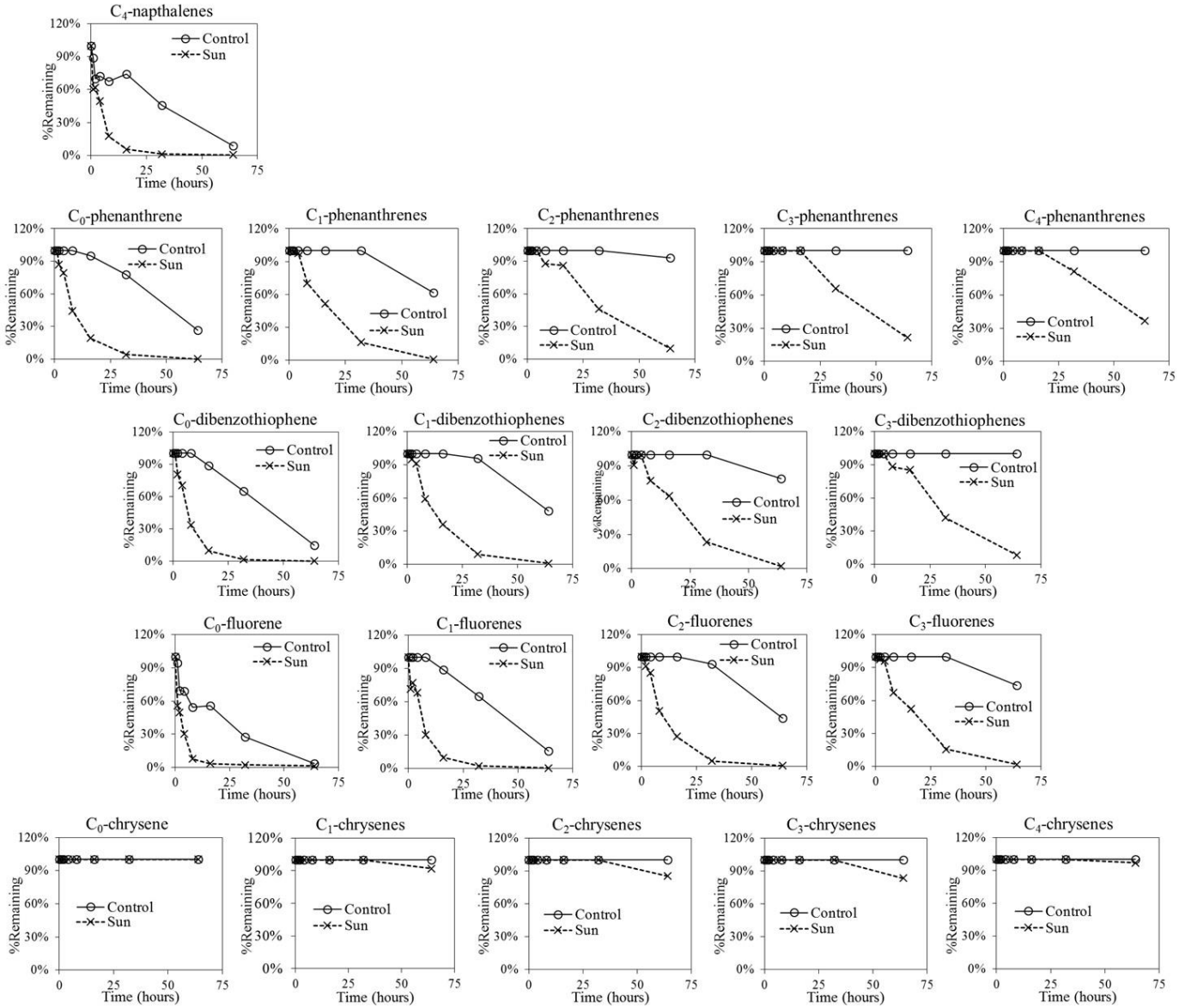

Figure 3.8: PAHs remaining in SOM samples at different kinetic points

3.3.3.4 ESOM

The weathering of PAHs present in ESOM in sunlight-control and sunlight-exposure samples are presented in Figure 3.9. Since the ESOM was prepared from SOM, there were no C_0-, C_1-, C_2- and C_3-naphthalenes. The remaining C_4-naphthalenes present in SOM weather as soon as the samples are exposed to sunlight irrespective whether the samples are sunlight-control or sunlight-exposure samples. The C_4-naphthalenes present in sunlight-exposure weathers at a faster rate compared to that of sunlight-control samples.

In control samples, C_0-, C_1-, C_2-, C_3- and C_4-phenanthrenes weathering decreases with increase in alkylation. In sunlight-exposure samples, C_0-, C_1-, C_2-, C_3- and C_4-phenanthrenes weathering increases with increase in exposure time and at the end of 64 hours of exposure more than 95% of compounds have weathered.

In sunlight-control samples, C_0-, C_1-, C_2- and C_3-dibenzothiophenes weathering decreases with increase in alkylation. In sunlight-exposure samples, C_0-, C_1-, C_2- and C_3-dibenzothiophenes weathering increases with increase in exposure time and at the end of 64 hours of sunlight exposure more than 97% of the compounds have weathered.

C_0-, C_1-, C_2-, and C_3-fluorenes remaining in ESOM weather as soon as the samples are exposed to sunlight irrespective whether the samples are sunlight-control or sunlight-exposure. The C_1-, C_2- and C_3-fluorenes compounds present in sunlight-exposure samples weathers at a faster rate compared to that of control samples.

In sunlight-control samples, C_0-, C_1-, C_2-, C_3- and C_4-chrysenes shows little or no weathering. In sunlight-exposure samples unlike in SOM, the C_0-, C_1-, C_2-, C_3- and C_4-chrysenes present in ESOM weather with increase in exposure time.

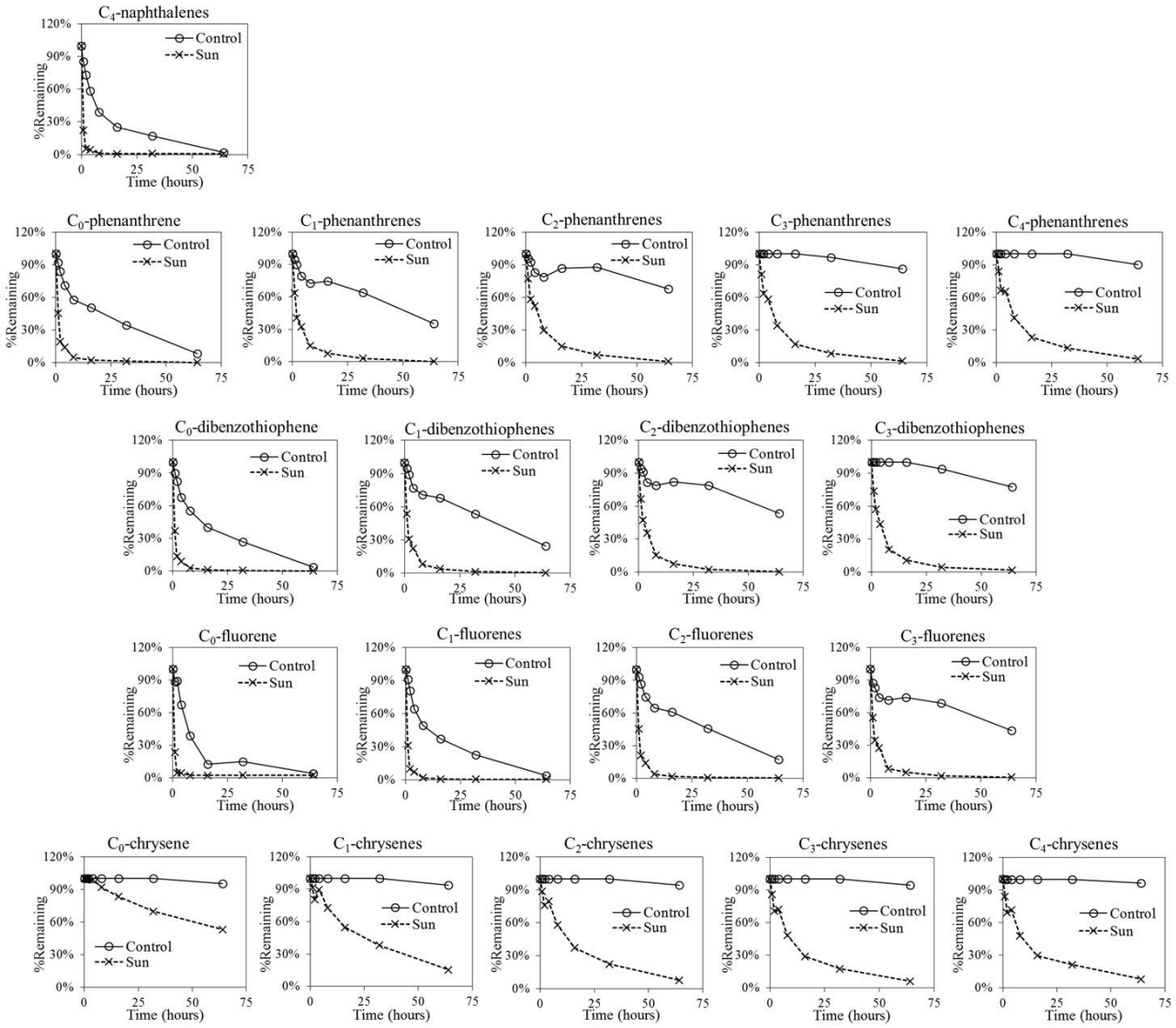

Figure 3.9: PAHs remaining in ESOM samples at different kinetic points

3.3.4 Estimation of physical and chemical properties

The vapor pressure and *HOMO-LUMO* were determined for all five groups of PAHs – 1) C_0- to C_4-naphthalenes, 2) C_0- to C_4-phenanthrenes, 3) C_0- to C_3-dibenzothiophenes, 4) C_0- to C_3-fluorenes and 5) C_0- to C_4-chrysenes. The estimated physical and chemical properties are presented in appendix Table A4 to A8.

3.3.4.1 Vapor Pressure

The evaporation rate is directly proportional to vapor pressure and higher vapor pressure implies that the compound is volatile and lower vapor pressure implies that the compound is non-volatile (Mackay and van Wesenbeeck, 2014; Stiver and Mackay, 1984). The vapor pressure decreases with increase in alkylation and molecular weight. C_0- to C_4-naphthalenes has the highest vapor pressure whereas C_0- to C_4-chrysenes has the least vapor pressure among the five groups of PAHs

3.3.4.2 HOMO-LUMO

When PAHs are exposed to sunlight or constant light conditions, the *HOMO-LUMO* gap can be used as an indicator of wavelengths being absorbed (Mekenyan et al., 1995). Mekenyan et al (1995) has stated that most phototoxic PAHs have a *HOMO-LUMO* gap of 6.8 – 7.6 eV and further explained the occurrence of this phenomenon which is as follows. The PAHs having higher *HOMO-LUMO* gap (> 7.6 eV), have the inability to absorb the wavelengths found in the sunlight and thus has increased chemical stability even when exposed to sunlight. For compounds having lesser *HOMO-LUMO* gap (<6.8 eV), the amount of energy absorbed is lesser and have lower stability in water to impart any effect. On the other hand, compounds having a *HOMO-LUMO* gap of 6.8 – 7.6 eV, absorb

more energy from the sunlight implying that these compounds are more photoactive. The *HOMO-LUMO* gap for naphthalene, phenanthrene, dibenzothiophene and fluorene and their respective alkylated homologues are greater than 7.6 eV. For chrysene and its alkylated homologues the *HOMO-LUMO* gap is about 7.6 eV.

3.4 Discussion

3.4.1 Naphthalene and its alkylated homologues

The vapor pressure of naphthalene and its alkylated homologues decreases with increase in alkylation, implying that as alkylation increases, weathering during to evaporation decreases. This is observed our dataset. Further vapor pressure is directly proportional to temperature and as temperature increases, vapor pressure increases and eventually the rate of evaporation (Sage and Sage, 2000). Naphthalene and its alkylated homologues weather at a faster rate in sunlight-exposure DWH samples compared to either sunlight-control DWH or DWH lab control samples.

HOMO-LUMO gap for naphthalene and its alkylated homologues is estimated to be greater than 7.6 eV and this indicates that photo-oxidation is not a major degradation pathway for this group of PAHs.

It is clear that for C_4-naphthalenes remaining in SOM, the major weathering pathway is through evaporation and their evaporation increases with increase in temperature when exposed to sunlight.

3.4.2 Phenanthrene and its alkylated homologues

The vapor pressure of phenanthrene and its alkylated homologues decreases with increase in alkylation, implying that as alkylation increases, weathering during to

evaporation decreases. This is observed in the dataset. As discussed earlier, vapor pressure is directly proportional to temperature and as temperature increases, vapor pressure increases and eventually the rate of evaporation(Sage and Sage, 2000). In DWH lab control, phenanthrene and its alkylated homologues shows little or no weathering, in sunlight-control samples of DWH, SOM and ESOM, shows moderate weathering but in sunlight-exposure samples of DWH, SOM and ESOM, the compounds weather more rapidly when exposed to sun.

HOMO-LUMO gap for phenanthrene and its alkylated homologues is estimated to be above 7.6 eV and this indicates that photo-oxidation is not a major degradation pathway for this group of PAHs.

It is clear that for phenanthrene and its alkylated homologues trapped in SOM, the major weathering pathway is through evaporation and its evaporation increases with increase in temperature when exposed to sunlight.

3.4.3 Dibenzothiophene and its alkylated homologues

The vapor pressure of dibenzothiophene and its alkylated homologues too decreases with increase in alkylation, implying that as alkylation increases, weathering during to evaporation decreases. This is observed in the dataset in DWH lab control samples. As temperature increases, vapor pressure proportionally increases and thus the evaporation (Sage and Sage, 2000). This could be seen in the dataset as dibenzothiophene and its alkylated homologues shows more weathering in sunlight-control samples and much more weathering in sunlight-exposed samples compared to DWH lab control samples.

HOMO-LUMO gap for dibenzothiophene and its alkylated homologues is estimated to be above 7.6 eV and this indicates that photo-oxidation is not a major degradation pathway for this group of PAHs.

Similar to that of phenanthrenes, it is clear that for dibenzothiophene and its alkylated homologues trapped in SOM, the major weathering pathway is through evaporation and its evaporation increases with increase in temperature when exposed to sunlight.

3.4.4 Fluorene and its alkylated homologues

The vapor pressure of fluorene and its alkylated homologues too decreases with increase in alkylation, implying that as alkylation increases, weathering during to evaporation decreases. This is observed in the dataset in DWH lab control samples. As temperature increases, vapor pressure proportionally increases and thus the evaporation (Sage and Sage, 2000). This could be seen in the dataset as fluorene and its alkylated homologues shows more weathering in sunlight-control samples and much more weathering in sunlight-exposure samples compared to DWH lab control samples.

HOMO-LUMO gap for fluorene and its alkylated homologues is estimated to be much above 7.6 eV and this indicates that photo-oxidation is not a major degradation pathway for this group of PAHs.

Similar to that of phenanthrenes and dibenzothiophenes, it is clear that for fluorene and its alkylated homologues trapped in SOM, the major weathering pathway is through evaporation and its evaporation increases with increase in temperature when exposed to sunlight.

3.4.5 Chrysene and its alkylated homologues

The vapor pressure of chrysene and its alkylated homologues is lowest compared to other four groups of PAHs. It is clear that evaporation is not the major weathering pathway for chrysene and its homologues unlike the other four groups of PAHs. The DWH lab control and sunlight-control samples of DWH, SOM and ESOM datasets also proves this.

HOMO-LUMO gap for chrysene and its alkylated homologues is estimated to be about 7.6 eV, implying that this group of compounds are able to absorb more energy from the sunlight and weather by photo-oxidation. This could be observed in our dataset. There is no weathering of chrysene and its alkylated homologues in either DWH lab control or sunlight-control samples of DWH, SOM and ESOM samples, but they weather rapidly in sunlight-exposure samples of DWH and ESOM. In sunlight-exposure SOM samples weathering increased with increase in alkylation, but the weathering rate is very slow compared to that of ESOM. This may be due to interference from sand particles present in the SOM samples as SOM is predominantly composed of sand (>87%).

Unlike other groups of PAHs, the major weathering pathway for chrysene and its alkylated homologues is indeed photo-oxidation and the SOM has to be exposed to sunlight to promote further weathering of chrysene and its alkylated homologues trapped in these deposits.

3.5 Conclusion

The sunlight has a major influence on the weathering patterns of all five groups of PAHs – (1) C_0- to C_4-naphthalenes, (2) C_0- to C_4-phenanthrenes, (3) C_0- to C_3-

dibenzothiophenes, (4) C_0- to C_3-fluorenes, (5) C_0- to C_4-chrysenes present in SOM. Sunlight enhances the weathering rate of PAHs trapped in SOM. Our data clearly shows that when the SOM is re-exposed to sunlight the PAHs trapped in these residues will undergo weathering primarily through evaporation and photo-oxidation. However, the daughter products formed due to photo-oxidation processes are largely unknown and therefore further studies are needed to identify the by-products of photo-oxidation reactions and to evaluate the ecological impacts of these degradation products.

Chapter 4

Development and application of an analytical method using gas chromatography/triple quadrupole mass spectrometry for characterizing alkylated chrysenes in crude oil samples

4.1 Introduction

Polycyclic aromatic hydrocarbons (PAHs) and their alkylated homologues are a class of common organic environmental contaminants that contain two or more aromatic rings (Neff, 1979). They are naturally found in organic substances such as crude oil, coal and creosote. They are also formed during incomplete combustion of coal, oil, gas or other organic substances (ATSDR, 1995; Lien et al., 2007). It is well established that alkylated homologues of certain PAHs (known as alkylated PAHs) can be high in abundance in environmental samples, and, in some cases, can be more toxic than their parent PAHs (Turcotte et al., 2011; Wang et al., 2007). Also, certain groups of alkylated PAHs in crude oil released into the marine environment, (for example, alkylated chrysenes), are highly resistant to natural weathering processes such as volatilization, photo-oxidation, and biodegradation (Chaillan et al., 2006; Wang et al., 1998a; Wang and Fingas, 2003). Furthermore, due to their low aqueous solubility, the relative concentrations of some of these PAHs can concentrate over time under certain environmental conditions (Wang et al., 1994c). These properties make chrysene and alkylated chrysenes excellent indicator compounds for assessing the impacts of large-scale environmental events such as oil spills.

In this study we focus on four homologues of alkylated chrysenes (C_1 to C_4-chrysenes). In general, alkylated chrysenes are commonly estimated using GC/MS methods (Fernández-González et al., 2008; Schantz and Kucklick, 2011; Wang and Fingas, 2003). The efficiency of GC/MS methods depend on the level of interference from the sample matrix, and lower detection limits can be achieved only after extensive sample clean-up procedures prior to analysis (Fernández-González et al., 2008). Recent advances in mass spectrometry have led to the development of triple quadrupole mass spectrometry (or GC/MS/MS) that allows identification of low concentration target analytes in complex samples with greater certainty by minimizing or removing matrix interferences (Pitarch et al., 2007). This is achieved by monitoring multiple reactions that yield precursor ions from the electron ionization process and characteristic product ions from collision cell reactions of selected precursor ions. Fernández-González et al. (2008) completed a comparison study and has shown that GC/MS/MS methods can avoid interferences in biota samples, and they can also yield lower detection limits. Pitarch et al. (2007) quantified various semi volatile organic compounds in water samples and concluded that GC/MS/MS methods can lead to excellent selectivity and sensitivity.

Currently, there are no published GC/MS/MS methods available for accurately identifying and quantifying different types of alkylated chrysenes present in environmental samples. The objective of this effort was to develop a robust analytical method using gas chromatography–triple quadrupole mass spectrometry to characterize alkylated chrysenes in crude oil and/or weathered oil spill samples. In this work, a new GC/MS/MS instrument was used to first study the mass fragmentation patterns of several commercially available alkylated chrysenes standards using full scan and product-ion scan modes. These

experimental data were then used to predict the mass fragmentation patterns of other isomers of chrysene homologues for which standards were not available. Both experimental and theoretical mass fragmentation data were then combined to develop a GC/MS/MS method for identifying and quantifying the total concentrations of C_1-, C_2-, C_3-, and C_4-chrysene homologues in crude oil samples. The developed method was tested to characterize alkylated chrysenes in MC252 crude oil which was spilled into the Gulf of Mexico waters during the 2010 *Deepwater Horizon* oil spill event. Note parts of this chapter were recently published in a Rapid Communications in Mass Spectrometry journal article, which was co-authored by this author (John et al., 2014).

4.2 Experimental methods

4.2.1 Materials

High purity standards chrysene (purity > 98%), C_1-chrysenes (1-methylchrysene, 2-methylchrysene, 3-methylchrysene), C_2-chrysene (6-ethylchrysene), C_3-chrysenes (6-n-propylchrysene, 1,3,6-trimethylchrysene) and C_4-chrysene (6-n-butylchrysene) were purchased from Chiron AS (Trondheim, Norway). All alkylated chrysene homologue standards were of purity greater than 99%. Chrysene-d_{12} (purity > 99.9%) was purchased from Supelco (Bellefonte, PA, USA). *p*-terphenyl-d_{14} (purity > 98.5%) and pyrene-d_{10} (purity > 98.6%) were purchased from AccuStandard (New Haven CT, USA). Hexane and dichloromethane were purchased from VWR International (Suwanee, GA, USA). All organic solvents used in this study were of reagent grade. GC capillary columns (J&W DB-EUPAH, 20 m x 0.18 mm x 0.14 µm, p/n 121-9627) and deactivated GC liners (splitless tapered glasswool) were purchased from Agilent Technologies (Wilmington, DE, USA). MC252 crude oil was provided by British Petroleum (BP).

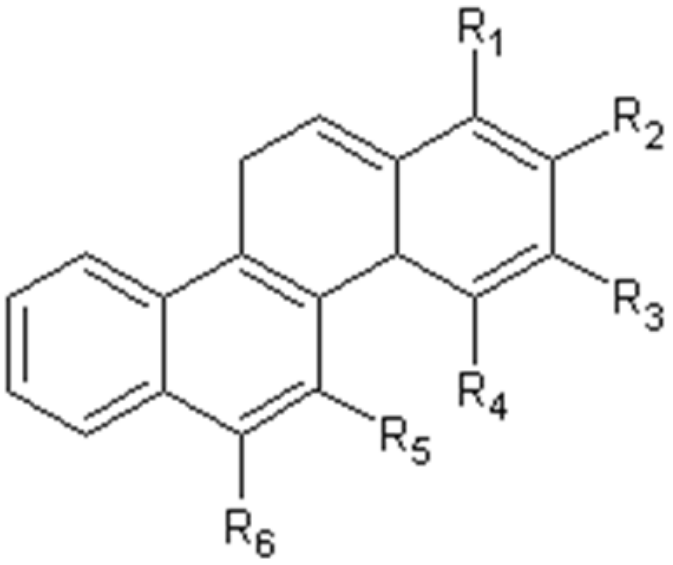

Chrysene	: $R_1 = R_2 = R_3 = R_4 = R_5 = R_6 = H$
1-methylchrysene	: $R_2 = R_3 = R_4 = R_5 = R_6 = H$; $R_1 = CH_3$
2-methylchrysene	: $R_1 = R_3 = R_4 = R_5 = R_6 = H$; $R_2 = CH_3$
3-methylchrysene	: $R_1 = R_2 = R_4 = R_5 = R_6 = H$; $R_3 = CH_3$
6-ethylchrysene	: $R_1 = R_2 = R_3 = R_4 = R_5 = H$; $R_6 = C_2H_5$
6-n-propylchrysene	: $R_1 = R_2 = R_3 = R_4 = R_5 = H$; $R_6 = C_3H_7$
1,3,6-trimethylchrysene	: $R_2 = R_4 = R_5 = H$; $R_1 = R_3 = R_6 = CH_3$
6-n-butylchrysene	: $R_1 = R_2 = R_3 = R_4 = R_5 = H$; $R_6 = C_4H_9$

Figure 4.1: Structure of chrysene and alkylated chrysene standards used in this study

4.2.2 Preparation of weathered oil under laboratory conditions

MC252 crude oil (1 mL) was transferred into an aluminum pan (5 cm diameter and 1.5 cm deep) and was evaporated for 7 days within a laboratory fume hood (Mott Manufacturing Limited, Ontario, Canada) at a face velocity of 200 feet per minute (fpm). The weathering process was completed at room temperature (22 ºC) and the resulting evaporated crude oil was designated as “Weathered MC252 oil”.

4.2.3 Column Chromatographic Fractionation

Fractionation of oil samples was conducted using methods similar to those discussed in earlier research (Luellen and Shea, 2002; Wang et al., 1994a). Activated silica

gel was prepared using the methods outlined in Wang et al., (1994a). Anhydrous sodium sulfate was purified by heating at 400°C. A glass column (10.1 mm diameter and 200 mm length) was plugged with glass wool, and about 3 g of activated silica gel was added to the column, followed by 1 g of anhydrous sodium sulfate. 20 mL of hexane was then added to the column. About 25 mg of oil sample was weighed in a 12 mL glass vial and spiked with surrogates *p*-terphenyl-d_{14} and pyrene-d_{10}. The contents were then extracted with 1 mL of hexane and transferred to the column. The vial was then sequentially washed with 2 mL of hexane, with 1 mL in each step, and the contents were transferred to the column. All solvents eluted from the column prior to this step were discarded. 12 mL of hexane was then used to elute aliphatic hydrocarbon fractions from the sample. The hexane-eluted fraction was labeled as F1. Next, a 50% hexane and 50% dichloromethane solvent mixture (15 mL) was used to elute all aromatic hydrocarbon fractions, and this fraction was labeled as F2. The F1 and F2 fractions were concentrated under a gentle stream of nitrogen gas and then reconstituted in 10 mL of hexane and hexane:dichloromethane solvent mixture (ratio of 1:1) for each fraction, respectively. The sample was filtered through 0.2 µm PTFE filters, spiked with internal standard (IS) chrysene-d_{12}, and analyzed for alkylated chrysenes. All the samples were prepared in duplicate and analyzed in triplicate.

4.2.4 Instrument

An Agilent 7890 gas chromatograph coupled with an Agilent 7000B triple quadrupole (QqQ) mass spectrometer, fitted with electron ionization (EI) source and a collision cell were used. Various analytical experiments were completed using this instrument running under different conditions including full scan, product-ion scan, and

multiple reaction monitoring (MRM) modes. The GC and MS conditions used are summarized in Table 4-1.

Table 4-1: Gas chromatograph and Mass spectrometer parameters

GC Conditions	
Column	DB-5MS (J&W Agilent Technologies, 20 mx 180 µm x 0.14 µm)
Inlet Temperature	300 °C
Inlet Pressure	22.151 psi
Carrier gas	Helium
Flow rate	0.8 mL/min
Injection mode	Pulsed splitless
Oven Program	50 °C (0.8 minutes hold); 40 °C/minute to 250 °C (2 minutes hold); 0.5 °C/minute to 260 °C (2 minutes hold); 30 °C/minute to 325 °C (1 minute hold)
Total run time	32.97 minutes
Injection volume	1 µL
Transfer line temperature	320 °C
MS Conditions	
Delta EMV	-70 eV
Acquisition parameters	Electron Ionization (EI)
Solvent Delay	2.5 minutes
MS source temperature	350 °C
Quadrupole temperatures	Q1 = Q2 = 180 °C

4.2.5 Full Scan Analysis

To identify the appropriate precursor ions, high concentrations of target analytes (5 mg/L) were prepared by diluting the standards in a solvent mixture of hexane and dichloromethane (ratio of 1:1). These samples were then run in the full scan mode, scanning from *m/z* of 50 to 300. Results of the full scan analysis were used to select the precursor ion for each homologue.

4.2.6 Product Ion Scan Analysis

Product ion (PI) scan analysis was completed to obtain the product ion spectrum of each precursor ion at various collision energies (ranging from 5 to 40 eV). For facilitating collision induced dissociation (CID) of the precursor ion, ultra high purity

nitrogen was delivered to the collision cell at a flow rate of 1.5 mL/min, and helium was delivered at a flow rate of 2.3 mL/min to quench the reactions. From the product ion spectrum of a precursor ion the most abundant set of product ions and the optimal level of collision energy required to obtain these ions, were selected.

4.2.7 Multiple Reaction Monitoring (MRM) Analysis

The combination of precursor ion, the most intense product ion and its corresponding optimal collision energy determined form the MRM transition for each analyte. For each analyte, two different MRM transitions were monitored - one as a quantitative transition and other as a confirmatory transition.

4.3 Results and discussion

4.3.1 Full Scan Analysis

The mass spectra of alkylated chrysene standards are shown in Figure 4.2. For C_1-chrysenes, the data show that the predominant ion is at *m/z* of 242 in the mass spectrum, corresponding to its molecular ion ($[M]^+$) as the aromatic ring cleavage process requires relatively higher energy (McLafferty and Tureček, 1993). Other characteristic ions at *m/z* of 241 and 239 are also observed. All three C_1-chrysene isomers have similar mass spectra.

For C_2-chrysene (6-ethylchrysene) the data show that the predominant ion is at *m/z* of 241 (Figure 4.2), which can be yielded by the rupture of benzylic bond of the ethyl group (McLafferty and Tureček, 1993). Other characteristic ions observed are at *m/z* of 256 ($[M]^+$) and 239.

For 1,3,6-trimethylchrysene, the data show that the predominant ion is at *m/z* of 270 ($[M]^+$) which is similar to C_1-chrysene reaction were higher energy is required to cleave

aromatic ring (McLafferty and Tureček, 1993); other major ions observed are at *m/z* of 255 and 239. The predominant ion for 6-n-propylchrysene is at *m/z* of 241 corresponding to rupture of benzylic bond of propyl group eliminating the ethyl group (McLafferty and Tureček, 1993); other major ions observed are at *m/z* of 270 ($[M]^+$) and 239.

For 6-n-butylchrysene, (a C_4-chrysene) the data show that the predominant ion in the mass spectrum is at *m/z* of 241 corresponding to rupturing of benzylic bond of butyl group eliminating propyl group (McLafferty and Tureček, 1993). Other characteristic ions observed are at *m/z* of 284 ($[M]^+$) and 239.

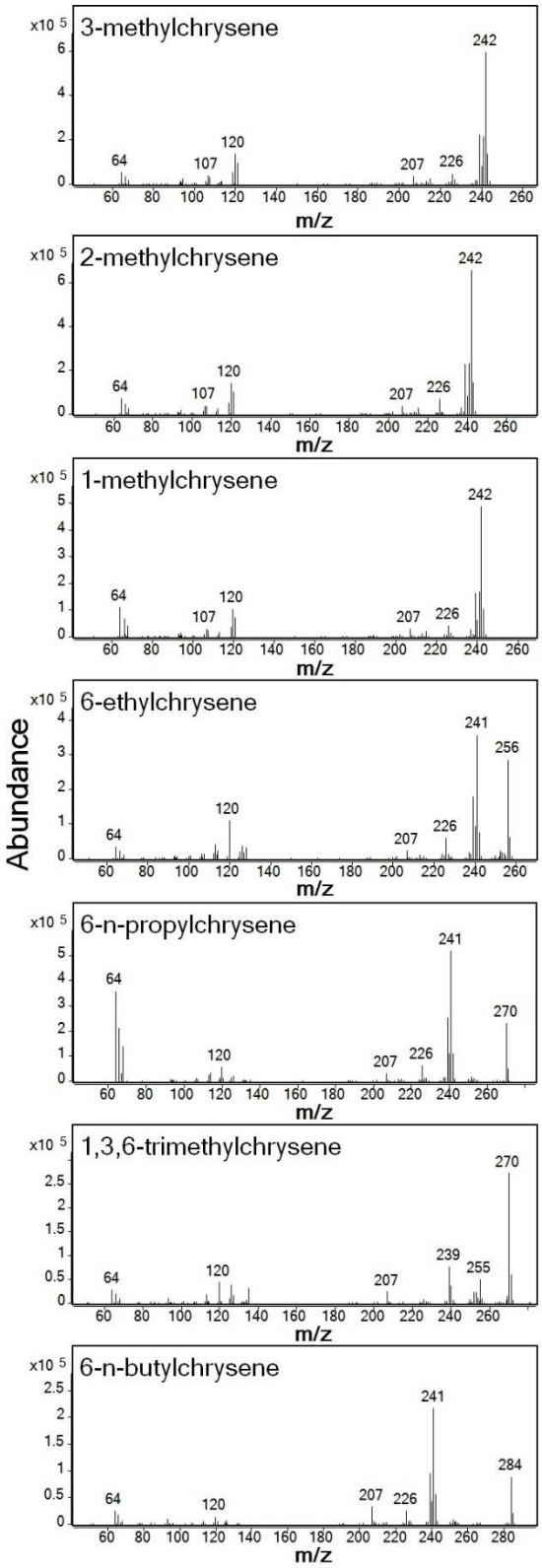

Figure 4.2: Full scan electron ionization mass spectra for the seven alkylated chrysene standards

4.3.2 Analysis of quantitative MRM transitions from experimental data

The parent chrysene molecule, chrysene-d_{12} and the surrogates *p*-terphenyl-d_{14} and pyrene-d_{10} have been studied extensively by others and the expected MRM transitions can be inferred from the literature data (Sapozhnikova and Lehotay, 2013; Xia et al., 2012). However, the product ion information is not available for any alkylated chrysenes. In all our PI scan experiments, we selected the molecular ions ($[M]^+$) as precursor ions since we observed prominent molecular ion peaks for all four alkylated chrysene homologues (Figure 4.2). The mass scan range in PI scan experiment for each pure alkylated chrysene standard varied from *m/z* of 50 to mass of the molecular ion ($[M]^+$).

Typical PI scans collected at 20 eV for all pure alkylated chrysene standards are shown in Figure 4.3. For all three C_1-chrysenes, the predominant product ion is at *m/z* of 241, and this corresponds to the loss of one hydrogen (McLafferty and Tureček, 1993) from the precursor ion at *m/z* of 242. Since CID of the precursor ion would depend on the amount of collision energy, we further extended the PI scan to estimate the optimal energy level for the transition that yielded maximum product ion response. The maximum intensity of predominant product ion (*m/z* of 241) occurred at a collision energy of 20 eV (Figure 4.4). The optimal MRM transition for C_1-chrysenes is 242 → 241 at collision energy of 20 eV.

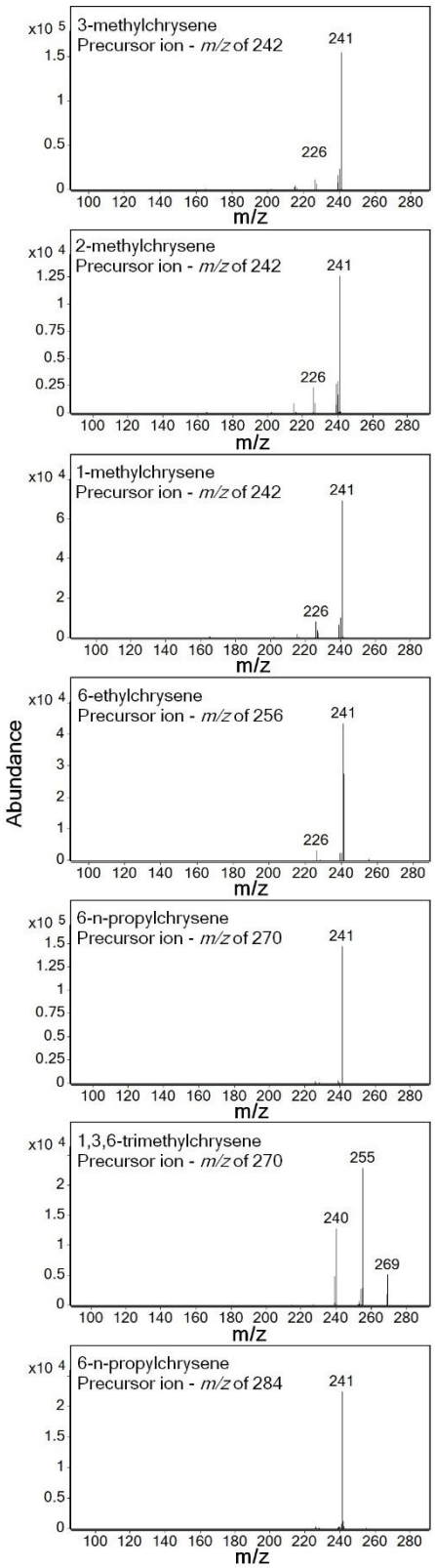

Figure 4.3: Product ion scan mass spectra for the seven alkylated chrysene standards at collision energy of 20 eV (precursor ions selected are reported in the respective figures)

For 6-ethylchrysene, a C_2-chrysene, the predominant product ion was observed at *m/z* of 241, which can be yielded by eliminating a methyl group from its $[M]^+$. The maximum intensity of predominant product ion occurred at the collision energy level of 15 eV (Figure 4.4). Therefore, the optimal MRM transition for this type of C_2-chrysene was 256 → 241 at a collision energy of 15 eV.

The data from Figure 4.3 shows that the most significant product ion for 1,3,6-trimethychrysene is at *m/z* of 255, which is yielded by a ring-alkyl bond cleavage reaction (McLafferty and Tureček, 1993). The most significant product ion for 6-n-propylchrysene is at *m/z* of 241, which is yielded by a reaction where the benzylic bond of the propyl group is ruptured, eliminating an ethyl group from its $[M]^+$ (*m/z* of 270). Based on these results, we selected 270 → 255 as the MRM transition for monitoring C_3-chrysenes that have three methyl groups and selected 270 → 241 as the MRM transition for monitoring C_3-chrysenes that have a propyl group. Figure 4.4 shows that the optimal collision energy levels for monitoring the ions at *m/z* of 255 and 241 are at 20 and 15 eV respectively. Therefore, the optimal MRM transitions of 270 → 255 and 270 → 241 are set at collision energies of 20 and 15 eV, respectively.

For 6-n-butylchrysene, a C_4-chrysene, the data (Figure 4.3) show that the most significant product ion is at *m/z* of 241, which is yielded by a reaction where the benzylic bond of the butyl group is ruptured eliminating a propyl group from its $[M]^+$ (*m/z* of 284). The maximum intensity of predominant product ion occurred at a collision energy of 15 eV (Figure 4.4). Therefore, the optimal MRM transition selected for this type of C_4-chrysene is 284 → 241 at collision energy of 15 eV.

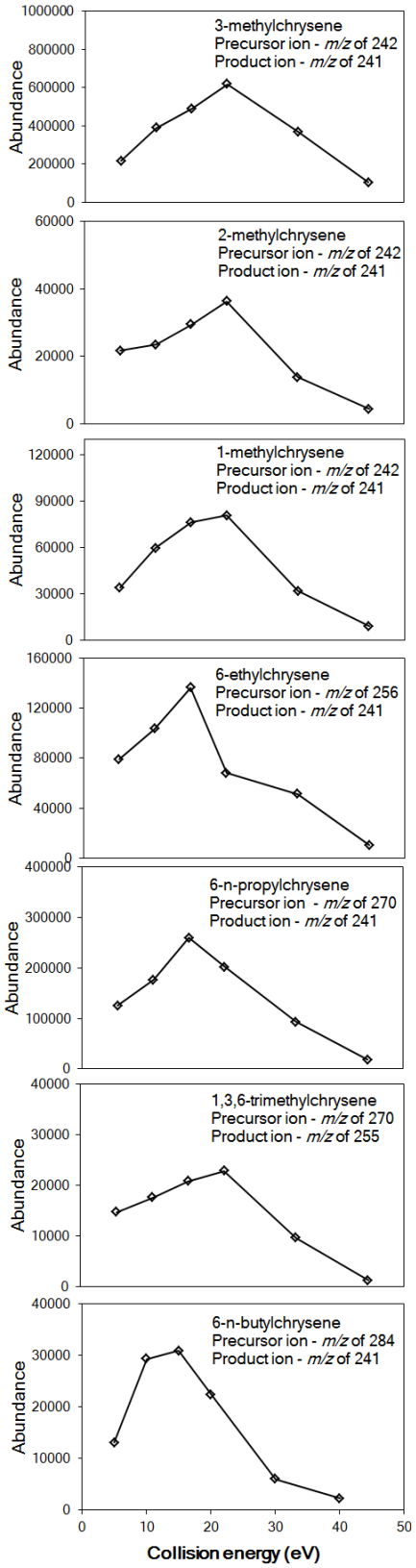

Figure 4.4: Collision energy optimization data for the seven alkylated chrysene standards (precursor and product ions selected are reported in the respective figures)

4.3.3 Analysis of quantitative MRM transitions from literature data

For C_2-chrysene, the PI scan data (of 6-ethylchrysene standard) indicated that 256 → 241 MRM transition would capture all ethyl-type C_2-chrysenes. However, C_2-chrysenes can also have two methyl groups. McLafferty and Tureček (McLafferty and Tureček, 1993) discussed dimethylbenzenes data to show that the predominant ion would be yielded by removing one of the methyl groups. Therefore, 256 → 241 MRM transition, which was originally identified to capture ethyl-type C_2-chrysenes, would also naturally capture C_2-chrysenes involving two methyl groups.

From the C_3-chrysene dataset, we know multiple MRM transitions are needed to capture compounds having three different types of alkylations. Based on the PI scan data of C_3-chrysene standards, we have already assigned 270 → 255 MRM transition for monitoring C_3-chrysenes having three methyl groups, and assigned 270 → 241 MRM transition for monitoring C_3-chrysenes having a propyl group. However, C_3-chrysene compounds can also have an ethyl and methyl groups. Based on our PI scan analysis of 1,3,6-trimethylchrysene (maximum intensity of product ion at *m/z* of 255 at 20 eV) and 6-n-propylchrysene (maximum intensity of product ion at *m/z* of 241 at 15 eV) it is easier to rupture the benzylic bond of the ethyl group than a ring-alkyl bond cleavage of a methyl group; hence, the significant product ion for C_3-chrysene having an ethyl group and a methyl group will be at *m/z* of 255. Isopropylchrysene is also a C_3-chrysene and the predominant ion would be at *m/z* of 255 corresponding to loss of one of the methyl groups similar to isopropylbenzene (Linstrom and Mallard). Therefore, the 270 → 255 MRM transition, originally assigned to monitor C_3-chrysenes having three methyl groups, would also capture C_3-chrysene having an ethyl group and a methyl group and isopropylchrysene.

For C_4-chrysene, the PI scan data (of 6-n-butylchrysene) indicated that 284 → 241 MRM transition would capture all butyl-type C_4-chrysenes. However, C_4-chrysenes can also have other alkylation types with compounds involving: a) four methyl groups, b) two ethyl groups c) a methyl and a propyl group d) isobutylchrysene and e) tert-butylchrysene. For C_4-chrysenes containing four methyl groups, the characteristic ion would be at *m/z* of 269 because of the loss of one of the methyl groups due to ring-alkyl cleavage, as illustrated for the 1,3,6-trimethylchrysene dataset. Therefore 284 → 269 MRM transition is used to capture all C_4-chrysenes containing four methyl groups. Interestingly for C_4-chrysenes containing two ethyl groups the characteristic ion would also be *m/z* of 269 due to the loss of one of the methyl groups from rupturing of the benzylic bond in one of the ethyl groups, as illustrated for the 6-ethylchrysene dataset. Furthermore, for tert-butylchrysene, the predominant ion would be at *m/z* of 269 corresponding to the loss of a methyl group, similar to tert-butylbenzene (Linstrom and Mallard). Therefore, 284 → 269 MRM transition, used to capture C_4-chrysenes having four methyl groups, would also naturally capture the C_4-chrysenes containing two ethyl groups and tert-butylchrysene. We selected the collision energy for this transition as 20 eV.

For C_4-chrysenes containing a methyl and a propyl group the characteristic ion would be at *m/z* of 255 because of the loss of ethyl from the propyl group due to the rupture of the benzylic bond of the propyl group, as illustrated using the 6-n-propylchrysene dataset. For isobutylchrysene, the predominant ion would be at *m/z* of 241corresponding to loss of $\cdot CH(CH_3)_2$ similar to isobutylbenzene (Linstrom and Mallard). Therefore 284 → 255 MRM transition is used to capture all C_4-chrysenes having a methyl and a propyl group and tert-butylchrysene, with the selected collision energy for this transition as 15 eV.

4.3.4 Selection of confirmatory MRM transitions from experimental data

The confirmatory MRM transitions are chosen to improve the selectivity and sensitivity of GC/MS/MS MRM methods (Nácher-Mestre et al., 2009). Full scan of all seven alkylated chrysene standards yielded *m/z* of 239, although the intensities differed. Furthermore, PI scans of all the compounds, when completed at higher collision energy levels, yielded *m/z* of 239. The overall response of this ion increased as the collision energy level was increased. Therefore, we used the following four confirmatory MRM transitions: 242 → 239, 256 → 239, 270 → 239 and 284 → 239 to verify C_1-, C_2-, C_3- and C_4-chrysene homologues respectively. The collision energy levels for all these confirmatory transitions are set at 40 eV. A detailed summary of the proposed MRM method is presented in Table 4-2. The relative abundance of quantitative transitions to that of confirmatory transitions for *p*-terphenyl-d_{14}, pyrene-d_{10}, chrysene, 3-methylchrysene, 2-methylchrysene, 1-methylchrysene, 6-ethylchrysene, 6-n-propylchrysene, 1,3,6-trimethylchrysene and 6-n-butylchrysene are 1.30, 1.14, 76.44, 1.48, 1.49, 1.53, 2.67, 3.85, 0.89 and 4.19, respectively.

Table 4-2: Summary of optimized MRM transitions used for quantifying various target compounds

Homologue/ Compound	Quantitative Transitions		Confirmatory Transitions	
	Ions (*m/z*)	Collision Energy (eV)	Ions (*m/z*)	Collision Energy (eV)
†*p*-terphenyl-d_{14}	212 → 208	40	212 → 210	40
†Pyrene-d_{10}	244 → 212	40	244 → 160	40
†Chrysene-d_{12}	240 → 236	40	-	-
†Chrysene	228 → 226	38	228 → 224	38
C_1-chrysenes	242 → 241	20	242 → 239	40
C_2-chrysenes	256 → 241	15	256 → 239	40
C_3-chrysenes	270 → 241 270 → 255	15 20	270 → 239	40
C_4-chrysenes	284 → 241 284 → 255 284 → 269	15 15 20	284 → 239	40

†These MRM transitions are selected from published literature

4.3.5 Application of the MRM Method for Characterizing MC252 Crude Oil

The developed MRM method was used to characterize a complex environmental sample, MC252 crude oil which was spilled during the 2010 *Deepwater Horizon* oil spill event (Hayworth and Clement, 2011b; Mulabagal et al., 2013). One of the major unknowns of this oil spill is the fate of toxic PAHs such as chrysene and its alkylated homologues. Therefore, detailed characterization of various components of chrysene in MC252 crude oil would help provide the preliminary data required for assessing the potential human and ecological risks resulting from the oil spill. Furthermore, Mulabagal et al.,(2013) reported hopane levels in MC252 oil spill residue recovered along the Alabama shoreline and showed that the relatively fresh looking, sticky brownish oil spill samples are not degrading and hence have the potential to remain in the environment for an extended period of time (Pauzi Zakaria et al., 2001). These studies support the importance of understanding the fate of various forms of chrysenes in oil spill samples.

To accurately quantitate the concentration of alkylated chrysenes in environmental samples, pure standards of various forms of alkylated chrysenes are required; however, several of these compounds might not be available commercially. Therefore, United States Environmental Protected Agency (USEPA) methods typically use relative response factors (RRF), which are estimated based on the response of parent chrysene, to make semi-quantitative estimates of alkylated chrysenes (USEPA, 2007a). Methods that employ a parent PAH to quantify alkylated homologues can introduce large quantitation errors (Burkhardt et al., 2005). In the published literature, other simpler methods have also been proposed to make highly approximate estimates for alkylated compounds. For example, during the *Deepwater Horizon* oil spill event, USEPA recommended using a constant (factor of 5 with respect to parent chrysene) to estimate the total amount of the alkylated chrysenes in oil spill samples (USEPA, 2010).

In this study, we used seven different alkylated chrysene standards. The MRM responses of these standards (at the concentration level of 100 ng/mL) are given in Figure 4.5. Their fragmentation patterns in full scan and PI scan analysis were presented in Figures 4.2 and 4.3 respectively. The data show that all three C_1-chrysene standards (3-methylchrysene, 2-methylchrysene and 1-methylchrysene) have similar mass fragmentation patterns, and they also show similar levels of response. Therefore, any one of these pure compounds can be used as the standard to quantify C_1-chrysenes. In this effort, we selected 3-methylchrysene, which is a standard compound used in previous research efforts (Schantz and Kucklick, 2011).

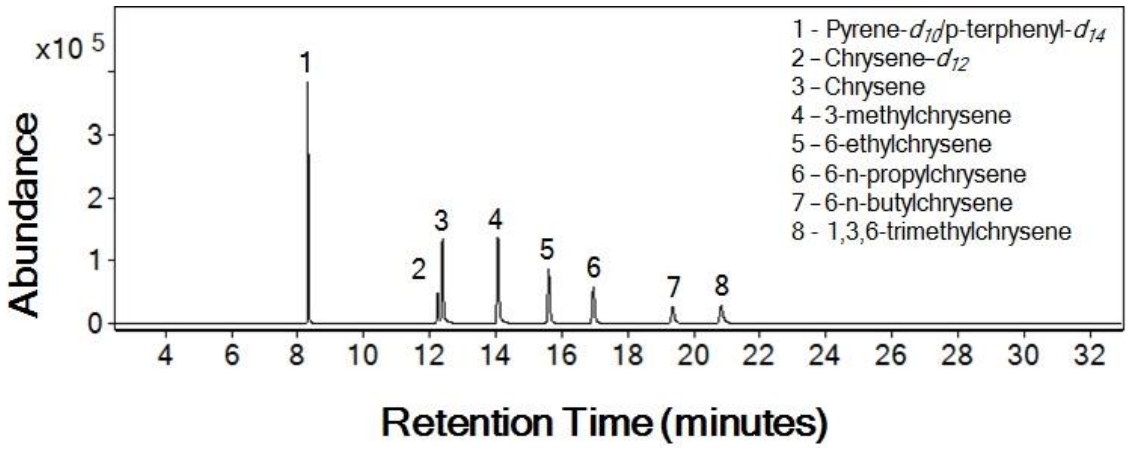

Figure 4.5: The total ion MRM chromatogram of the standard solution used for calibration

Since only one isomer is commercially available for C_2- and C_4-chrysene homologues (6-ethylchrysene for C_2 and 6-n-butylchrysene for C_4, respectively), these two compounds were used as representative calibration standards for these two homologues.

In the case of C_3-chrysenes, we had two standards that represent two distinct types of alkylation that have two different MRM transitions. We used 6-n-propylchrysene for quantifying C_3-chrysenes having the MRM transition of 270 → 241, and 1,3,6-trimethylchrysene for quantifying the MRM transition of 270 → 255.

The quantitation approach used here (which uses a distinct calibration standard for each homologue) is a robust approach for quantifying different types of chrysene homologues. A calibration stock solution consisting of 10 mg/mL of parent chrysene, 3-methylchrysene, 6-ethylchrysene, 6-n-propylchrysene, 1,3,6-trimethylchrysene, 6-n-butylchrysene, and two surrogate standards *p*-terphenyl-d_{14} and pyrene-d_{10} was prepared in a solvent mixture of hexane and dichloromethane in a ratio of 1:1. The solution was then diluted to prepare calibration standards having concentrations of 1, 2, 5, 10, 20, 50, 100, 200 and 500 ng/mL. The calibration curves were constructed using the standard

solutions. The linearity of the calibration curve was confirmed by ensuring the r^2 values were greater than 0.99 (USEPA, 2007b).

4.3.6 LOD/LOQ and Recovery Data

Limit of detection (LOD) and limit of quantitation (LOQ) for the representative compounds were determined by measuring a series of blanks with no analyte. The blank mean value and the standard deviation (SD) were calculated for each representative compounds. LOD is estimated as the mean blank value plus three times SD. LOQ is estimated as mean blank value plus ten times SD(MacDougall and Crummett, 1980). The LOD and LOQ values for the representative compounds are presented in Table 4-3.

The MC252 crude oil extract was spiked to increase the concentration by 10 and 20 ng/mL (using the following pure standards: chrysene, 3-methylchrysene, 2-methylchrysene, 1-methylchrysene, 6-ethylchrysene, 6-n-propylchrysene, 1,3,6-trimethylchrysene and 6-n-butylchrysene) prior to GC/MS/MS analysis. The recovery levels were computed using the following equation(USEPA, 1996):

$$\%R = \left(\frac{C_S - C_U}{C_n}\right) X\ 100 \qquad eqn(4.1)$$

where $\%R$ is the measured percentage recovery level, C_S and C_U are the concentration levels of the target analyte in the spiked and non-spiked samples, and C_n is the spiked concentration level (10 and 20 ng/mL). The recovery levels are summarized in Table 4-3. The overall spiked target recovery levels observed ranged from 85 to 120% and these values are well within typical spiked compounds recovery levels (USEPA, 1996).

Table 4-3: LOD and LOQ values, and percentage recovery values from spiking studies

Compound	LOD (ng/mL)	LOQ (ng/mL)	%R	
			Mean	%RSD
Chrysene	0.57	0.62	113.0	5.8
3-methylchrysene	0.11	0.12	101.8	12.6
2-methylchrysene	0.12	0.14	84.8	11.0
1-methylchrysene	0.12	0.14	84.1	9.9
6-ethylchrysene	0.92	0.93	89.8	7.0
6-n-propylchrysene	1.09	1.10	88.8	7.6
1,3,6-trimethylchrysene	0.77	0.80	118.3	6.6
6-n-butylchrysene	1.00	1.05	109.0	6.0

4.3.7 Results for MC252 Crude Oil Sample

The crude oil fractions F1 and F2 (discussed in the methods section) were analyzed and alkylated chrysenes were found only in the F2 fraction. In order to enhance sensitivity, within the MRM method, we set distinct time segments to monitor each homologue. The total ion chromatogram for the crude oil and the extracted ion chromatograms for each MRM transition are given in Figure 4.6.

To quantify the concentrations, the extracted chromatographic peaks that satisfied both quantitative and confirmatory MRM transitions of a homologue were selected and quantified using the respective calibration standard. The estimated concentration values of chrysene and its alkylated homologues in MC252 crude oil are summarized in Table 4-4. The two surrogate compounds, *p*-terphenyl-d_{14} and pyrene-d_{10}, were also quantified; the relative recovery of surrogate compounds were found to be ranging between 80% to 120% , which is well within the USEPA recommended levels for surrogate recovery in environmental samples (USEPA, 1996).

National Institute of Standards and Testing (NIST) compiled the analytical results of MC252 oil characterization studies completed by 26 different laboratories and released

a summary report (Schantz and Kucklick, 2011). Table 4-4 compares the values of the different types of chrysenes estimated in our study against this reference dataset presented in the NIST report. The data show that the concentration estimates for chrysene and its homologues evaluated in our study are well within the range reported in the report.

Table 4-4: Comparison of estimated values of various chrysenes using the proposed GC/MS/MS method against NIST data reported for MC252 crude oil

Homologue	**Concentration (mg/kg)**			
	Current study	**NIST report**		
		Mean	**Median**	**Range**
Chrysene	57 ± 3	44.8	47.5	20.7 – 64.4
C_1-chrysenes	128 ± 7	108	108	72.4 – 134
C_2-chrysenes	91 ± 4	130	128	92.5 – 163
C_3-chrysenes	166 ± 5	91.3	92.7	39.4 – 140
C_4-chrysenes	31 ± 1	65.4	70.9	39.1 – 87.8

We also prepared a synthetic weathered oil sample by evaporating the original MC252 crude oil under a fume hood for 7 days, resulting in a loss of bulk oil mass of 44% (estimated by the gravimetric method). Since chrysene and its homologues are semi-volatile organic compounds (relatively resistant to volatilization), ideally, they would have concentrated in the weathered sample by about 44%. The weathered MC252 oil sample was analyzed using the MRM method discussed above. The concentration levels of various chrysenes measured in the synthetic sample are summarized in Table 4-5, and these values were also used to estimate the net weathering level of the oil using the following equation (Mulabagal et al., 2013).

$$P = \left(1 - \frac{C_S}{C_W}\right) X\ 100 \quad eqn\ (4.2)$$

where P is the percentage weathering level with respect to the source crude oil, C_S and C_W are the concentrations of chrysenes in MC252 and weathered MC252 crude oil

samples, respectively. The average level of weathering estimated using the total amount of chrysene was 47%, which is close to the gravimetric estimate of 44%. Other estimates computed based on individual chrysenes (Table 4-5) showed less than 20% of variability from the gravimetric estimate.

Table 4-5: Method validation data acquired using lab-weathered MC252 crude oil sample

Homologue	**Concentration in lab weathered MC252 crude oil (mg/kg)**	**% weathering of oil**
Chrysene	92 ± 2	39
C_1-chrysenes	221 ± 5	42
C_2-chrysenes	170 ± 3	46
C_3-chrysenes	341 ± 10	51
C_4-chrysenes	67 ± 2	54
Total	891	47

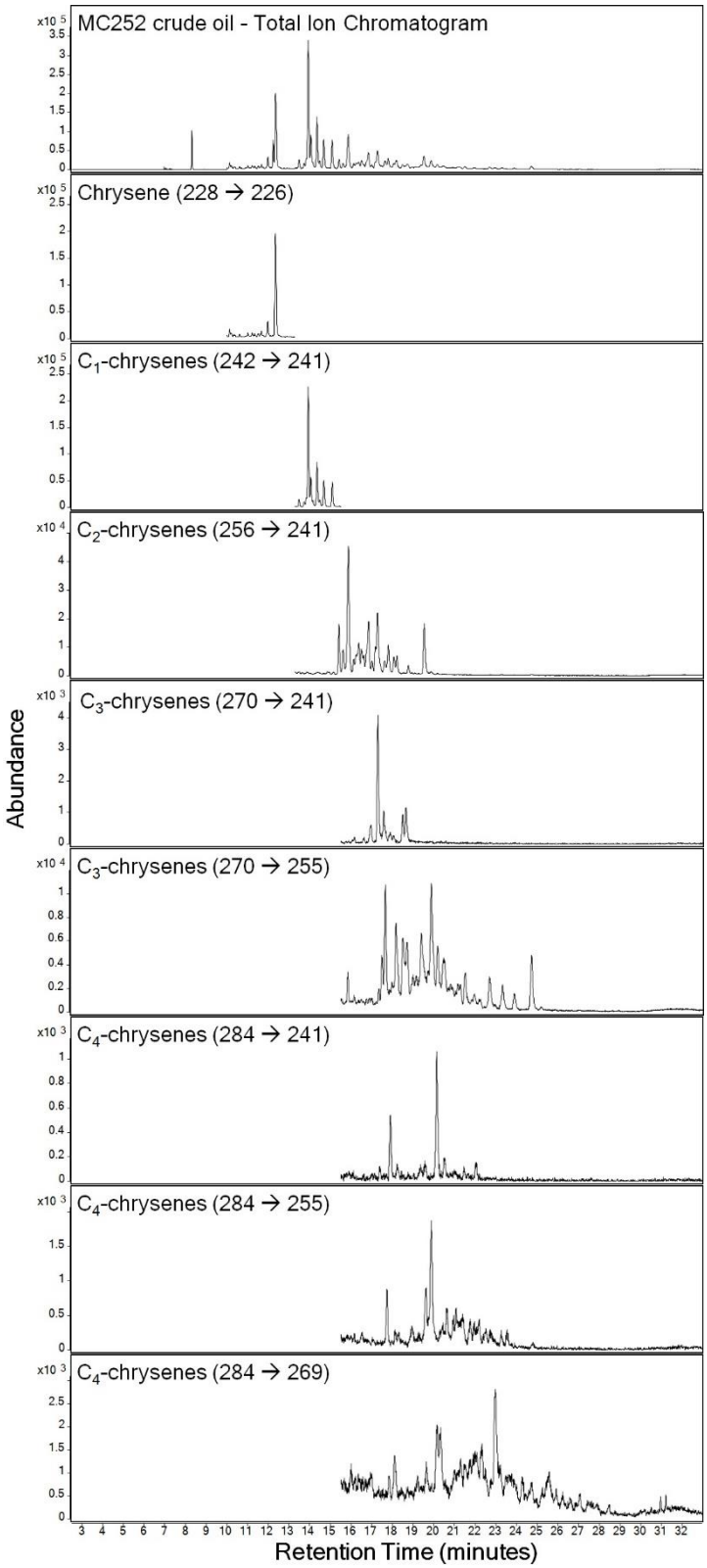

Figure 4.6: Total ion chromatogram and extracted-ion chromatograms for various MRM transitions used for quantifying chrysene and alkylated chrysene homologues in the MC252 crude oil sample

4.4 Conclusions

The objective of this study was to develop a GC/MS/MS MRM method for identifying and quantifying chrysene and its alkylated homologues in crude oil samples. The method was developed based on full-scan and product-ion scan data collected for seven different alkylated standards using a novel MS/MS instrument (Agilent's 7000B MS/MS system). The full scan data, product-ion scan data, and the collision cell energy optimization data for all seven standards are provided. Based on these experimental data, coupled together with literature-derived information, the mass fragmentation patterns of other isomers of chrysene homologues for which standards are not commercially available were proposed. This information was used to develop a GC/MS/MS method for identifying and quantifying the total concentrations of C_1-, C_2-, C_3-, and C_4-chrysenes in crude oil samples. The developed method was employed to characterize MC252 crude oil, which was spilled into the Gulf of Mexico during the *Deepwater Horizon* oil spill event. The results show the chrysene levels estimated by the proposed method are mostly well within the range of values previously reported in the literature. The proposed method is a promising approach for quantifying chrysene homologues in more complex environmental samples such as crude oils and weathered oil-spill-waste samples.

Chapter 5

Enhancing oil dispersants for destabilizing water-in-oil crude oil emulsions

5.1 Introduction

The explosion and sinking of the *Deepwater Horizon* (DWH) drilling platform, while exploring for oil on the Macondo Prospect (MC252) in the Gulf of Mexico (GOM), resulted in the discharge of an estimated 785 million liters of crude oil into the GOM between April 20, 2010 and July 15, 2010 (Lehr et al., 2010a; McNutt et al., 2012). Of this estimated total volume, approximately 611 million liters has been accounted for through direct recovery, evaporation and dissolution, natural and chemical dispersion, and burning or skimming (Lehr et al., 2010a). Two recent studies (Chanton et al., 2014; Valentine et al., 2014) suggest that between 14-113 million liters of MC252 oil may be deposited on the deep sea floor in the vicinity of the MC252 well, in an area ranging from 3,200-24,000 km^2. It is likely that a large fraction of the remaining 62-161 million liters of oil washed onto northern GOM shorelines in Florida, Alabama, Mississippi, and Louisiana (Hayworth et al., 2011; Hayworth and Clement, 2011a; Michel et al., 2013a; Operational Science Advisory Team (OSAT-3), 2013).

MC252 oil impacting northern GOM shorelines was predominantly in the form of water-in-oil (W/O) emulsions, a chemically weathered, highly viscous, neutrally buoyant material sometimes referred to as mousse (Daling and StrØm, 1999; Liu et al., 2012b). W/O emulsions form when raw crude oil is released in aquatic systems (Fingas and Fieldhouse, 2004; Fingas et al., 1993); and once formed, they are extremely difficult to

destabilize, even when treated with dispersants (Daling and StrØm, 1999; Hayworth and Clement, 2012). Stable W/O emulsions contain 50%-80% water by volume, which results in a significant increase in the volume of oil-related material requiring cleanup. Additionally, the density and viscosity of W/O emulsions increases relative to the density and viscosity of the original raw crude oil (Fingas and Fieldhouse, 2003), which has important implications with respect to the physical, chemical, and transport behavior of the emulsion. Generally, W/O emulsions will extend deeper into the water column, will evaporate and spread more slowly, and will be less influenced by wind in their transport behavior relative to non-emulsified oil (Fingas and Fieldhouse, 2003).

Previous studies have shown that stable W/O emulsions form as a result of surfactant-like behavior of asphaltenes within the crude oil (Al-Sabagh et al., 2002; J. and Burgess, 2003; McLean and Kilpatrick, 1997; McLean et al., 1998; Menon and Wasan, 1998; Pozdnyshev et al., 1969; Thingstad and Pengerud, 1983a). Asphaltenes constitute the non-volatile, high molecular weight fraction of oil. They are defined on the basis of their solubility—they are soluble in carbon disulfide but insoluble in light alkanes such as n-pentane and n-heptane. Importantly, asphaltenes are more soluble in crude oil when associated with polar resins and other polar constituents of crude oil. It is thought that asphaltenes stabilize W/O emulsions by collecting at the water-oil interface as colloidal aggregates. These asphaltenic molecules are thought to aggregate through hydrogen bonding and proton/electron donor-acceptor interactions and are solvated on their edges primarily by polar resins. There is evidence that as W/O emulsions are forming, polar resin molecules (which initially serve to solvate asphaltene aggregates) are shed, leading to film stabilization. The end result is a viscous, cross-linked, three-dimensional, mechanically

rigid film at the water droplet-oil interface which resists coalescence of water droplets dispersed in the emulsion (McLean and Kilpatrick, 1997; McLean et al., 1998).

Studies directed at developing methods for destabilizing W/O emulsions have focused on the use of commercially-available oil dispersants as de-emulsifiers (Limited et al., 2006). Results indicate that dispersants are largely ineffective as de-emulsifiers, especially for emulsions with relatively high viscosities. This is thought to be a result of the inability of the dispersant surfactants to "displace" asphaltenes stabilizing the oil-water interface. This observation, along with the observation that asphaltenes solubility increases in oil when associated with polar resins and other polar constituents in the oil, suggests that modifying the composition and fraction of polar constituents in commercial dispersants may increase asphaltenes solubility, decrease oil-water interface stability, and enhance the de-emulsification ability of these dispersants.

In this study, we investigate the effectiveness of the commercially-available dispersant COREXIT9500A, modified to enhance its polar fraction, in the destabilization of artificial (laboratory-developed) W/O emulsions formed from laboratory-weathered Louisiana light sweet crude oil. This oil is the official surrogate MC252 (DWH) oil provided to researchers by the US Department of Interior (Pelz et al., 2011). Two polar additives to COREXIT9500A were considered (1-octanol and hexylamine) based on their mechanistic differences in destabilizing emulsions and their negligible environmental risk. (Sjöblom et al., 2003; Wasan et al., 1979).

5.2 Materials and Methods

5.2.1 Oil, Dispersant, and Additives

Louisiana light sweet crude oil (MC252 surrogate oil) and the chemical dispersant COREXIT9500A were supplied by OHMSETT, NJ, USA. Hexylamine and 1-octanol were supplied by Sigma-Aldrich, USA. Sodium chloride was supplied by VWR, USA. Artificial seawater (ASW) was prepared by dissolving sodium chloride in deionized water (3.3 wt%). MC252 surrogate oil was weathered by placing 200 mL of crude oil in a 1000 mL crystallizing jar under natural sunlight for 4 days. Unweathered and weathered MC252 surrogate oil are referred to as MC and EMC, respectively.

5.2.2 Preparation of Artificial Mousse

Previous studies have shown that crude oil exposed to simulated sunlight formed stable emulsions compared to fresh oil and non-exposed oil (Thingstad and Pengerud, 1983b). This is due in part to the formation of photo-oxidation products which acted as emulsifying agents (Lee, 1999). Artificial mousse (AM) was prepared from EMC which was exposed to sunlight for 4 days prior to preparation to form stable W/O emulsion. AM was prepared using a previously developed method (Fingas et al., 1996). EMC (15 g) and ASW (35 g) was placed in a commercial blender and mixed at 15000 rpm for 1 minute, after which oil/water mixture adhering to the blender container walls was scraped to the bottom of the blender container using rubber scraper. This process was repeated twice, and then the contents were transferred to 50 mL centrifuge tubes and allowed to stand for 8 hours. The contents were then centrifuged at 15000 rpm for 1 hour, resulting in the formation of three distinctly separate phases: a top layer containing oil, a bottom layer containing coalesced water, and a middle layer containing the AM used in this study.

5.2.3 Asphaltenes Content

MC and EMC asphaltenes content was quantified using the American Society for Testing and Materials (ASTM) method D3279 (D3279, 1988). Since AM was prepared using EMC, the asphaltenes content of AM is equivalent to that of EMC. Approximately 1 g of MC or EMC sample was placed in a 125 mL Erlenmeyer flask and 100 mL of n-hexane was added. The flask was then fitted with reflux condenser and heated at 45°C for 20 minutes. The contents were then passed through a glass-fiber filter, and the filter was dried and weighed to determine the asphaltenes content (mass percent) of the samples.

5.2.4 Determining Water Content

MC, EMC and AM water content were measured using ASTM method D4006 (D4006, 1987). MC, EMC, or AM (5 -10 g) were placed in a 1 L round bottom flask and xylene was added for a 400 mL total volume. Heat was applied to the bottom of the flask to drive water into a trap; the mass percentage of water present in the sample was determined using eqn (5.1)

$$Mass\% = \frac{(A - B)}{M} X\ 100 \qquad eqn(5.1)$$

where A is volume of water in the trap, B is volume of water in the solvent blank, and M is the weight of the sample taken.

5.2.5 Measuring Viscosity

The viscosities of MC and EMC were measured using a Brookefield Viscometer (Model: DV-II+) employing spindle (size 21) and small sample adapter. About 8 g of either MC or EMC oil was placed in the small sample adapter, the spindle was inserted into the adapter and the viscometer was turned on to measure viscosity.

AM viscosity was measured using a Thermo Analytical AR2000e dynamic shear rheometer following a previously established method (Fingas and Fieldhouse, 2003). A stress sweep from 100 to 10,000 mPa at a frequency of 1/second was performed. After the sample was thermally equilibrated (25°C for 2 minutes), viscosity was measured by spreading the sample onto a 25 mm diameter base plate and raising a 25 mm diameter measuring plate to a 0.5 gap.

5.2.6 Modified Dispersant

Modified dispersants were prepared by adding either hexylamine or 1-octanol to COREXIT9500A in the proportions 20, 40, 60, 80 and 100% v/v. The list of modified dispersants are given in Tables 5-1 and 5-2.

Table 5-1: Modified dispersants containing 1-octanol as additive

Modified dispersant	COREXIT9500A % (v/v)	1-octanol % (v/v)
O20	80	20
O40	60	40
O60	40	60
O80	20	80
O100	0	100

Table 5-2: Modified dispersants containing hexylamine as additive

Modified dispersant	COREXIT9500A % (v/v)	Hexylamine % (v/v)
H20	80	20
H40	60	40
H60	40	60
H80	20	80
H100	0	100

5.2.7 Oil Standards

Oil standards were prepared as stated in previous studies (Venosa and Holder, 2013; Venosa et al., 2002) A stock solution of dispersant–oil mixture in dichloromethane was prepared by adding 80 µL of dispersant to 2 mL of oil, and then 18 mL of dichloromethane was added. Since the additives were colorless, the color of the modified dispersant varies with change in composition of the additive. In order to avoid any variation in UV-Vis absorbance due to this color variation, stock solution for each modified dispersant were prepared. A total of 24 oil standards were prepared – control, 5 modified dispersants containing hexylamine and another 5 modified dispersants containing 1-octanol for both MC and EMC. EMC was used as the AM oil standard, since AM was prepared from EMC.

Determinations of stock solution concentrations were based on the mass measurements after each addition. For generating a 4-point calibration curve, specific volumes of the stock standard solution were added (25, 50, 100, 200 µL) to 30 mL ASW in a 125 mL separatory funnel. Liquid/liquid extraction was performed by adding 5 mL of dichloromethane. The liquid/liquid extraction process was repeated for another two times. Extracts were then combined and concentrated under gentle stream of nitrogen, adjusted to a final volume of 10 mL and then stored at 5°C until analysis. Extracts were analyzed using UV-Vis spectrophotometer for absorbance at wavelengths 340, 370, and 400 nm (Venosa and Holder, 2013). The area under the absorbance vs. wavelength curve between wavelengths 340 and 400 nm was determined by applying the trapezoidal rule according to equation (eqn(5.2)).

$$Area = \frac{(Abs_{340} + Abs_{370})\ X\ 30}{2} + \frac{(Abs_{370} + Abs_{400})\ X\ 30}{2} \qquad eqn(5.2)$$

The volume of oil-dispersant mixture taken and their respective *Area* were plotted to compute calibration slope and intercept. The calibration slope and intercept are given in Table 5-3.

Table 5-3: Calibration slope, intercept and R^2 for calibration stock solutions containing different modified dispersants

Oil	Dispersant	Calibration slope	Intercept	R^2
MC	Control	4.319	-1.108	0.999
	C100	3.150	0.456	0.995
	O20	2.759	4.473	0.994
	O40	2.883	3.015	0.999
	O60	3.249	2.920	0.999
	O80	3.465	0.782	0.997
	O100	4.393	0.114	0.998
	H20	3.914	-0.698	0.999
	H40	3.688	2.323	0.998
	H60	4.373	3.882	0.997
	H80	4.429	0.260	0.996
	H100	4.069	1.140	0.990
EMC	Control	6.653	0.915	0.999
	C100	7.341	-6.230	0.999
	O20	4.968	2.884	0.998
	O40	6.793	-3.049	1.000
	O60	5.374	-0.187	1.000
	O80	5.592	3.973	0.996
	O100	6.323	2.026	0.999
	H20	5.425	2.726	0.998
	H40	5.582	3.324	0.999
	H60	5.754	1.926	0.997
	H80	5.996	-1.021	0.999
	H100	5.929	1.805	0.999

5.2.8 Dispersion Effectiveness

Dispersion effectiveness is the measure of ability of the dispersant to disperse the oil into water-phase. It is measured by analyzing the water-phase for oil. Dispersants having higher dispersion effectiveness would disperse more oil into water-phase. The dispersant effectiveness experiment generally followed the approach as stated by Venosa and Holder (2013). A 150 mL trypsinizing flask fitted with a PTFE stopcock at the bottom was used. 120 mL of ASW was added into the trypsinizing flask. About 100 mg of oil was then carefully added to the surface of the ASW. For AM, 100 mg oil equivalent (about 286 g of AM) was added to the surface of ASW. This helps to normalize the dispersant effectiveness for AM to that of the oil, allowing comparison for MC, EMC and AM. 4 µl of dispersant is added to the surface of the oil. The ratio of dispersant to oil was 1/25 (v/w) (Venosa and Holder, 2013). The baffled flask was then placed on orbital shaker and shaken at 200 rpm for 10 minutes. The contents were allowed to settle for 10 minutes to allow non-dispersed oil to return to the water surface before removing the subsurface water sample. At the end of settling time, 2 mL of subsurface water sample was drained from the stopcock and discarded, then 30 mL of subsurface water sample was collected and transferred to a 125 mL separatory funnel and extracted three times with 5 mL dichloromethane. The extract was then concentrated under a gentle stream of nitrogen, adjusted to a final volume of 10 mL and stored at 5°C before analysis. The oil extracts were analyzed using UV-Vis spectrophotometer for absorbance at wavelengths 340, 370, and 400 nm (Venosa and Holder, 2013) similar to that of calibration solution. The area under the absorbance vs. wavelength curve between wavelengths 340 and 400 nm was

determined by applying eqn(5.2). The area was then used to compute the dispersion effectiveness (DE) using eqn(5.3).

$$DE(\%) = \frac{(Area - Intercept)}{Calibration\ curve\ slope}\ X\ \frac{V_{tw}}{V_{ew}}\ X\ \frac{\rho_{oil}}{W_{oil}\ X\ 1000}\ X\ 100 \qquad eqn(5.3)$$

Where V_{tw} is the total volume of ASW taken, V_{ew} is the volume of ASW extracted, ρ_{oil} is the density of the oil and W_{oil} is the weight of the oil added to the flask.

5.2.9 Microscopic Analysis of W/O Emulsions

About 50 mg oil equivalent of AM was weighed in a glass vial. 2 µl of dispersant was added to the AM and mixed well using a vortex mixer. About 2 mL of mineral oil was added and the contents were mixed again. AM was diluted using mineral oil for clear observation using a microscope. About 500 µl of this mixture was carefully transferred to a 24 well plate and observed under a microscope (Advanced Microscopy Group, Model AMAFD1000).

5.3 Results and Discussion

Viscosity, water content, and asphaltenes content for MC, EMC, and AM samples are given in Table 5-4. As these data show, the loss of volatile constituents from raw crude oil, the resultant concentrating of asphaltenic constituents, and the inclusion of water within the oil matrix resulted in an approximately 2 order of magnitude increase in w/o emulsion viscosity relative to the raw crude oil. This dramatic increase in viscosity from MC to AM is responsible for much of the macroscopic behavior of w/o emulsions in marine systems.

Table 5-4: Viscosity, water content and asphaltenes content in MC, EMC and AM

Property	**MC**	**EMC**	**AM**
Viscosity (cps)	14	201	3773
Water content (mass %)	BD	BD	65
Asphaltenes content (mass %)	0.19	0.49	0.49

BD: below detection limit

Figure 5.1 shows the dispersant effectiveness of modified dispersants on MC, EMC and AM. Little or no oil was dispersed when no dispersant was used. Dispersion effectiveness increased with increase in additive composition in the modified dispersant from 0% to approximately 40% additive, and then decreased from > 40% additive. This suggests that there is an optimal amount of both COREXIT9500A and polar additive, above which the effectiveness of the modified dispersant to disperse and de-emulsify oil is reduced.

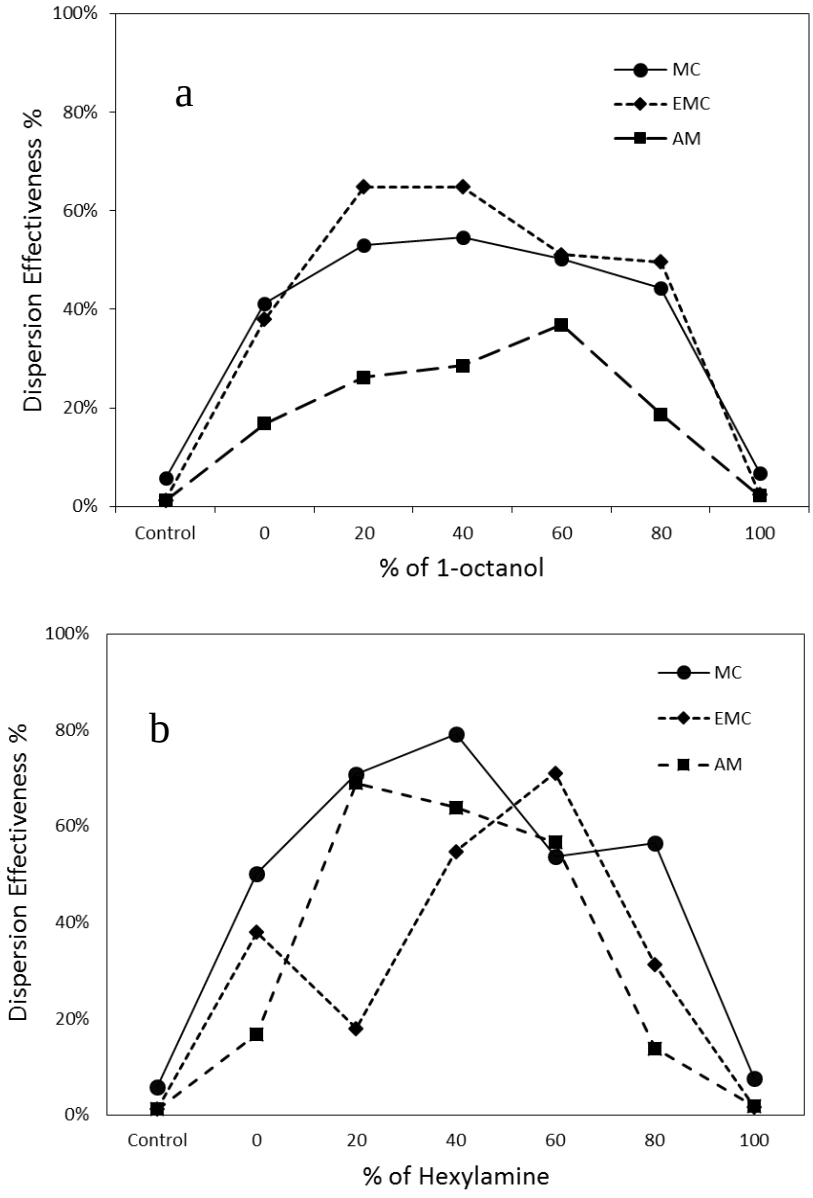

Figure 5.1: Dispersion effectiveness of modified dispersants – (a) 1-octanol and (b) hexylamine

5.3.1 Change in properties of oil with weathering

The viscosity of EMC increased by one order when compared to MC due to loss of the volatile components through evaporation (Trudel et al., 2010). The viscosity of AM increased by two orders of magnitude compared to MC. This is result of weathered oil forming W/O emulsions. When observed under microscope, water droplets were found dispersed in the oil (Figure 5.2). This observation suggests that the increase in interfacial surface area between water droplets and the weathered oil matrix is responsible for the increase in AM viscosity.

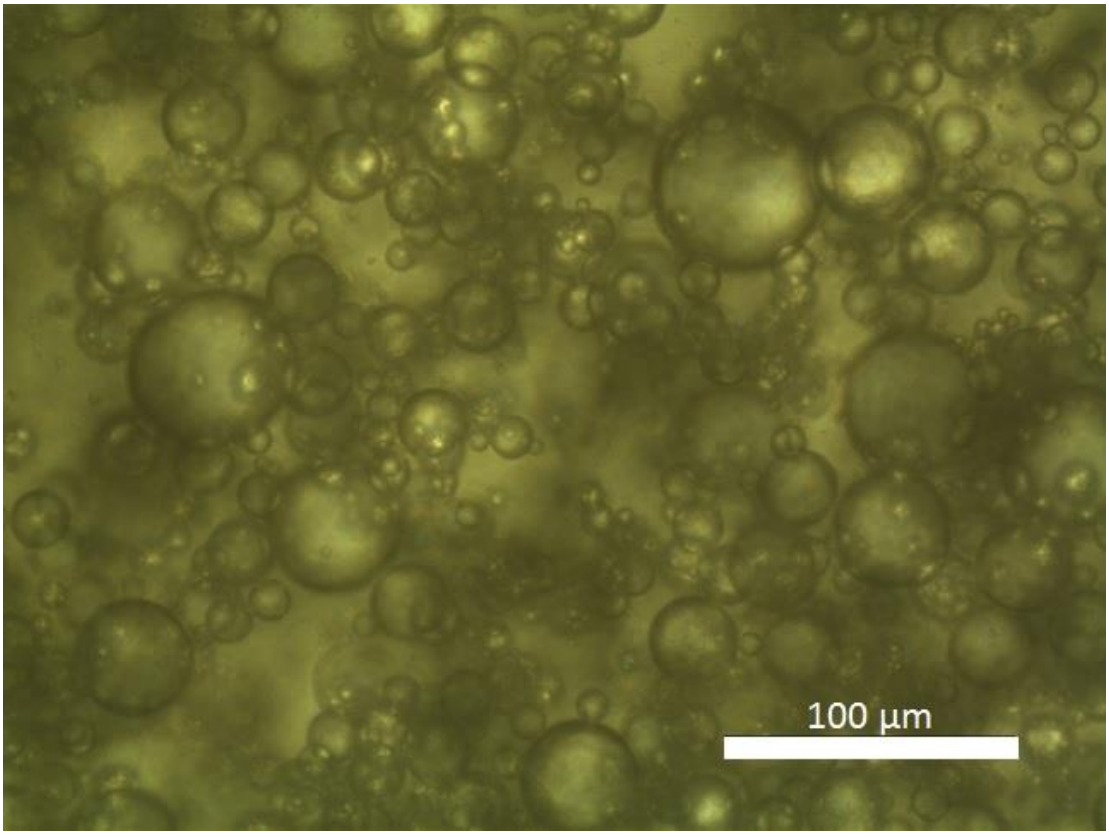

Figure 5.2: Microscopic image showing water droplets dispersed in oil in AM

5.3.2 Selection of additives

Chemical additives are used in the petroleum industry to break down W/O emulsions which are formed at well-head chokes and valves. The principal role of chemical additives is the reduction of interfacial tension and the enhancement of water droplets coalescence at the oil-water interface (Djuve et al., 2001). Two additives that were selected to modify COREXIT9500A were 1-octanol and hexylamine. These compounds were selected based on their mechanistic differences in destabilizing emulsions. 1-octanol is a short-chain alcohol, which acts to break down existing intermolecular hydrogen bonds between asphaltenes molecules, replacing them with alcohol-asphaltenes hydrogen bonds (Sjöblom et al., 2003). Wasan et al. (1979) observed a similar destabilization effect on W/O emulsions originating from a medium-chain alcohols. Hexylamine acts to disintegrate asphaltenes through interaction between the nitrogen group (base) and the acid groups present in the interfacial film. A consequence of this interaction is that the properties of the interfacial film are modified, with this film becoming hydrophilic to stabilize the aqueous droplets (Sjöblom et al., 2003; Sjöblom et al., 1990).

5.3.3 Microscopic image analysis of AM

A microscopic image of AM after addition of COREXIT9500A is shown in Figure 5.3. Figures 5.4 and 5.5 show microscopic images of AM after addition of modified dispersants containing the additives at different compositions. The microscopic images show that the addition of dispersants reduces the size of water droplets present in the W/O emulsion. This is an advantageous process, as the size of droplets decreases, the shear-thinning effect increases (Pal, 1996), leading to a decrease in viscosity of the emulsion, thus increasing potential dispersability of the W/O emulsion.

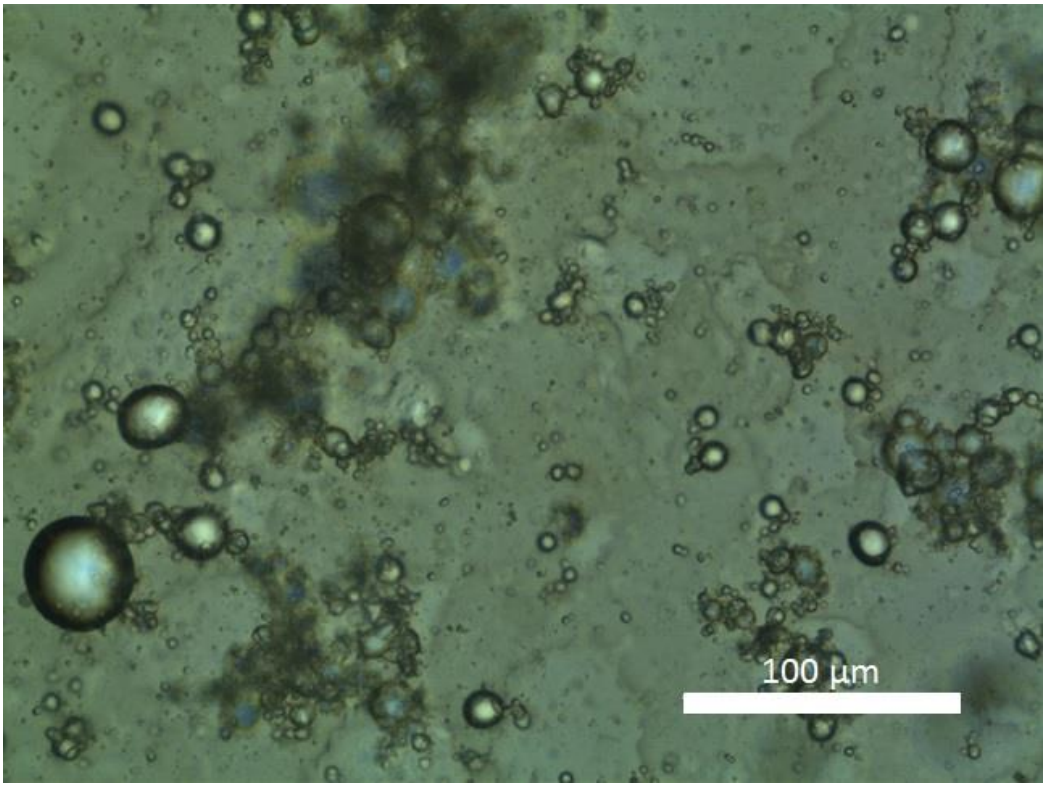

Figure 5.3: Microscopic image of AM after addition of COREXIT9500A

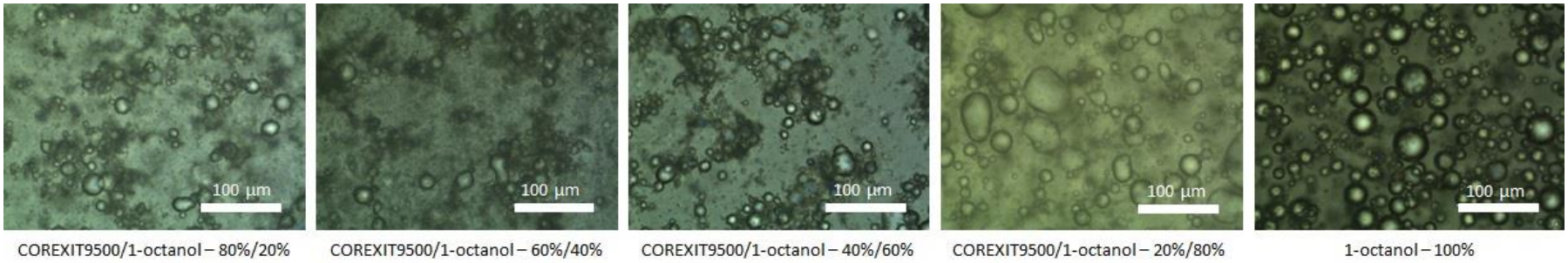

Figure 5.4: Microscopic images of AM after addition of modified COREXIT9500A containing different compositions of 1-octanol

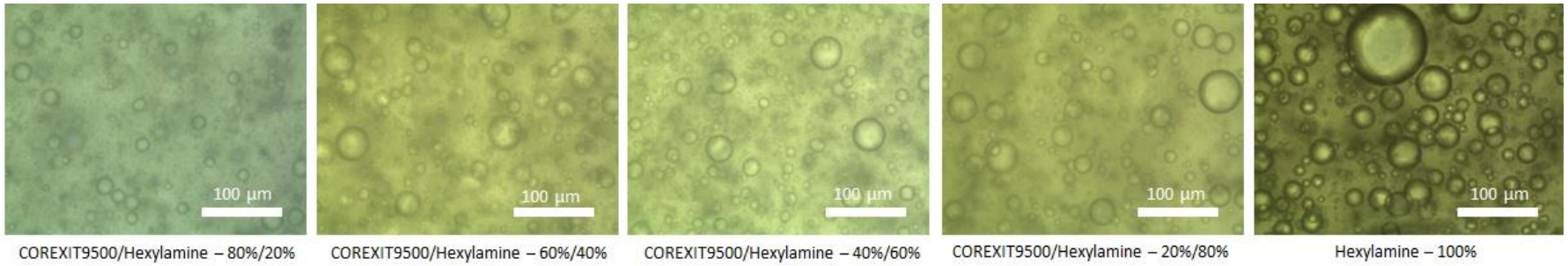

Figure 5.5: Microscopic images of AM after addition of modified COREXIT9500A containing different compositions of 1-octanol

5.4 Conclusion

In summary, addition of dispersants to the W/O emulsion reduces the size of water droplets, which increases the shear-thinning effect leading to decrease in viscosity and increasing the flow properties of W/O emulsion. Also, the chemical additives alter the chemistry of the water-oil interface, reducing the interfacial tension and leads to coalescence of water droplets thus breaking the W/O emulsion. Then the dispersant COREXIT9500A present in the modified dispersant disperses the oil which was released from the emulsion.

Chapter 6

Conclusions and Recommendations

6.1 Conclusions

The *Deepwater Horizon* oil spill accident in the summer of 2010 is the largest maritime environmental disaster in the history of US which impacted its shores location along Florida, Alabama, Mississippi, Louisiana and Texas. Our research primarily focused on Alabama shoreline. The coastline of Alabama is priceless, majorly due to its economic and environmental values. Oil from the spill first arrived on Alabama shorelines in early June 2010. It was predominantly in the form of water-in-oil (W/O) emulsion also known as "mousse". An unknown quantity of mousse interacted with suspended sediments in the near-shore environment, settled down to seafloor, transforming into submerged oil mats (SOMs) and surface residual balls (SRBs). SRBs continue to wash ashore to this day. The main focus of this dissertation was to monitor the activity of SOMs/SRBs in Alabama's beach environment and investigate the transformation of polycyclic aromatic hydrocarbons present in these oil spill residues. Further, this study also focused on how to enhance the ability of a commercially available dispersants to de-stabilize and disperse mousse.

The activity of SOMs/SRBs was documented over a period of four years beginning 2010, along the shores of Alabama; SOMs/SRBs activity was documented during three timeline periods – (1) pre-arrival period (May 2010), (2) cleanup period (June 2010 – January 2013) and (3) post-cleanup period (June 2013 – August 2014). Based on all field

observations, chemical analysis data and other published literature information we conclude the following : (1) it is highly unlikely that Alabama's beaches will return to background tarball levels in the foreseeable future; (2) virtually all oil found on Alabama beaches match the physical characteristics of MC252 SRBs; (3) chemical analysis of SRBs over a period of four years show that the concentration of PAHs remain at essentially the same concentration of MC252 oil which first arrived on Alabama beaches in June 2010; and (4) the presence of SRBs in the near-shore beach environment has a potential to pose long term risks to Alabama's shoreline ecosystem.

Sunlight enhances the weathering of PAHs present in crude oil through photo-oxidation. The effect of sunlight was studied on five groups of PAHs: (1) C_0- to C_4-naphthalenes, (2) C_0- to C_4-phenanthrenes, (3) C_0-to C_3-dibenzothiophenes, (4) C_0- to C_3-fluorenes, (5) C_0- to C_4-chrysenes present in both raw MC252 crude oil and MC252's SOMs. Our dataset show that the PAHs present in MC252 and SOMs weather primarily through evaporation and photo-oxidation. Among all five groups of PAHs, C_0- to C_4-chrysenes present in SOMs have the lowest rate of weathering. The daughter products formed as result of photo-oxidation weathering process are largely unknown.

C_0- to C_4-chrysenes are a group of compounds present in crude oil which are highly resistant to natural weathering processes, and thus could potentially serve as excellent indicators to assess large-scale impacts from oil spills. A GC/MS/MS MRM method was developed for identifying and quantifying chrysene and its alkylated homologues and this method was used to quantify C_0- to C_4-chrysenes in MC252 oil. The estimated concentrations of C_0- to C_4-chrysenes matched closely with those values reported in the

literature. The proposed GC/MS/MS MRM method provides a promising approach for quantifying C_0- to C_4-chrysenes in complex oil spill residues.

Oil which washed ashore during the *Deepwater Horizon* accident was predominantly in the form of highly viscous water-in-oil (W/O) emulsion known as "mousse". Dispersants are largely ineffective as de-emulsifiers. In this study, we modified the commercially available dispersant COREXIT9500A by adding two polar additives (1-octanol and hexylamine). Our dataset shows that the addition of these additives enhances the effectiveness of the dispersant. We propose that this increase in effectiveness is due to two main factors: (1) the addition of COREXIT9500A reduces the size of water droplets in mousse, which increases the shear-thinning effect leading to decrease in viscosity and increasing the flow properties of mousse and thus its dispersion, (2) addition of additives alter the chemistry of the water-oil interface in W/O emulsion; reducing the interfacial tension and leads to coalescence of water droplets thus breaking the W/O emulsion.

6.2 Recommendations for future research

This study investigated the activity of oil spill residues along Alabama beaches, developed analytical methods to characterize C_0- to C_4-chrysenes in oil spill residues and modified COREXIT9500A to enhance its effectiveness to disperse W/O emulsions. There are still a number of scientific issues that require further investigations. Some possible future research directions are described below.

The oil that washed ashore in June 2010 was weathered by more than 40% compared to that of source MC252 (unweathered) oil (Mulabagal et al., 2013). However, the concentration of PAHs in oil spill residues which were collected over a four year period

show that some PAHs remain at essentially the same levels as the first arrival oil of June 2010. Several studies considered the ecological impact of fresh MC252 oil, but very few have focused on ecological impacts of weathered oil. Therefore, studies considering the ecological impacts of DWH oil spill residues in the near-shore environment are needed.

Sunlight plays a major role on weathering of PAHs present in oil spill residues. Sunlight could also increase the toxicity of the oil as it enhances the formation of photo-oxidized products. Photo-oxidized products tend to have higher polarity and thus have higher bioavailability and can eventually increase the toxicity of spilled oil. However, the majority of daughter compounds formed as a result of photo-oxidation are largely unknown. Research focused on identifying photo-oxidized transformation products and their potential ecological impacts are needed.

The effectiveness and toxicity of COREXIT9500A have been extensively studied. In this dissertation experiments were conducted using COREXIT9500A modified with two additives (1-octanol and hexylamine). Although, the effectiveness of the modified dispersant in destabilizing W/O emulsions was demonstrated the potential ecological impacts of the modified dispersant and the oil that is dispersed by the modified dispersant are largely unknown. Thus studies investigating the potential ecological impacts posed by modified dispersants are warranted.

References

(SCCP), S.C.C.P., 2011. Report by the UC SCCP Core Group (http://www.restorethegulf.gov/sites/default/files/u306/Signed%20SCCP1.pdf) Accessed 2/17/2014.

(USCOE), U.S.A.o.C.o.E., 2002. Coastal Engineering Manual, Engineering Manual, 1110-2-1100, U.S. Army of Corps of Engineers, Washington, D.C.

Abdulkadar, A.H.W., Kunhi, A.A.M., Jassim, A.-J., Abdulla, A.-A., 2003. Determination of benzo(a)pyrene by GC/MS/MS in retail olive oil samples available in Qatar. Food Additives & Contaminants 20, 1164-1169.

Aeppli, C., Carmichael, C.A., Nelson, R.K., Lemkau, K.L., Graham, W.M., Redmond, M.C., Valentine, D.L., Reddy, C.M., 2012. Oil Weathering after the Deepwater Horizon Disaster Led to the Formation of Oxygenated Residues. Environmental Science & Technology 46, 8799-8807.

Aeppli, C., Nelson, R.K., Radović, J.R., Carmichael, C.A., Valentine, D.L., Reddy, C.M., 2014. Recalcitrance and Degradation of Petroleum Biomarkers upon Abiotic and Biotic Natural Weathering of Deepwater Horizon Oil. Environmental Science & Technology 48, 6726-6734.

Al-Sabagh, A.M., Nehal, S.A., Amal, M.N., Gabr, M., 2002. Synthesis and evaluation of some polymeric surfactants for treating crude oil—Part II. Destabilization of naturally occurring water-in-oil emulsions by polyalkylphenol formaldehyde amine resins. Polymers for Advanced Technology 13, 7.

Atlas, R.M., Hazen, T.C., 2011. Oil Biodegradation and Bioremediation: A Tale of the Two Worst Spills in U.S. History. Environmental Science & Technology 45, 6709-6715.

ATSDR, 1995. Chemical and physical information, in: Toxicological Profile for Polycyclic Aromatic Hydrocarbons (PAHs), ATSDR, Atlanta, Georgia, USA

Berg, R., 2012. Tropical Cyclone Report, Hurricane Isaac (AL092012), 21 August - 1 September 2012. National Hurricane Center, 28 January 2013 (http://

www.nhc.noaa.gov/data/tcr/AL092012_Isaac.pdf) Accessed 2/17/2014.

Bernabeu, A.M., Rey, D., Rubio, B., Vilas, F., Domínguez, C., Bayona, J.M., Albaigés, J., 2009. Assessment of Cleanup Needs of Oiled Sandy Beaches: Lessons from the Prestige Oil Spill. Environmental Science & Technology 43, 2470-2475.

Boehm, P.D., Fiest, D.L., 1982. Subsurface distributions of petroleum from an offshore well blowout. The Ixtoc I blowout, Bay of Campeche. Environmental Science & Technology 16, 67-74.

BP, 2014. Active Cleanup from Deepwater Horizon Accident Ends in Florida, Alabama and Mississippi (http://www.bp.com/en/global/corporate/press/press-releases/active-cleanup-for-deepwater-horizon-accident-ends.html) Accessed 2/17/2014.

Brown, D.P., 2011. Tropical Cyclone Report, Tropical Storm Lee (AL132011), 2–5 September 2011. National Hurricane Center, 15 December 2011. <http://www.nhc.noaa.gov/data/tcr/AL132011_Lee.pdf> accessed 17.02.14).

Burkhardt, M.R., Zaugg, S.D., Burbank, T.L., Olson, M.C., Iverson, J.L., 2005. Pressurized liquid extraction using water/isopropanol coupled with solid-phase extraction cleanup for semivolatile organic compounds, polycyclic aromatic hydrocarbons (PAH), and alkylated PAH homolog groups in sediment. Analytica Chimica Acta 549, 104-116.

Burns, W.A., Mankiewicz, P.J., Bence, A.E., Page, D.S., Parker, K.R., 1997. A principal-component and least-squares method for allocating polycyclic aromatic hydrocarbons in sediment to multiple sources. Environmental Toxicology and Chemistry 16, 1119-1131.

Camilli, R., Reddy, C.M., Yoerger, D.R., Van Mooy, B.A.S., Jakuba, M.V., Kinsey, J.C., McIntyre, C.P., Sylva, S.P., Maloney, J.V., 2010. Tracking Hydrocarbon Plume Transport and Biodegradation at Deepwater Horizon. Science 330, 201-204.

Camino-Sánchez, F.J., Zafra-Gómez, A., Pérez-Trujillo, J.P., Conde-González, J.E., Marques, J.C., Vílchez, J.L., 2011. Validation of a GC–MS/MS method for simultaneous determination of 86 persistent organic pollutants in marine sediments by pressurized liquid extraction followed by stir bar sorptive extraction. Chemosphere 84, 869-881.

Carls, M.G., Babcock, M.M., Harris, P.M., Irvine, G.V., Cusick, J.A., Rice, S.D., 2001. Persistence of oiling in mussel beds after the Exxon Valdez oil spill. Marine Environmental Research 51, 167-190.

Chaillan, F., Gugger, M., Saliot, A., Couté, A., Oudot, J., 2006. Role of cyanobacteria in the biodegradation of crude oil by a tropical cyanobacterial mat. Chemosphere 62, 1574-1582.

Chanton, J., Zhao, T., Rosenheim, B.E., Joye, S., Bosman, S., Brunner, C., Yeager, K.M., Diercks, A.R., Hollander, D., 2015. Using Natural Abundance Radiocarbon To Trace the Flux of Petrocarbon to the Seafloor Following the Deepwater Horizon Oil Spill. Environmental Science & Technology 49, 847-854.

Chanton, J., Zhao, T., Rosenheim, B.E., Joye, S.B., Bosman, S., Brunner, C.A., Yeager, K.M., Diercks, A.R., Hollander, D., 2014. Using Natural Abundance Radiocarbon to trace the Flux of Petrocarbon to the Seafloor following the Deepwater Horizon Oil Spill. Environmental science & technology 49, 8.

Chao, X., Shankar, N.J., Cheong, H.F., 2001. Two- and three-dimensional oil spill model for coastal waters. Ocean Engineering 28, 1557-1573.

D3279, A., 1988. Standard Test Method for n-Heptane Insolubles, in: Drews, A.W. (Ed.), Manual on Hydrocarbon Analysis: 4th Edition. ASTM, Philadelphia, PA, USA, pp. 650 - 652.

D4006, A., 1987. Standard Test Method for Water in Crude Oil by Distillation, in: Drews, A.W. (Ed.), Manual on Hydrocarbon Analysis: 4th Edition. ASTM, Philadelphia, PA, USA, pp. 713 - 722.

Daling, P.S., StrØm, T., 1999. Weathering of Oils at Sea: Model/Field Data Comparisons. Spill Science & Technology Bulletin 5, 63-74.

Dalyander, P.S., Long, J.W., Plant, N.G., Thompson, D.M., 2014. Assessing mobility and redistribution patterns of sand and oil agglomerates in the surf zone. Marine Pollution Bulletin 80, 200-209.

Dass, C., 2001. Principles and Practice of Biological Mass Spectrometry. Wiley-Interscience.

Díez, S., Jover, E., Bayona, J.M., Albaigés, J., 2007. Prestige Oil Spill. III. Fate of a Heavy Oil in the Marine Environment. Environmental Science & Technology 41, 3075-3082.

Díez, S., Sabaté, J., Viñas, M., Bayona, J.M., Solanas, A.M., Albaigés, J., 2005. The Prestige oil spill. I. Biodegradation of a heavy fuel oil under simulated conditions. Environmental Toxicology and Chemistry 24, 2203-2217.

Djuve, J., Yang, X., Fjellanger, I.J., Sjöblom, J., Pelizzetti, E., 2001. Chemical destabilization of crude oil based emulsions and asphaltene stabilized emulsions. Colloid & Polymer Sci 279, 232-239.

Douglas, G.S., Bence, A.E., Prince, R.C., McMillen, S.J., Butler, E.L., 1996. Environmental Stability of Selected Petroleum Hydrocarbon Source and Weathering Ratios. Environmental Science & Technology 30, 2332-2339.

Dubansky, B., Whitehead, A., Miller, J.T., Rice, C.D., Galvez, F., 2013. Multitissue Molecular, Genomic, and Developmental Effects of the Deepwater Horizon Oil Spill on Resident Gulf Killifish (Fundulus grandis). Environmental Science & Technology 47, 5074-5082.

Dutta, T.K., Harayama, S., 2000. Fate of Crude Oil by the Combination of Photooxidation and Biodegradation. Environmental Science & Technology 34, 1500-1505.

EIA, 2014. World Oil Transit Checkpoints. (Available at: http://www.eia.gov/beta/international/regions-topics.cfm?RegionTopicID=WOTC. Accessed on July 28, 2015).

EIA, 2015. Global Petroleum and Other Liquids (Available at: http://www.eia.gov/forecasts/steo/report/global_oil.cfm. Accessed on July 28/2015), Short-Term Energy Outlook.

Fernández-González, V., Muniategui-Lorenzo, S., López-Mahía, P., Prada-Rodríguez, D., 2008. Development of a programmed temperature vaporization-gas chromatography–tandem mass spectrometry method for polycyclic aromatic hydrocarbons analysis in biota samples at ultratrace levels. Journal of Chromatography A 1207, 136-145.

Fingas, M., Fieldhouse, B., 2003. Studies of the formation process of water-in-oil emulsions. Marine Pollution Bulletin 47, 369-396.

Fingas, M., Fieldhouse, B., 2009. Studies on crude oil and petroleum product emulsions: Water resolution and rheology. Colloids and Surfaces A: Physicochemical and Engineering Aspects 333, 67-81.

Fingas, M., Fieldhouse, B., Mullin, J., 1996. Studies of Water-in-Oil Emulsions: The Role of Asphaltenes and Resins, Proceedings of the Nineteenth Arctic Marine Oilspill Program Technical Seminar, Environment Canada, Ottawa, Ontario, Canada, pp. 73-88.

Fingas, M.F., 1997. Studies on the evaporation of crude oil and petroleum products: I. the relationship between evaporation rate and time. Journal of Hazardous Materials 56, 227-236.

Fingas, M.F., Fieldhouse, B., 2004. Formation of water-in-oil emulsions and application to oil spill modeling. Journal of Hazardous Materials 107, 14.

Fingas, M.F., Fieldhouse, B., Bier, I., Conrod, D., Tennyson, E.J., 1993. Development of a test for water-in-oil emulsion breakers, Proceedings of the Sixteenth Arctic and Marine Oil Spill Program Technical Seminar, Calgary, Alberta, Canada, pp. 909-955.

Garrett, R.M., Pickering, I.J., Haith, C.E., Prince, R.C., 1998. Photooxidation of Crude Oils. Environmental Science & Technology 32, 3719-3723.

Gonçalves, C., Carvalho, J.J., Azenha, M.A., Alpendurada, M.F., 2006. Optimization of supercritical fluid extraction of pesticide residues in soil by means of central composite design and analysis by gas chromatography–tandem mass spectrometry. Journal of Chromatography A 1110, 6-14.

González, J.J., Viñas, L., Franco, M.A., Fumega, J., Soriano, J.A., Grueiro, G., Muniategui, S., López-Mahía, P., Prada, D., Bayona, J.M., Alzaga, R., Albaigés, J., 2006. Spatial and temporal distribution of dissolved/dispersed aromatic hydrocarbons in seawater in the area affected by the Prestige oil spill. Marine Pollution Bulletin 53, 250-259.

Gundlach, E.R., Finkelstein, K.J., Sadd, J.L., 1981. IMPACT AND PERSISTENCE OF IXTOC I OIL ON THE SOUTH TEXAS COAST. International Oil Spill Conference Proceedings 1981, 477-485.

Guo, W.J., Wang, Y.X., 2009. A numerical oil spill model based on a hybrid method. Marine Pollution Bulletin 58, 726-734.

Haib, J., Hofer, I., Renaud, J.-M., 2003. Analysis of multiple pesticide residues in tobacco using pressurized liquid extraction, automated solid-phase extraction clean-up and gas chromatography–tandem mass spectrometry. Journal of Chromatography A 1020, 173-187.

Hall, G.J., Frysinger, G.S., Aeppli, C., Carmichael, C.A., Gros, J., Lemkau, K.L., Nelson, R.K., Reddy, C.M., 2013. Oxygenated weathering products of Deepwater Horizon oil come from surprising precursors. Marine Pollution Bulletin 75, 140-149.

Hamoda, M.F., Hamam, S.E.M., Shaban, H.I., 1989. Volatilization of crude oil from saline water. Oil and Chemical Pollution 5, 321-331.

Hayworth, J., Clement, T., Valentine, J., 2011. Deepwater Horizon oil spill impacts on Alabama beaches. Hydrology and Earth System Sciences 15, 3639.

Hayworth, J.S., Clement, T.P., 2011a. BP's Operation Deep Clean: Is dilution the solution to beach pollution? Environmental Science & Technology 45, 1.

Hayworth, J.S., Clement, T.P., 2011b. BP's Operation Deep Clean: Could Dilution be the Solution to Beach Pollution? Environmental Science and Technology-Columbus 45, 4201.

Hayworth, J.S., Clement, T.P., 2012. Provenance of Corexit-related chemical constituents found in nearshore and inland Gulf Coast waters. Marine Pollution Bulletin 64, 10.

Hayworth, J.S., Prabakhar Clement, T., 2012. Provenance of Corexit-related chemical constituents found in nearshore and inland Gulf Coast waters. Marine Pollution Bulletin 64, 2005-2014.

Hayworth, J.S., Prabakhar Clement, T., John, G.F., Yin, F., 2015. Fate of Deepwater Horizon oil in Alabama's beach system: Understanding physical evolution processes based on observational data. Marine Pollution Bulletin 90, 95-105.

Hoffmann, E.d., Stroobant, V., 2001. Mass Spectrometry - Principles and Applications, Second ed. John Wiley & Sons, Ltd.

Incardona, J.P., Swarts, T.L., Edmunds, R.C., Linbo, T.L., Aquilina-Beck, A., Sloan, C.A., Gardner, L.D., Block, B.A., Scholz, N.L., 2013. Exxon Valdez to Deepwater Horizon: Comparable toxicity of both crude oils to fish early life stages. Aquatic Toxicology 142–143, 303-316.

J., J., Burgess, D.J., 2003. Rheology and stability of water-in-oil-in-water multiple emulsions containing Span 83 and Tween 80. AAPS PharmSci. 5.

John, G.F., Yin, F., Mulabagal, V., Hayworth, J.S., Clement, T.P., 2014. Development and application of an analytical method using gas chromatography/triple quadrupole mass spectrometry for characterizing alkylated chrysenes in crude oil samples. Rapid Communications in Mass Spectrometry 28, 948-956.

Johnson, Y.S., 2012. Determination of Polycyclic Aromatic Hydrocarbons in Edible Seafood by QuEChERS-Based Extraction and Gas Chromatography-Tandem Mass Spectrometry. Journal of Food Science 77, T131-T137.

Joye, S., 2013. Oil Spills and Industry History (Available at: http://www.joyeresearchgroup.uga.edu/public-outreach/marine-oil-spills/history. Accessed on July 26, 2015).

Kim, M., Yim, U.H., Hong, S.H., Jung, J.-H., Choi, H.-W., An, J., Won, J., Shim, W.J., 2010. Hebei Spirit oil spill monitored on site by fluorometric detection of residual oil in coastal waters off Taean, Korea. Marine Pollution Bulletin 60, 383-389.

Kostka, J.E., Prakash, O., Overholt, W.A., Green, S.J., Freyer, G., Canion, A., Delgardio, J., Norton, N., Hazen, T.C., Huettel, M., 2011. Hydrocarbon-Degrading Bacteria and the Bacterial Community Response in Gulf of Mexico Beach Sands Impacted by the Deepwater Horizon Oil Spill. Applied and Environmental Microbiology 77, 7962-7974.

Kujawinski, E.B., Kido Soule, M.C., Valentine, D.L., Boysen, A.K., Longnecker, K., Redmond, M.C., 2011. Fate of Dispersants Associated with the Deepwater Horizon Oil Spill. Environmental Science & Technology 45, 1298-1306.

Laffon, B., Rábade, T., Pásaro, E., Méndez, J., 2006. Monitoring of the impact of Prestige oil spill on Mytilus galloprovincialis from Galician coast. Environment International 32, 342-348.

Lee, C.I., Kim, M.C., Kim, H.C., 2009. Temporal variation of chlorophyll a concentration in the coastal waters affected by the Hebei Spirit oil spill in the West Sea of Korea. Marine Pollution Bulletin 58, 496-502.

Lee, R.F., 1999. Agents Which Promote and Stabilize Water-in-Oil Emulsions. Spill Science & Technology Bulletin 5, 117-126.

Lee, R.F., 2003. Photo-oxidation and Photo-toxicity of Crude and Refined Oils. Spill Science & Technology Bulletin 8, 157-162.

Lehr, B., Bristol, S., Possolo, A., 2010a. Oil Budget Calculator, Deepwater Horizon. The Federal Interagency Solutions Group, Oil Budget Calculator Science and Engineering Team.

Lehr, B., Briston, S., Possolo, A., 2010b. Oil Budget Calculator, Deepwater Horizon. The Federal Interagency Solutions Group, Oil Budget Calculator Science and Engineering Team. .

Lessard, R.R., DeMarco, G., 2000. The Significance of Oil Spill Dispersants. Spill Science & Technology Bulletin 6, 59-68.

Li, H., Boufadel, M.C., 2010. Long-term persistence of oil from the Exxon Valdez spill in two-layer beaches. Nature Geosci 3, 96-99.

Lien, G.-W., Chen, C.-Y., Wu, C.-F., 2007. Analysis of polycyclic aromatic hydrocarbons by liquid chromatography/tandem mass spectrometry using atmospheric pressure chemical ionization or electrospray ionization with tropylium post-column derivatization. Rapid Communications in Mass Spectrometry 21, 3694-3700.

Limited, S.R.E.R., Consultancy, A.L., Inc, M., 2006. DISPERSANT EFFECTIVENESS TESTING ON WATER-IN-OIL EMULSIONS AT OHMSETT For U.S. Department of the Interior Minerals Management Service Herndon, VA . (Available at: http://www.bsee.gov/Technology-and-Research/Oil-Spill-Response-Research/Reports/500-599/542AA/, Accessed on November 13, 2015).

Linstrom, P.J., Mallard, W.G.E., NIST Chemistry WebBook, NIST Standard Reference Database Number 69, National Institute of Standards and Technology, Gaithersburg MD, 20899. Available at http://webbook.nist.gov. (Accessed on December 16, 2013). NIST Chemistry WebBook, NIST Standard Reference Database Number 69, National Institute of Standards and Technology, Gaithersburg MD, 20899. Available at http://webbook.nist.gov. (Accessed on December 16, 2013).

Liu, Z., Liu, J., Zhu, Q., Wu, W., 2012a. The weathering of oil after the Deepwater Horizon oil spill: insights from the chemical composition of the oil from the sea surface, salt marshes and sediments. Environmental Research Letters 7, 035302.

Liu, Z., Liu, J., Zhu, Q., Wu, W., 2012b. The weathering of oil after the Deepwater Horizon oil spill: insights from the chemical composition of the oil from the sea surface, salt marshes and sediments. Environmental research letters 7, 14.

Luellen, D.R., Shea, D., 2002. Calibration and Field Verification of Semipermeable Membrane Devices for Measuring Polycyclic Aromatic Hydrocarbons in Water. Environmental Science & Technology 36, 1791-1797.

MacDougall, D., Crummett, W.B., 1980. Guidelines for data acquisition and data quality evaluation in environmental chemistry. Analytical Chemistry 52, 2242-2249.

Mackay, D., van Wesenbeeck, I., 2014. Correlation of Chemical Evaporation Rate with Vapor Pressure. Environmental Science & Technology 48, 10259-10263.

Martínez Vidal, J.L., Arrebola, F.J., Mateu-Sánchez, M., 2002. Application of gas chromatography–tandem mass spectrometry to the analysis of pesticides in fruits and vegetables. Journal of Chromatography A 959, 203-213.

McDaniel, L.D., Basso, J., Pulster, E., Paul, J.H., Sand patties provide evidence for the presence of Deepwater Horizon oil on the beaches of the West Florida Shelf. Marine Pollution Bulletin.

McLafferty, F.W., Tureček, F., 1993. Interpretation of mass spectra, Fourth ed. University Science Books, Sausalito, California.

McLean, J.D., Kilpatrick, P.K., 1997. Effects of asphaltene solvency on stability of water-in-crude-oil emulsions. J. Colloid and Interface Sci. 189, 12.

McLean, J.D., Spiecker, P.M., Sullivan, A.P., Kilpatrick, P.K., 1998. The role of petroleum asphaltenes in the stabilization of water-in-oil emulsions, in: Mullins, O.C., Sheu, E.Y. (Eds.), Structure and Dynamics of Asphaltenes. Plenum Press, New York.

McMaster, M., McMaster, C., 1998. GC/MS A Practical Users Guide. Wiley-VCH. New York.

McNair, H.M., Miller, J.M., 2009. Basic gas chromatography. John Wiley & Sons.

McNutt, M.K., Camilli, R., Crone, T.J., Guthrie, G.D., Hsieh, P.A., Ryerson, T.B., Savas, O., Shaffer, F., 2012. Review of flow rate estimates of the Deepwater Horizon oil spill. Proceedings of the National Academy of Sciences 109, 20260-20267.

Mekenyan, O.G., Ankley, G.T., Veith, G.D., Call, D.J., 1995. QSARs for Photoinduced Toxicity of Aromatic Compounds. SAR and QSAR in Environmental Research 4, 139-145.

Menon, V.B., Wasan, D.T., 1998. A review of the factors affecting the stability of solids-stabilized emulsions. Sep. Sci. Technol. 23, 12.

Michel, J., Owens, E.H., Zengel, S., Graham, A., Nixon, Z., Allard, T., Holton, W., Reamer, P.D., Lamarche, A., White, M., Rutherford, N., Childs, C., Mauseth, G., Challenger, G., Taylor, E., 2013a. Extent and Degree of Shoreline Oiling: Deepwater Horizon Oil Spill, Gulf of Mexico, USA. PLOS ONE 8, 9.

Michel, J., Owens, E.H., Zengel, S., Graham, A., Nixon, Z., Allard, T., Holton, W., Reimer, P.D., Lamarche, A., White, M., 2013b. Extent and degree of shoreline oiling: Deepwater Horizon oil spill, Gulf of Mexico, USA. PloS one 8, e65087.

Michel, J., Owens, E.H., Zengel, S., Graham, A., Nixon, Z., Allard, T., Holton, W., Reimer, P.D., Lamarche, A., White, M., Rutherford, N., Childs, C., Mauseth, G., Challenger, G., Taylor, E., 2013c. Extent and Degree of Shoreline Oiling: <italic>Deepwater Horizon</italic> Oil Spill, Gulf of Mexico, USA. PLoS ONE 8, e65087.

Mulabagal, V., Yin, F., John, G.F., Hayworth, J.S., Clement, T.P., 2013. Chemical fingerprinting of petroleum biomarkers in Deepwater Horizon oil spill samples collected from Alabama shoreline. Marine Pollution Bulletin 70, 147-154.

Mumtaz, M., George, J., Gold, K., Cibulas, W., Derosa, C., 1996. ATSDR evaluation of health effects of chemicals. IV. Polycyclic aromatic hydrocarbons (PAHs): understanding a complex problem. Toxicology and industrial health 12, 742-971.

Nácher-Mestre, J., Serrano, R., Portolés-Nicolau, T., Hernández, F., Benedito-Palos, L., Pérez-Sánchez, J., 2009. A reliable analytical approach based on gas chromatography coupled to triple quadrupole and time-of-flight mass analyzers for the determination and confirmation of polycyclic aromatic hydrocarbons in complex matrices from aquaculture activities. Rapid Communications in Mass Spectrometry 23, 2075-2086.

Natter, M., Keevan, J., Wang, Y., Keimowitz, A.R., Okeke, B.C., Son, A., Lee, M.-K., 2012. Level and Degradation of Deepwater Horizon Spilled Oil in Coastal Marsh Sediments and Pore-Water. Environmental Science & Technology 46, 5744-5755.

Neff, J.M., 1979. Polycyclic aromatic hydrocarbons in the aquatic environment: sources, fates and biological effects. Applied Science Publishers (London).

NIST, 2011a. Formulas which begin with C10H8 (Available at - http://webbook.nist.gov/cgi/formula/C10H8. Accessed on October 8, 2015), Formula Browser.

NIST, 2011b. Formulas which begin with C11H10 (Available at - http://webbook.nist.gov/cgi/formula/C11H10. Accessed on October 8, 2015), Formula Browser.

NIST, 2011c. Formulas which begin with C12H8S (Available at - http://webbook.nist.gov/cgi/formula/C12H8S. Accessed on October 8, 2015), Formula Browser.

NIST, 2011d. Formulas which begin with C12H12 (Available at - http://webbook.nist.gov/cgi/formula/C12H12. Accessed on October 8, 2015), Formula Browser.

NIST, 2011e. Formulas which begin with C13H10 (Available at - http://webbook.nist.gov/cgi/formula/C13H10. Accessed on October 8, 2015), Formula Browser.

NIST, 2011f. Formulas which begin with C13H10S (Available at - http://webbook.nist.gov/cgi/formula/C13H10S. Accessed on October 8, 2015), Formula Browser.

NIST, 2011g. Formulas which begin with C13H14 (Available at - http://webbook.nist.gov/cgi/formula/C13H14. Accessed on October 8, 2015), Formula Browser.

NIST, 2011h. Formulas which begin with C14H10 (Available at - http://webbook.nist.gov/cgi/formula/C14H10. Accessed on October 8, 2015) Formula Browser.

NIST, 2011i. Formulas which begin with C14H12 (Available at - http://webbook.nist.gov/cgi/formula/C14H12. Accessed on October 8, 2015), Formula Browser.

NIST, 2011j. Formulas which begin with C14H12S (Available at - http://webbook.nist.gov/cgi/formula/C14H12S. Accessed on October 8, 2015), Formula Browser.

NIST, 2011k. Formulas which begin with C14H16 (Available at - http://webbook.nist.gov/cgi/formula/C14H16. Accessed on October 8, 2015), Formula Browser.

NIST, 2011l. Formulas which begin with C15H12 (Available at - http://webbook.nist.gov/cgi/formula/C15H12. Accessed on October 8, 2015), Formula Browser.

NIST, 2011m. Formulas which begin with C15H14 (Available at - http://webbook.nist.gov/cgi/formula/C15H14. Accessed on October 8, 2015), Formula Browser.

NIST, 2011n. Formulas which begin with C15H14S (Available at - http://webbook.nist.gov/cgi/formula/C15H14S. Accessed on October 8, 2015), Formula Browser.

NIST, 2011o. Formulas which begin with C16H14 (Available at - http://webbook.nist.gov/cgi/formula/C16H14. Accessed on October 8, 2015) Formula Browser.

NIST, 2011p. Formulas which begin with C16H16 (Available at - http://webbook.nist.gov/cgi/formula/C16H16. Accessed on October 8, 2015), Formula Browser.

NIST, 2011q. Formulas which begin with C17H16 (Available at - http://webbook.nist.gov/cgi/formula/C17H16. Accessed on October 8, 2015), Formula Browser.

NIST, 2011r. Formulas which begin with C18H12 (Available at - http://webbook.nist.gov/cgi/formula/C18H12. Accessed on October 8, 2015), Formula Browser.

NIST, 2011s. Formulas which begin with C18H18 (Available at - http://webbook.nist.gov/cgi/formula/C18H18. Accessed on October 8, 2015), Formula Browser.

NIST, 2011t. Formulas which begin with C19H14 (Available at - http://webbook.nist.gov/cgi/formula/C19H14. Accessed on October 8, 2015), Formula Browser.

NIST, 2011u. Formulas which begin with C20H16 (Available at - http://webbook.nist.gov/cgi/formula/C20H16. Accessed on October 8, 2015), Formula Browser.

NIST, 2011v. Formulas which begin with C21H18 (Available at - http://webbook.nist.gov/cgi/formula/C21H18. Accessed on October 8, 2015), Formula Browser.

NIST, 2011w. Formulas which begin with C22H20 (Available at - http://webbook.nist.gov/cgi/formula/C22H20. Accessed on October 8, 2015), Formula Browser.

NRC, 2003. Oil in the Sea III:: Inputs, Fates, and Effects. national academies Press.

O'Sullivan, A.J., Richardson, A.J., 1967. The Torrey Canyon Disaster and Intertidal Marine Life. Nature 214, 448-542.

Operational Science Advisory Team (OSAT-3), U.A.C., 2013. Investigation of Recurring Residual Oil in Discrete Shoreline Areas in the Eastern Area of Responsibility, in: Report to the Federal On-Scene Coordinator, D.H., October, 2013 (Ed.).

OSAT-1, 2010. Summary Report ofor Sub-sea and Sub-surface oil and dispersant detection: Sampling and Monitoring. (Accessed on March 6, 2014. Available at: http://www.restorethegulf.gov/sites/default/files/documents/pdf/OSAT_Report_FINAL_17DEC.pdf).

OSAT-2, 2011. Summary report for fate and effects of remnant oil in the beach environment (Accessed on January 12, 2014. http://www.restorethegulf.gov/sites/default/files/u316/OSAT-2%20Report%20no%20ltr.pdf).

OSAT-3, 2013. Investigation of Recurring Residual Oil in Discrete Shoreline Areas in the Eastern Area of Responsibility. (Accessed on March 3, 2014. Available at: http://www.restorethegulf.gov/sites/default/files/u372/OSAT%20III%20Eastern%20States.pdf).

OSAT-3, 2014. Investigation of Recurring Residual Oil in Discrete Shoreline Areas in the Eastern Area of Responsibility. (Accessed on March 3, 2014. Available at: http://www.restorethegulf.gov/sites/default/files/u372/OSAT%20III%20Eastern%20States.pdf).

Pal, R., 1996. Effect of droplet size on the rheology of emulsions. AIChE Journal 42, 3181-3190.

Patton, J.S., Rigler, M.W., Boehm, P.D., Fiest, D.L., 1981. Ixtoc 1 oil spill: flaking of surface mousse in the Gulf of Mexico. Nature 290, 235-238.

Pauzi Zakaria, M., Okuda, T., Takada, H., 2001. Polycyclic Aromatic Hydrocarbon (PAHs) and Hopanes in Stranded Tar-balls on the Coasts of Peninsular Malaysia: Applications of Biomarkers for Identifying Sources of Oil Pollution. Marine Pollution Bulletin 42, 1357-1366.

Pelz, O., Brown, J., Huddleston, M., Rand, G., Gardinali, P., Stubblefield, W., BenKinney, M.T., Ahnell, A., 2011. Selection of a Surrogate MC252 Oil as a Reference Material for Future Aquatic Toxicity Tests and Other Studies, Society of Environmental Toxicology and Chemistry (SETAC) 2011, John B. Hynes Veterans Memorial Convention Center in Boston, Massachusetts.

Peterson, C.H., Rice, S.D., Short, J.W., Esler, D., Bodkin, J.L., Ballachey, B.E., Irons, D.B., 2003. Long-Term Ecosystem Response to the Exxon Valdez Oil Spill. Science 302, 2082-2086.

Piatt, J.F., Anderson, P., 1996. Response of common murres to the Exxon Valdez oil spill and long-term changes in the Gulf of Alaska marine ecosystem, American fisheries society symposium, pp. 720-737.

Pitarch, E., Medina, C., Portolés, T., López, F.J., Hernández, F., 2007. Determination of priority organic micro-pollutants in water by gas chromatography coupled to triple quadrupole mass spectrometry. Analytica Chimica Acta 583, 246-258.

Pozdnyshev, G.N., Petrov, A.A., Makarova, A.M., 1, 23-27., 1969. Separation of crude oil into oils, resins, and asphaltenes by extraction. Chem. Mat. Sci. 5, 5.

Prince, R.C., Elmendorf, D.L., Lute, J.R., Hsu, C.S., Haith, C.E., Senius, J.D., Dechert, G.J., Douglas, G.S., Butler, E.L., 1994. 17.alpha.(H)-21.beta.(H)-hopane as a conserved

internal marker for estimating the biodegradation of crude oil. Environmental Science & Technology 28, 142-145.

Prince, R.C., Garrett, R.M., Bare, R.E., Grossman, M.J., Townsend, T., Suflita, J.M., Lee, K., Owens, E.H., Sergy, G.A., Braddock, J.F., Lindstrom, J.E., Lessard, R.R., 2003. The Roles of Photooxidation and Biodegradation in Long-term Weathering of Crude and Heavy Fuel Oils. Spill Science & Technology Bulletin 8, 145-156.

Radović, J.R., Aeppli, C., Nelson, R.K., Jimenez, N., Reddy, C.M., Bayona, J.M., Albaigés, J., 2014. Assessment of photochemical processes in marine oil spill fingerprinting. Marine Pollution Bulletin 79, 268-277.

Reddy, C.M., Eglinton, T.I., Hounshell, A., White, H.K., Xu, L., Gaines, R.B., Frysinger, G.S., 2002. The West Falmouth Oil Spill after Thirty Years: The Persistence of Petroleum Hydrocarbons in Marsh Sediments. Environmental Science & Technology 36, 4754-4760.

Sage, M.L., Sage, G.W., 2000. Vapor Pressure, in: Boethling, R.S., Mackay, D. (Eds.), Handbook of Property Estimation Methods for Chemicals. Lewis Publishers.

Sapozhnikova, Y., Lehotay, S.J., 2013. Multi-class, multi-residue analysis of pesticides, polychlorinated biphenyls, polycyclic aromatic hydrocarbons, polybrominated diphenyl ethers and novel flame retardants in fish using fast, low-pressure gas chromatography–tandem mass spectrometry. Analytica Chimica Acta 758, 80-92.

Schantz, M.M., Kucklick, J.R., 2011. Interlaboratory Analytical Comparison Study to Support Deepwater Horizon Natural Resource Damage Assessment: Description and Results for Crude Oil QA10OIL01. National Institute of Standards and Technology, Gaithersburg, MD 20899, USA, Gaithersburg, MD 20899.

Sjöblom, J., Aske, N., Harald Auflem, I., Brandal, Ø., Erik Havre, T., Sæther, Ø., Westvik, A., Eng Johnsen, E., Kallevik, H., 2003. Our current understanding of water-in-crude oil emulsions.: Recent characterization techniques and high pressure performance. Advances in Colloid and Interface Science 100–102, 399-473.

Sjöblom, J., Söderlund, H., Lindblad, S., Johansen, E.J., Skjärvö, I.M., 1990. Water-in-crude oil emulsions from the Norwegian continental shelf. Colloid & Polymer Sci 268, 389-398.

Song, L., Cho, D.S., Bhandari, D., Gibson, S.C., McNally, M.E., Hoffman, R.M., Cook, K.D., 2011. Liquid chromatography/dopant-assisted atmospheric pressure chemical ionization mass spectrometry for the analysis of non-polar compounds. International Journal of Mass Spectrometry 303, 173-180.

Spiecker, P.M., Gawrys, K.L., Trail, C.B., Kilpatrick, P.K., 2003. Effects of petroleum resins on asphaltene aggregation and water-in-oil emulsion formation. Colloids and Surfaces A: Physicochemical and Engineering Aspects 220, 9-27.

Stiver, W., Mackay, D., 1984. Evaporation rate of spills of hydrocarbons and petroleum mixtures. Environmental Science & Technology 18, 834-840.

Team, O.B.C.S.a.E., 2010. Oil Budget Calculator Deepwater Horizon Technical Documentation (http://www.restorethegulf.gov/sites/default/files/documents/pdf/OilBudgetCalc_Full_HQ-Print_111110.pdf) Accessed 2/17/2014.

Thingstad, T., Pengerud, B., 1983a. The formation of 'chocolate mousse' from Statfjord crude oil and seawater. Marine Pollution Bulletin 14, 3.

Thingstad, T., Pengerud, B., 1983b. The formation of “chocolate mousse” from Statfjord crude oil and seawater. Marine Pollution Bulletin 14, 214-216.

Trudel, K., Belore, R.C., Mullin, J.V., Guarino, A., 2010. Oil viscosity limitation on dispersibility of crude oil under simulated at-sea conditions in a large wave tank. Marine Pollution Bulletin 60, 1606-1614.

Turcotte, D., Headley, J.V., Abudulai, N.L., Hodson, P.V., Stephen Brown, R., 2011. Identification of phase II in vivo metabolites of alkyl-anthracenes in rainbow trout (Oncorhynchus mykiss). Chemosphere 85, 1585-1591.

Turner, R.E., Overton, E.B., Meyer, B.M., Miles, M.S., Hooper-Bui, L., 2014. Changes in the concentration and relative abundance of alkanes and PAHs from the Deepwater Horizon oiling of coastal marshes. Marine Pollution Bulletin 86, 291-297.

Urbano, M., Elango, V., Pardue, J.H., 2013. Biogeochemical characterization of MC252 oil:sand aggregates on a coastal headland beach. Marine Pollution Bulletin 77, 183-191.

USEPA, 1993. Provisional guidance for quantitative risk assessmentof polycyclic aromatic hydrocarbons (Available at: http://cfpub.epa.gov/ncea/cfm/recordisplay.cfm).

USEPA, 1996. Method 8000B - Determinative chromatographic separations (Accessed on September 20, 2013). Available at http://www.epa.gov/osw/hazard/testmethods/sw846/pdfs/8000b.pdf.

USEPA, 2007a. Method 8270D Semivolatile Organic Compounds by Gas Chromatography/Mass Spectrometry (GC/MS) (accessed April 10, 2013). Available at http://www.epa.gov/osw/hazard/testmethods/sw846/pdfs/8270d.pdf.

USEPA, 2007b. Method 8272 - Parent and Alkyl polycyclic aromatics in sediment pore water by solid-phase microextraction and gas chromatography/mass spectrometry in selected ion monitoring mode (accessed September 20, 2013). Available at http://www.epa.gov/osw/hazard/testmethods/pdfs/8272.pdf.

USEPA, 2010. Explanation of PAH benchmark calculations using EPA PAH ESB approach Originally developed by Dave Mount, ORD Duluth (Accessed August 24, 2013). Available at: http://www.epa.gov/bpspill/water/explanation-of-pah-benchmark-calculations-20100622.pdf.

Valentine, D.L., Fisher, G.B., Bagby, S.C., Nelson, R.K., Reddy, C.M., Sylva, S.P., Woo, M.A., 2014. Fallout plume of submerged oil from Deepwater Horizon. Proceedings of the National Academy of Sciences 111, 5.

Varlet, V., Serot, T., Monteau, F., Bizec, B.L., Prost, C., 2007. Determination of PAH profiles by GC–MS/MS in salmon processed by four cold-smoking techniques. Food Additives & Contaminants 24, 744-757.

Venosa, A.D., Holder, E.L., 2013. Determining the dispersibility of South Louisiana crude oil by eight oil dispersant products listed on the NCP Product Schedule. Marine Pollution Bulletin 66, 73-77.

Venosa, A.D., King, D.W., Sorial, G.A., 2002. The Baffled Flask Test for Dispersant Effectiveness: A Round Robin Evaluation of Reproducibility and Repeatability. Spill Science & Technology Bulletin 7, 299-308.

Walorczyk, S., 2007. Development of a multi-residue screening method for the determination of pesticides in cereals and dry animal feed using gas chromatography–

triple quadrupole tandem mass spectrometry. Journal of Chromatography A 1165, 200-212.

Wang, S.D., Shen, Y.M., Zheng, Y.H., 2005. Two-dimensional numerical simulation for transport and fate of oil spills in seas. Ocean Engineering 32, 1556-1571.

Wang, Z., Fingas, M., Blenkinsopp, S., Sergy, G., Landriault, M., Sigouin, L., Foght, J., Semple, K., Westlake, D.W.S., 1998a. Comparison of oil composition changes due to biodegradation and physical weathering in different oils. Journal of Chromatography A 809, 89-107.

Wang, Z., Fingas, M., Blenkinsopp, S., Sergy, G., Landriault, M., Sigouin, L., Lambert, P., 1998b. Study of the 25-Year-Old Nipisi Oil Spill: Persistence of Oil Residues and Comparisons between Surface and Subsurface Sediments. Environmental Science & Technology 32, 2222-2232.

Wang, Z., Fingas, M., Li, K., 1994a. Fractionation of a Light Crude Oil and Identification and Quantitation of Aliphatic, Aromatic, and Biomarker Compounds by GC-FID and GC-MS, Part I. Journal of Chromatographic Science 32, 361-366.

Wang, Z., Fingas, M., Li, K., 1994b. Fractionation of a Light Crude Oil and Identification and Quantitation of Aliphatic, Aromatic, and Biomarker Compounds by GC-FID and GC-MS, Part II. Journal of Chromatographic Science 32, 367-382.

Wang, Z., Fingas, M., Sergy, G., 1994c. Study of 22-Year-Old Arrow Oil Samples Using Biomarker Compounds by GC/MS. Environmental Science & Technology 28, 1733-1746.

Wang, Z., Fingas, M.F., 2003. Development of oil hydrocarbon fingerprinting and identification techniques. Marine Pollution Bulletin 47, 423-452.

Wang, Z., Li, K., Lambert, P., Yang, C., 2007. Identification, characterization and quantitation of pyrogenic polycylic aromatic hydrocarbons and other organic compounds in tire fire products. Journal of Chromatography A 1139, 14-26.

Wang, Z., Stout, S.A., Fingas, M., 2006. Forensic Fingerprinting of Biomarkers for Oil Spill Characterization and Source Identification. Environmental Forensics 7, 105-146.

Wasan, D.T., McNamara, J.J., Shah, S.M., Sampath, K., Aderangi, N., 1979. The Role of Coalescence Phenomena and Interfacial Rheological Properties in Enhanced Oil Recovery: An Overview. Journal of Rheology 23, 181-207.

website, R.t.G., 2014. (http://www.restorethegulf.gov/task-force) Accessed 2/17/2014.

Wong, J.W., Zhang, K., Tech, K., Hayward, D.G., Krynitsky, A.J., Cassias, I., Schenck, F.J., Banerjee, K., Dasgupta, S., Brown, D., 2010. Multiresidue Pesticide Analysis of Ginseng Powders Using Acetonitrile- or Acetone-Based Extraction, Solid-Phase Extraction Cleanup, and Gas Chromatography−Mass Spectrometry/Selective Ion Monitoring (GC-MS/SIM) or −Tandem Mass Spectrometry (GC-MS/MS). Journal of Agricultural and Food Chemistry 58, 5884-5896.

Wood, J.H., Long, G.R., Morehouse, D.F., 2004. Long-Term World Oil Supply Scenarios (Available at: http://www.netl.doe.gov/energy-analyses/pubs/EIA_LongTermOilSupply.pdf. Accessed on July 28, 2015).

Xia, K., Hagood, G., Childers, C., Atkins, J., Rogers, B., Ware, L., Armbrust, K., Jewell, J., Diaz, D., Gatian, N., Folmer, H., 2012. Polycyclic Aromatic Hydrocarbons (PAHs) in Mississippi Seafood from Areas Affected by the Deepwater Horizon Oil Spill. Environmental Science & Technology 46, 5310-5318.

Yim, U.H., Ha, S.Y., An, J.G., Won, J.H., Han, G.M., Hong, S.H., Kim, M., Jung, J.-H., Shim, W.J., 2011. Fingerprint and weathering characteristics of stranded oils after the Hebei Spirit oil spill. Journal of Hazardous Materials 197, 60-69.

Yim, U.H., Kim, M., Ha, S.Y., Kim, S., Shim, W.J., 2012. Oil Spill Environmental Forensics: the Hebei Spirit Oil Spill Case. Environmental Science & Technology 46, 6431-6437.

Yin, F., Hayworth, J.S., Clement, T.P., 2015a. A Tale of Two Recent Spills—Comparison of 2014 Galveston Bay and 2010 Deepwater Horizon Oil Spill Residues. PLoS ONE 10, e0118098.

Yin, F., John, G.F., Hayworth, J.S., Clement, T.P., 2015b. Long-term monitoring data to describe the fate of polycyclic aromatic hydrocarbons in Deepwater Horizon oil submerged off Alabama's beaches. Science of The Total Environment 508, 46-56.

Yin, F., John, G.F., Mulabagal, V., Hayworth, J.S., Clement, T.P., 2014. A long-term investigation of spatial and temporal distribution of polycyclic aromatic hydrocarbons in

Deepwater Horizon oil spill samples collected from Alabama shoreline, Gulf of Mexico Oil Spill and Ecosystem Science Conference, Mobile, AL, USA.

Appendix

Table A1: GC and MS parameters for F1 fraction

GC Parameters	
Column	DB-5MS (J&W Agilent Technologies, 20 mx 180 µm x 0.14 µm)
Inlet Temperature	290°C
Inlet Pressure	24.67 psi
Carrier gas	Helium
Flow rate	1 mL/min
Injection mode	Pulsed splitless
Oven Program	35°C (0.8 minutes hold); 7°C/minute to 120°C; 5°C/minute to 240°C; 3°C/minute to 320°C
Total run time	63.61 minutes
Injection volume	1 µL
Transfer line temperature	320 °C
MS Parameters	
Delta EMV	-70 eV
Acquisition parameters	Electron Impact (EI)
Solvent Delay	2.5 minutes
MS source temperature	280 °C
Quadrupole	Q1 = Q2 = 180 °C
SIM Mode – Ions monitored	
Compound	**Ion (m/z)**
Hopanes	191
Steranes	217 and 218

Table A2: GC and MS parameters for F2 fraction for analysis in MRM mode

GC Parameters	
Column	DB-5MS (J&W Agilent Technologies, 20 mx 180 µm x 0.14 µm)
Inlet Temperature	300°C
Inlet Pressure	23.4 psi
Carrier gas	Helium
Flow rate	1 mL/min
Injection mode	Pulsed splitless
Oven Program	50°C (0.8 minutes hold); 70°C/minute to 180°C; 7°C/minute to 230°C (1 minute hold); 40°C/minute to 280°C (1 minute hold); 25°C/minute to 330°C (5 minute hold)
Total run time	20.05 minutes
Injection volume	1 µL
Transfer line temperature	320 °C
MS Parameters	
Delta EMV	-70 eV
Acquisition parameters	Electron Impact (EI)
Solvent Delay	2.5 minutes
MS source temperature	350°C
Quadrupole	Q1 = Q2 = 180 °C

MRM Mode – Ions monitored

Compound	**Time segment**	**MRM transitions (m/z)**	**Collision energy (eV)**	**Type**
Biphenyl	1	154.0 → 152.0	25	Target
		154.0 → 153.0	25	
Naphthalene-d_8	1	136.0 → 108.0	19	Surrogate
Acenapthylene	1	152.0 → 150.0	40	Target
		152.0 → 151.0	40	
Acenapthene-d_{10}	1	162.0 → 160.0	25	Surrogate
Acenapthene	1	154.0 → 152.0	40	Target
		153.0 → 152.0	40	
Phenanthrene-d_{10}	2	188.0 → 160.0	19	Surrogate
Anthracene	2	178.0 → 176.0	34	Target
Fluoranthene	3	202.0 → 201.0	30	Target
		202.0 → 200.0	50	
Pyrene	3	202.0 → 201.0	30	Target
		202.0 → 200.0	50	
p-Terphenyl-d_{14}	4	244.0 → 212.0	40	Internal standard
Benzo(*a*)anthracene	4	228.0 → 226.0	38	Target
		228.0 → 224.0	38	
Benzo(*b*)fluoranthene	5	252.0 → 250.0	42	Target
		250.0 → 248.0	40	
Benzo(*k*)fluoranthene	5	252.0 → 250.0	42	Target
		250.0 → 248.0	40	
Benzo(*j*)fluoranthene	5	252.0 → 250.0	42	Target
		250.0 → 248.0	40	
Benzo(*e*)pyrene	5	252.0 → 250.0	42	Target
		250.0 → 248.0	40	
Benzo(*a*)pyrene-d_{12}	5	264.0 → 260.0	39	Surrogate
Benzo(*a*)pyrene	5	252.0 → 250.0	42	Target
		250.0 → 248.0	40	
Perylene	6	252.0 → 250.0	40	Target
		250.0 → 248.0	40	
Dibenz(*a,h*)anthracene	6	278.0 → 276.0	42	Target
		276.0 → 274.0	38	
Dibenz(*a,c*)anthracene	6	278.0 → 276.0	42	Target
		276.0 → 274.0	38	
Indeno(1,2,3-*cd*)pyrene	6	276.0 → 274.0	42	Target
Benzo(*ghi*)perylene	6	276.0 → 274.0	42	Target

Table A3: GC and MS parameters for F2 fraction for analysis in SIM mode

GC Parameters		
Column	DB-5MS (J&W Agilent Technologies, 20 mx 180 µm x 0.14 µm)	
Inlet Temperature	300°C	
Inlet Pressure	19.5 psi	
Carrier gas	Helium	
Flow rate	1 mL/min	
Injection mode	Pulsed splitless	
Oven Program	50°C (1 minute hold); 5°C/minute to 300°C (12 minutes hold)	
Total run time	63 minutes	
Injection volume	1 µL	
Transfer line temperature	320 °C	
MS Parameters		
Delta EMV	-70 eV	
Acquisition parameters	Electron Impact (EI)	
Solvent Delay	2.5 minutes	
MS source temperature	350 °C	
Quadrupole	Q1 = Q2 = 180 °C	
SIM Mode – Ions monitored		
Compound	**Target ion (m/z)**	**RRF standard**
C_0-naphthalene	128	-
C_1-naphthalenes	142	2-Methylnaphthalene
C_2-naphthalenes	156	2,6-Methylnaphthalene
C_3-naphthalenes	170	2,3,5-Methylnaphthalene
C_4-naphthalenes	184	2,3,5-Methylnaphthalene
C_0-phenanthrene	178	-
C_1-phenanthrenes	192	1-Methylphenanthrene
C_2-phenanthrenes	206	1-Methylphenanthrene
C_3-phenanthrenes	220	1-Methylphenanthrene
C_4-phenanthrenes	234	1-Methylphenanthrene
C_0-dibenzothiophene	184	-
C_1-dibenzothiophenes	198	Dibenzothiophene
C_2-dibenzothiophenes	212	Dibenzothiophene
C_3-dibenzothiophenes	226	Dibenzothiophene
C_0-fluorene	166	-
C_1-fluorenes	180	Fluorene
C_2-fluorenes	194	Fluorene
C_3-fluorenes	208	Fluorene
C_0-chrysene	228	-
C_1-chrysenes	242	Chrysene
C_2-chrysenes	256	Chrysene
C_3-chrysenes	270	Chrysene
C_4-chrysenes	284	Chrysene
p-terphenyl-d_{14}	244	-

Table A4: Estimated vapor pressure, *HOMO*, *LUMO* and *HOMO-LUMO* for naphthalene and its alkylated homologues

Compound	**Vapor Pressure at 25°C (mm Hg)**	**HOMO (eV)**	**LUMO (eV)**	**HOMO-LUMO (eV)**
C_0-naphthalene				
Naphthalene	4.04E-02	8.84	0.41	8.43
C_1 naphthalenes				
1-methylnapthalene	3.68E-02	8.71	0.41	8.30
2-methylnapthalene	3.45E-02	8.74	0.39	8.35
3-methylnapthalene	3.45E-02	8.74	0.39	8.35
C_2 naphthalenes				
1-ethylnaphthalene	1.72E-02	8.71	0.39	8.32
2-ethylnaphthalene	1.77E-02	8.77	0.38	8.39
1,2-dimethylnaphthalene	1.21E-02	8.62	0.36	8.26
1,3-dimethylnaphthalene	1.35E-02	8.63	0.37	8.26
1,4-dimethylnaphthalene	1.03E-02	8.57	0.40	8.17
1,5-dimethylnaphthalene	3.50E-03	8.57	0.40	8.17
1,6-dimethylnaphthalene	1.28E-02	8.63	0.37	8.26
2,3-dimethylnapthalene	1.73E-03	8.68	0.36	8.32
2,6-dimethylnapthalene	2.45E-03	8.67	0.34	8.33
2,7-dimethylnapthalene	2.45E-03	8.70	0.34	8.36
C_3 naphthalenes				
1,2,4-trimethylnaphthalene	2.53E-03	8.52	0.36	8.16
1,2,5-trimethylnaphthalene	4.06E-03	8.52	0.36	8.16
1,2,6-trimethylnaphthalene	4.84E-03	8.57	0.33	8.24
1,2,7-trimethylnaphthalene	4.84E-03	8.59	0.33	8.26
1,3,5-trimethylnaphthalene	2.52E-03	8.52	0.37	8.15
1,3,6-trimethylnaphthalene	4.84E-03	8.59	0.34	8.25
1,3,7-trimethylnaphthalene	4.84E-03	8.57	0.37	8.20
1,4,5-trimethylnaphthalene	2.52E-03	8.43	0.39	8.04
1,4,6-trimethylnaphthalene	2.52E-03	8.53	0.37	8.16
1,6,7-trimethylnaphthalene	2.25E-03	8.58	0.35	8.23
2,3,5-trimethylnaphthalene	2.25E-03	8.55	0.35	8.20
2,3,6-trimethylnaphthalene	2.52E-03	8.61	0.32	8.29
1-ethyl-3-methylnaphthalene	2.89E-03	8.66	0.37	8.29
1-ethyl-4-methylnaphthalene	2.89E-03	8.61	0.40	8.21
1-ethyl-5-methylnaphthalene	2.89E-03	8.60	0.40	8.20
2-ethyl-7-methylnaphthalene	2.89E-03	8.71	0.34	8.37
2-ethyl-5-methylnaphthalene	2.89E-03	8.64	0.37	8.27
2-ethyl-1-methylnaphthalene	2.89E-03	8.64	0.37	8.27
1-propylnaphthalene	7.21E-03	8.70	0.40	8.30
2-propylnaphthalene	3.31E-03	8.78	0.38	8.40
1-(1-methylethyl)-)naphthalene	1.03E-02	8.73	0.40	8.33
2-(1-methylethyl)-)naphthalene	1.02E-02	8.76	0.38	8.38
C_4 naphthalenes				
1,4,6,7-tetramethylnaphthalene	7.79E-04	8.42	0.35	8.07
1,2,6,8-tetramethylnaphthalene	7.79E-04	8.40	0.31	8.09
1,3,5,8-tetramethylnaphthalene	7.79E-04	8.35	0.35	8.00
1,2,5,8-tetramethylnaphthalene	7.79E-04	8.34	0.34	8.00
1,2-diethylnaphthalene	1.03E-03	8.66	0.36	8.30
1,6-diethylnaphthalene	1.03E-03	8.68	0.37	8.31
1,7-diethylnaphthalene	1.03E-03	8.65	0.37	8.28
2,3-diethylnaphthalene	1.03E-03	8.66	0.34	8.32
2-methyl-1-propylnapthalene	1.03E-03	8.66	0.37	8.29
3-methyl-2-propylnapthalene	1.03E-03	8.68	0.35	8.33
2-methyl-3-propylnapthalene	1.03E-03	8.68	0.35	8.33
2-butylnaphthalene	2.98E-03	8.75	0.38	8.37
1-butylnaphthalene	3.44E-03	8.70	0.40	8.30
1-isopropyl-2-methylnaphthalene	2.09E-03	8.66	0.35	8.31
2-isopropyl-3-methylnaphthalene	2.09E-03	8.69	0.36	8.33
tert-butylnaphthalene	5.63E-03	8.71	0.38	8.33

Table A5: Estimated vapor pressure, *HOMO*, *LUMO* and *HOMO-LUMO* for phenanthrene and its alkylated homologues

Compound	Vapor Pressure at 25°C (mm Hg)	HOMO (eV)	LUMO (eV)	HOMO-LUMO (eV)
C_0-phenanthrenes				
Phenanthrene	4.32E-05	8.74	0.53	8.21
C_1-phenanthrenes				
1-methylphenanthrene	2.45E-05	8.64	0.52	8.12
2-methylphenanthrene	6.67E-05	8.72	0.50	8.22
3-methylphenanthrene	6.67E-05	8.64	0.52	8.12
4-methylphenanthrene	2.45E-05	8.62	0.52	8.10
9-methylphenanthrene	5.01E-05	8.61	0.53	8.08
C_2-phenanthrenes				
3,6-dimethylphenanthrene	7.59E-06	8.55	0.50	8.05
2,7-dimethylphenanthrene	7.59E-06	8.70	0.48	8.22
1,4-dimethylphenanthrene	1.82E-05	8.50	0.51	7.99
2,5-dimethylphenanthrene	1.82E-05	8.62	0.49	8.13
9,10-dimethylphenanthrene	7.59E-06	8.53	0.51	8.02
1-ethylphenanthrene	2.12E-05	8.67	0.52	8.15
2-ethylphenanthrene	2.12E-05	8.72	0.51	8.21
3-ethylphenanthrene	2.12E-05	8.66	0.52	8.14
9-ethylphenanthrene	5.43E-05	8.64	0.53	8.11
C_3-phenanthrenes				
2,3,5-trimethylphenanthrene	8.20E-06	8.52	0.47	8.05
1,2,8-trimethylphenanthrene	8.20E-06	8.56	0.48	8.08
1,6,7-trimethylphenanthrene	8.20E-06	8.53	0.47	8.06
1,6,9-trimethylphenanthrene	8.20E-06	8.45	0.49	7.96
1,4,8-trimethylphenanthrene	8.20E-06	8.47	0.52	7.95
1,3,7-trimethylphenanthrene	8.20E-06	8.55	0.48	8.07
1,3,4-trimethylphenanthrene	8.20E-06	8.45	0.50	7.95
3,6,9-trimethylphenanthrene	8.20E-06	8.44	0.49	7.95
2,3,9-trimethylphenanthrene	8.20E-06	8.49	0.48	8.01
2,3,4-trimethylphenanthrene	8.20E-06	8.52	0.47	8.05
1-n-propylphenanthrene	9.02E-06	8.65	0.52	8.13
2-n-propylphenanthrene	9.02E-06	8.72	0.50	8.22
9-n-propylphenanthrene	9.02E-06	8.62	0.52	8.10
9-ethyl-10-methylphenanthrene	7.73E-06	8.54	0.50	8.04
1-ethyl-2-methylphenanthrene	7.73E-06	8.64	0.49	8.15
6-ethyl-1-methylphenanthrene	7.73E-06	8.56	0.51	8.05
2-isopropylphenanthrene	1.67E-05	8.70	0.49	8.21
3-isopropylphenanthrene	1.67E-05	8.66	0.52	8.14
C_4-phenanthrenes				
1,6,7,10-tetramethylphenanthrene	3.18E-06	8.38	0.46	7.92
1,4,7,10-tetramethylphenanthrene	3.18E-06	8.38	0.48	7.90
1,3,6,8-tetramethylphenanthrene	3.18E-06	8.41	0.47	7.94
2,7-diethylphenanthrene	3.91E-06	8.69	0.46	8.23
2,5-diethylphenanthrene	3.91E-06	8.61	0.48	8.13
1,2-diethylphenanthrene	3.91E-06	8.64	0.49	8.15
9-tertbutylphenanthrene	8.99E-06	8.64	0.50	8.14
3-tertbutylphenanthrene	8.99E-06	8.65	0.51	8.14
9-isobutylphenanthrene	7.09E-06	8.63	0.53	8.10
2-Isopropyl-10-methylphenanthrene	6.08E-06	8.58	0.48	8.10
2-methyl-1-propylphenanthrene	3.91E-06	8.64	0.49	8.15
9-methyl-10-propylphenanthrene	3.91E-06	8.54	0.51	8.03
1-methyl-2-propylphenanthrene	3.91E-06	8.63	0.49	8.14

Table A6: Estimated vapor pressure, *HOMO*, *LUMO* and *HOMO-LUMO* for dibenzothiophene and its alkylated homologues

Compound	**Vapor Pressure at 25°C (mm Hg)**	**HOMO (eV)**	**LUMO (eV)**	**HOMO-LUMO (eV)**
C_0-dibenzothiophene				
Dibenzothiophene	6.84E-05	8.60	0.63	7.97
C_1-dibenzothiophenes				
1-methyldibenzothiophene	2.32E-05	8.52	0.60	7.92
2-methyldibenzothiophene	2.32E-05	8.52	0.60	7.92
3-methyldibenzothiophene	2.32E-05	8.58	0.61	7.97
4-methyldibenzothiophene	2.32E-05	8.53	0.59	7.94
C_2-dibenzothiophenes				
2-ethyldibenzothiophene	1.00E-05	8.53	0.60	7.93
3-ethyldibenzothiophene	1.00E-05	8.57	0.61	7.96
4-ethyldibenzothiophene	1.00E-05	8.54	0.58	7.96
1,2-dimethyldibenzothiophene	1.09E-05	8.45	0.57	7.88
1,4-dimethyldibenzothiophene	1.09E-05	8.48	0.57	7.91
1,6-dimethyldibenzothiophene	1.09E-05	8.49	0.57	7.92
1,7-dimethyldibenzothiophene	1.09E-05	8.51	0.59	7.92
1,8-dimethyldibenzothiophene	1.09E-05	8.45	0.57	7.88
1,9-dimethyldibenzothiophene	1.09E-05	8.46	0.61	7.85
2,3-dimethyldibenzothiophene	1.09E-05	8.49	0.58	7.91
2,4-dimethyldibenzothiophene	1.09E-05	8.47	0.56	7.91
2,6-dimethyldibenzothiophene	1.09E-05	8.47	0.56	7.91
2,7-dimethyldibenzothiophene	1.09E-05	8.49	0.58	7.91
3,4-dimethyldibenzothiophene	1.09E-05	8.51	0.58	7.93
3,7-dimethyldibenzothiophene	1.09E-05	8.55	0.60	7.95
4,6-dimethyldibenzothiophene	1.09E-05	8.51	0.56	7.95
C_3-dibenzothiophenes				
1,4,6-trimethyldibenzothiophene	4.37E-06	8.43	0.53	7.90
1,2,4-trimethyldibenzothiophene	4.37E-06	8.40	0.54	7.86
3,4,6-trimethyldibenzothiophene	4.37E-06	8.48	0.54	7.94
1,4,8-trimethyldibenzothiophene	4.37E-06	8.40	0.54	7.86
2,6,7-trimethyldibenzothiophene	4.37E-06	8.45	0.55	7.90
3,4,7-trimethyldibenzothiophene	4.37E-06	8.49	0.56	7.93
2,4,7-trimethyldibenzothiophene	4.37E-06	8.44	0.55	7.89
1,4,7-trimethyldibenzothiophene	4.37E-06	8.45	0.56	7.89
1,3,7-trimethyldibenzothiophene	4.37E-06	8.49	0.58	7.91
2,4,8-trimethyldibenzothiophene	4.37E-06	8.40	0.53	7.87
4-ethyl,6-methyl-dibenzothiophene	4.73E-06	8.50	0.56	7.94

Table A7: Estimated vapor pressure, *HOMO*, *LUMO* and *HOMO-LUMO* for fluorene and its alkylated homologues

Compound	**Vapor Pressure at 25°C (mm Hg)**	**HOMO (eV)**	**LUMO (eV)**	**HOMO-LUMO (eV)**
C_0-Fluorenes				
Fluorene	3.30E-04	8.84	0.33	0.33
C_1-Fluorenes				
1-methylfluorene	3.53E-04	8.77	0.31	0.31
2-methylfluorene	3.98E-04	8.79	0.31	0.31
3-methylfluorene	3.98E-04	8.70	0.33	0.33
4-methylfluorene	3.98E-04	8.80	0.31	0.31
C_2-Fluorenes				
2-ethylfluorene	1.52E-04	8.80	0.31	0.31
9-ethylfluorene	2.34E-04	8.79	0.32	0.32
1,9-dimethylfluorene	2.02E-04	8.70	0.32	0.32
2,3-dimethylfluorene	1.56E-04	8.66	0.30	0.30
C_3-Fluorenes				
9-propylfluorene	9.23E-05	8.78	0.31	0.31
9-(1-methylethyl)fluorene	1.77E-04	8.79	0.32	0.32

Table A8: Estimated vapor pressure, *HOMO*, *LUMO* and *HOMO-LUMO* for chrysene and its alkylated homologues

Compound	**Vapor Pressure at 25°C (mm Hg)**	**HOMO (eV)**	**LUMO (eV)**	**HOMO-LUMO (eV)**
C_0-chrysenes				
Chrysene	1.56E-09	8.50	0.78	7.72
C_1-chrysenes				
1-methylchrysene	1.35E-08	8.44	0.77	7.67
2-methylchrysene	2.53E-07	8.45	0.76	7.69
3-methylchrysene	2.53E-07	8.45	0.76	7.69
4-methylchrysene	1.35E-08	8.41	0.78	7.63
5-methylchrysene	5.45E-07	8.43	0.78	7.65
6-methylchrysene	5.45E-07	8.40	0.77	7.63
C_2-chrysenes				
2-ethylchrysene	1.06E-07	8.44	0.76	7.68
3-ethylchrysene	1.06E-07	8.46	0.76	7.70
5-ethylchrysene	1.06E-07	8.42	0.76	7.66
6-ethylchrysene	1.06E-07	8.39	0.77	7.62
2,3-dimethylchrysene	1.14E-07	8.41	0.74	7.67
5,12-dimethylchrysene	1.14E-07	8.33	0.77	7.56
1,2-dimethylchrysene	1.14E-07	8.39	0.74	7.65
C_3-chrysenes				
6-propylchrysene	4.44E-08	8.39	0.77	7.62
1-ethyl-2-methylchrysene	4.82E-08	8.40	0.74	7.66
6-ethyl-5-methylchrysene	4.82E-08	8.37	0.75	7.62
6-(1-methylethyl)chrysene	8.06E-08	8.41	0.77	7.64
4-(1-methylethyl)chrysene	8.06E-08	8.42	0.77	7.65
C_4-chrysenes				
6-butylchrysene	4.78E-08	8.39	0.77	7.62
6,12-diethylchrysene	2.02E-08	8.29	0.76	7.53
2-isobutylchrysene	3.36E-08	8.45	0.75	7.70
6-isobutylchrysene	3.36E-08	8.41	0.76	7.65
1,2,7,8-tetramethylchrysene	2.01E-08	8.30	0.70	7.60